1. Report No. FHWA/TX-14/0-6622-2	2. Government Accession No.	3. Recipient's Catalog No.
4. Title and Subtitle DEVELOPMENT OF TEXAS MECHANISTIC-EMPIRICAL FLEXIBLE PAVEMENT DESIGN SYSTEM (TxME)		5. Report Date September 2013 Published: January 2014
		6. Performing Organization Code
7. Author(s) Sheng Hu, Fujie Zhou, and Tom Scullion		8. Performing Organization Report No. Report 0-6622-2
9. Performing Organization Name and Address Texas A&M Transportation Institute College Station, Texas 77843-3135		10. Work Unit No. (TRAIS)
		11. Contract or Grant No. Project 0-6622
12. Sponsoring Agency Name and Address Texas Department of Transportation Research and Technology Implementation Office 125 E. 11th Street Austin, Texas 78701-2483		13. Type of Report and Period Covered Technical Report: September 2012–August 2013
		14. Sponsoring Agency Code

15. Supplementary Notes

Project performed in cooperation with the Texas Department of Transportation and the Federal Highway Administration.

Project Title: Implementation of a Texas Mechanistic-Empirical Thickness Design System (TxME)

URL: http://tti.tamu.edu/documents/0-6622-2.pdf

16. Abstract

The FPS design system implemented in the mid-1990s has limitations in that it does not use any results from laboratory testing so it is impossible to determine benefits from improved base materials or superior asphalt mixes. The development of the new flexible pavement design system, TxME, will enable Texas pavement designers to take full advantage of new or premium materials, with a full consideration of the influential factors including pavement structure, traffic loading, and environmental conditions. The features of TxME include 1) Mechanistic-Empirical modeling, 2) performance-based material characterization, 3) traffic load spectrum incorporation, 4) design input variability-based reliability methodology, 5) incremental distress prediction, 6) fast running speed, 7) user-friendly interface, and 8) convenient connection with FPS.

This report documents the work and findings during this study. Sensitivity analysis shows that TxME can make rational predictions under different combinations of pavement structure, climate, and traffic load. As a first stage, the researchers recommend that TxME be used as a performance check tool for design options recommended by the FPS design system. More calibration and model fine-tuning work still needs to be done.

17. Key Words: TxME, Mechanistic Empirical, Flexible Pavement Design, Asphalt, Rutting, Cracking, Implementation	18. Distribution Statement No restrictions. This document is available to the public through NTIS: National Technical Information Service Alexandria, Virginia 22312 http://www.ntis.gov		
19. Security Classif. (of this report) Unclassified	20. Security Classif. (of this page) Unclassified	21. No. of Pages 180	22. Price

Form DOT F 1700.7 (8-72)   **Reproduction of completed page authorized**

DEVELOPMENT OF TEXAS MECHANISTIC-EMPIRICAL FLEXIBLE PAVEMENT DESIGN SYSTEM (TxME)

by

Sheng Hu, Ph.D., P.E.
Assistant Research Engineer
Texas A&M Transportation Institute

Fujie Zhou, Ph.D, P.E.
Research Engineer
Texas A&M Transportation Institute

and

Tom Scullion, P.E.
Senior Research Engineer
Texas A&M Transportation Institute

DISCLAIMER

The contents of this report reflect the views of the authors, who are responsible for the facts and the accuracy of the data presented here. The contents do not necessarily reflect the official view or policies of the Federal Highway Administration (FHWA) or the Texas Department of Transportation (TxDOT). This report does not constitute a standard, specification, or regulation, nor is it intended for construction, bidding, or permit purposes.

The United States Government and the State of Texas do not endorse products or manufacturers. Trade or manufacturers' names appear here solely because they are considered essential to the object of this report.

The researcher in charge was Dr. Fujie Zhou, P.E. (Texas, #95969).

ACKNOWLEDGMENTS

TABLE OF CONTENTS

LIST OF FIGURES

LIST OF TABLES

LIST OF ABBREVIATIONS

AADTT   Average Annual Daily Truck Traffic

AASHTO   American Association of State Highway and Transportation Officials

AC   Asphalt Concrete

CAM   Crack Attenuating Mixture

CA   Cracking Amount

CV   Coefficient of Variation

DDF   Directional Distribution Factor

EICM   Enhanced Integrated Climatic Model

ESAL   Equivalent Single Axle Load

FEM   Finite Element Method

FHWA   Federal Highway Administration

FWD   Falling Weight Deflectometer

FPS   Flexible Pavement Design System

HMA   Hot-Mix Asphalt

LDF   Lane Distribution Factor

M-E   Mechanistic-Empirical

MAF   Monthly Adjustment Factor

MEPDG   Mechanistic-Empirical Pavement Design Guide

MLET   Multi-layer Linear Elastic Theory

NCHRP   National Cooperative Highway Research Program

NN   Neural Network

OT   Overlay Tester (based on Tex-248-F)

SIF   Stress Intensity Factor

SMA   Stone Matrix Asphalt

TTI   Texas A&M Transportation Institute

TxACOL   Texas Asphalt Concrete Overlay Design System

TxDOT   Texas Department of Transportation

TxME   Texas Mechanistic-Empirical Flexible Pavement Design System

CHAPTER 1.
INTRODUCTION

1.1 BACKGROUND AND OBJECTIVES

The current flexible pavement design system (FPS) used by the Texas Department of Transportation (TxDOT) has limitations in that it does not use any results from laboratory testing so it is impossible to determine benefits from improved base materials or superior asphalt mixes (Liu and Scullion 2006). Developments over the last several decades have offered an opportunity for more rational and rigorous pavement design procedures. Substantial work has already been completed in Texas, nationally and internationally, in all aspects of modeling, materials characterization, and structural design. These and other assets provided the technical infrastructure that made it possible to develop the Texas Mechanistic-Empirical (TxME) flexible pavement design system. The development of this new system will enable Texas pavement designers to take full advantage of new or premium materials, with a full consideration of the influential factors including pavement structure, traffic volume, and environmental conditions.

The main objectives of this project are:

- Identify available models and test procedures that allow mechanistic-empirical prediction of pavement performance for different Texas flexible pavement types and environmental conditions.
- Identify or develop a methodology for incorporating axle load spectrum into pavement design.
- Identify a practical reliability approach, which can take the design input variability into account.
- Implement all the available models, load spectrum methodology, climate effects, and reliability approach into the TxME design program.
- Connect the TxME program with the FPS design program, and use TxME as a performance check tool for design options recommended by FPS.

In the first year of this project, a comprehensive literature review was made to identify and recommend available performance models and reliability approaches. Additionally, the framework of TxME was proposed and the main user interface of the software was developed. The work was summarized in the published Report 0-6622-1 (Hu et al. 2012a). Thus the Report 0-6622-2 mainly focuses on how these models and approaches are implemented into the TxME program. Sensitivity analyses were also performed to analyze the impact of design inputs and demonstrate the advantages of TxME.

1.2 REPORT ORGANIZATION

This report is organized into the following seven chapters:

- Chapter 1: Introduction, providing a brief description of the project background, objectives, and report organization.
- Chapter 2: Overview of TxME, summarizing the overall design, inputs and outputs, user interface, and functions.
- Chapter 3: Implementation of models, presenting how the performance models are implemented into the program. These models include asphalt layer fatigue cracking model, asphalt layer rutting model, asphalt layer thermal cracking model, granular base/subgrade rutting model, stabilized base fatigue cracking model, and endurance limit model. The preliminary calibrations for some models are also discussed.
- Chapter 4: Methodology for incorporating axle load spectrum, discussing how the damage is superposed in terms of each axle load, with respect to each distress type.
- Chapter 5: Reliability approach implementation, describing how the system takes the design input variability into account and how to determine the reliability-based results using the Rosenblueth method (Rosenblueth 1975).
- Chapter 6: Sensitivity analysis, comparing the distress prediction based on different combinations of pavement structure, material properties, climate, and traffic loads.
- Chapter 7: Conclusions and Recommendations.

Additionally, this report includes three appendices, which provide more information on default material properties, program specifications, and rutting distributions, respectively:

- Appendix A: Default Material Properties of Most Common Pavement Materials from Texas Districts.
- Appendix B: Program Specifications for TxME.
- Appendix C: Rutting Distribution in Individual Layers.

CHAPTER 2.
OVERVIEW OF TxME

The TxME design system aims to enable TxDOT designers to take full advantage of new or premium materials and to make more economically reliable designs. The main features of TxME include:

- Mechanistic-Empirical modeling.
- Performance-based material characterization.
- Traffic load spectrum incorporation.
- Consideration of local climate history.
- Design input variability-based reliability methodology.
- Incremental distress prediction.
- Fast running speed.
- User-friendly interface.
- Convenient connection with FPS.

Three types of flexible pavement structures can be handled in the TxME, including:
- Surface treated.
- Conventional or thin HMA.
- Perpetual pavement.

For any type of pavement design and analysis, there are four categories of input:

- Pavement structure and associated material properties.
- Traffic loading.
- Climate.
- Reliability-related input, including performance criteria and variability, etc.

To provide an overview of TxME, the following discusses these four categories of input and related output for each pavement type.

2.1 PAVEMENT STRUCTURE AND ASSOCIATED MATERIAL PROPERTIES

The user interface aspects of the main screen, pavement structure screen, and material properties input screen are briefly illustrated below.

2.1.1 Main Screen

Figure 2-1 presents the main screen of the TxME. In this screen, four major input categories are listed on the left side of the node tree, such as Structure, Climate, Traffic, and Reliability. Double-clicking each node activates the corresponding input window on the right side.
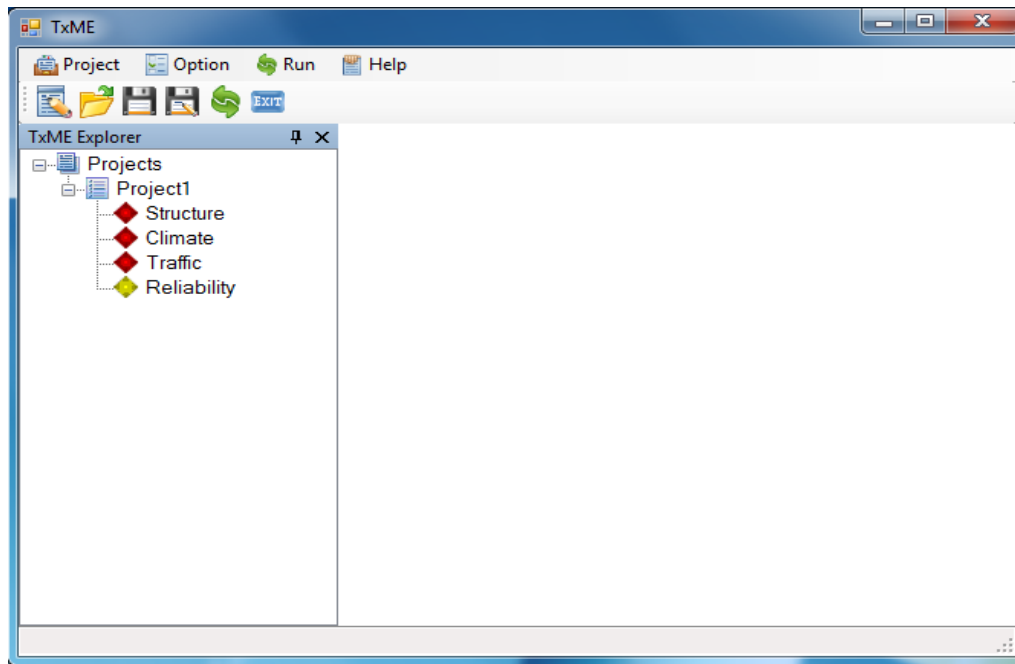
Figure 2-1. Main Screen of User Interface.

2.1.2 Pavement Structure

Figure 2-2 presents the pavement structure input screen. On this screen, the upper left window shows the pavement type and location; the upper right window lists available AC layer material, base layer material, and sub-base layer material icons; the lower left window shows the pavement structure; and the lower right window shows the layer material properties.

Users can build their own pavement structures by dragging the layer material icons into the pavement structure window. To remove a layer from the pavement structure window, users just need to click the layer and choose "Remove this layer" from the pop-up menu.
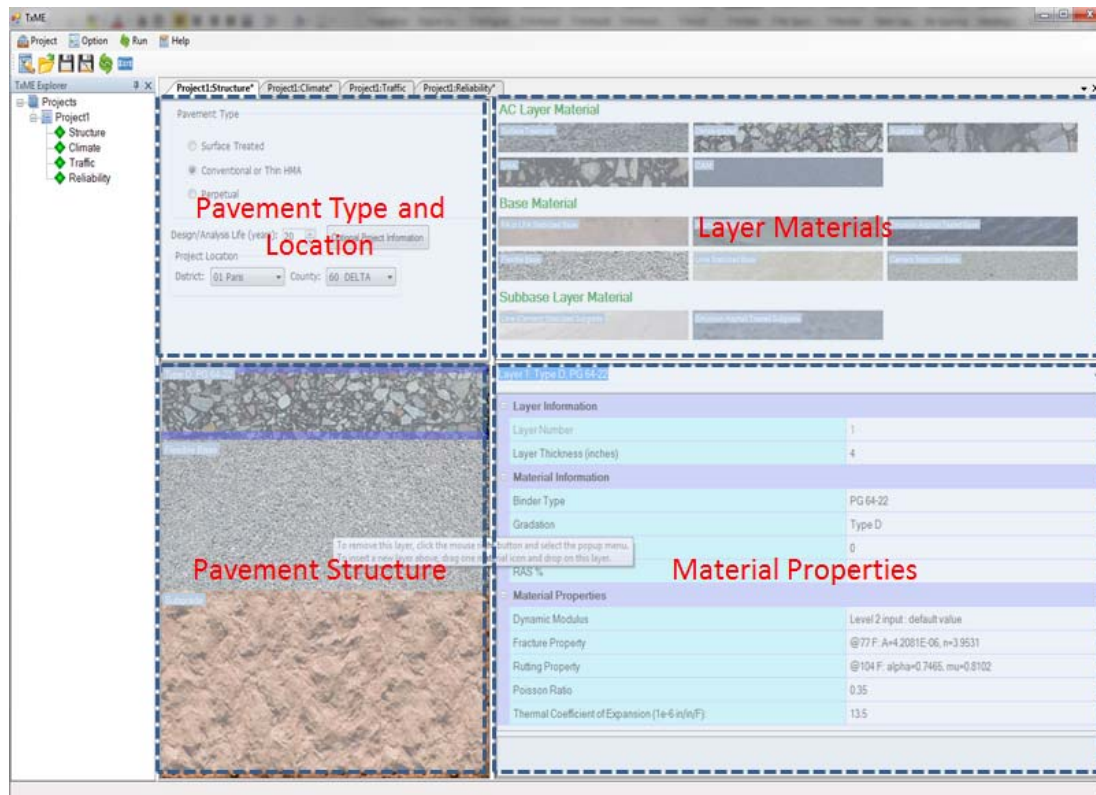
Figure 2-2. Pavement Structure Information Screen.

2.1.3 Material Properties

As in Figure 2-2, by clicking each layer in the pavement structure window, users can browse or edit this layer thickness and layer material properties in the material properties window. For some property inputs such as Thickness, Poisson's Ratio, etc., the user only needs to input a single parameter. For more complicated inputs such as dynamic modulus and fracture/rutting properties, the user needs to click on the item drop down menu, and the expanded input screen will pop up. Several material property input screens are illustrated below, including:

- Figure 2-3, presenting the dynamic modulus inputs for AC layers.
- Figures 2-4 and 2-5, presenting AC layer fracture property and rutting property inputs, respectively.
- Figure 2-6, presenting the stabilized base material property inputs.
- Figure 2-7 and 2-8, presenting flexible base or subgrade modulus inputs, including typical modulus and modulus considering moisture impact, respectively.
- Figure 2-9, presenting the flexible base or subgrade material rutting property inputs, with monthly values.

Figure 2-3. AC Layer Dynamic Modulus Input Screen.

Figure 2-4. AC Layer Fracture Properties Input Screen.

Figure 2-5. AC Layer Rutting Properties Input Screen.

Figure 2-6. Stabilized Base Material Properties Input Screen.

**Figure 2-7. Flexible Base/Subgrade Typical Modulus Input Screen
(without Considering Moisture Impact).**

Figure 2-8. Flexible Base/Subgrade Modulus Input Screen (Considering Moisture Impact).

Figure 2-9. Flexible Base/Subgrade Rutting Properties Input Screen.

2.2 TRAFFIC LOADING

There are two levels of traffic inputs in TxME: one is Equivalent Single Axle Load (ESAL) input and the other is axle load spectrum input. The following illustrates the difference between these inputs.

2.1.1 Traffic ESALs (Level 2) Input

Figure 2-10 shows the traffic ESALs (Level 2) input screen. The most important input is the total ESAL number during 20 years (one lane and one direction). The ADT-Beginning and ADT-End represent average daily traffic in the beginning and in the end, respectively. These values are used to determine the vehicle growth rate. The tire pressure is used to determine the tire contact area. The operational speed (could be posted speed limit, or lower in urban traffic) impacts the AC layer modulus since it relates to loading time.

Figure 2-10. Traffic ESALs (Level 2) Input Screen.

2.1.2 Axle Load Spectrum (Level 1) Input

Figure 2-11 is the traffic (truck classes 4–13) axle load spectrum (Level 1) input screen. In this screen, the left window shows the general information and axle configuration information such as average annual daily truck traffic (AADTT) number, operational speed, tire pressure, axle spacing, etc.; the upper right window shows the vehicle class distribution and growth rate information; and the lower right window shows the axle numbers for each vehicle class. By clicking the "Monthly Adjustment" or "Axle Load Distribution" button in Figure 2-11, screens such as Figure 2-12 or Figure 2-13 pop up. These screens let users define the axle load distributions for each vehicle class and their monthly variations.

Figure 2-11. Traffic Load Spectrum (Level 1) Input Screen.

Figure 2-12. Traffic Monthly Adjustment Input Screen.

Figure 2-13. Traffic Axle Load Distribution Input Screen.

Axle Load Distribution

View
- ○ Cumulative Distribution
- ● Distribution

Axles
- ○ Steering Axle ● Other Single Axle ○ Tandem Axle
- ○ Tridem Axle ○ Quad Axle

Axle Factors by Axle Type

>	Season	Veh. Class	Total	3000	4000	5000	6000	7000	8000	9000	10000	11000	12000	13000	14000	1500(
	January	4	100.00	1.8	0.96	2.91	3.99	6.8	11.47	11.3	10.97	9.88	8.54	7.33	5.55	4.23
	January	5	100.00	10.05	13.21	16.42	10.61	9.22	8.27	7.12	5.85	4.53	3.46	2.56	1.92	1.54
	January	6	100.00	2.47	1.78	3.45	3.95	6.7	8.45	11.85	13.57	12.13	9.48	6.83	5.05	3.74
	January	7	100.00	2.14	0.55	2.42	2.7	3.21	5.81	5.26	7.39	6.85	7.42	8.99	8.15	7.77
	January	8	100.00	11.65	5.37	7.84	6.99	7.99	9.63	9.93	8.51	6.47	5.19	3.99	3.38	2.73
	January	9	100.00	1.74	1.37	2.84	3.53	4.93	8.43	13.67	17.68	16.71	11.57	6.09	3.52	1.91
	January	10	100.00	3.64	1.24	2.36	3.38	5.18	8.35	13.85	17.35	16.21	10.27	6.52	3.94	2.33
	January	11	100.00	3.55	2.91	5.19	5.27	6.32	6.98	8.08	9.68	8.55	7.29	7.16	5.65	4.77
	January	12	100.00	6.68	2.29	4.87	5.86	5.97	8.86	9.58	9.94	8.59	7.11	5.87	6.61	4.55

Export Axle File   Open Axle File

OK   Cancel

2.3 CLIMATE

There are two ways to attach the climatic information to a given project location: users can either assign a specific weather station or use interpolated climatic data based on the coordinates of the location.

Figure 2-14 presents the climate input screen when users choose a specific weather station. Generally, the left part of the screen allows the user to select a weather station, and the right part shows the summary of the weather data, such as average temperature or precipitation. The tables on the right side will not appear until after a station location is selected (OK button activated). The user can look into more detailed information like hourly data by clicking the "Hourly data" tab on the upper right part of the screen.

Figure 2-14. Climate for a Specific Weather Station Input Screen.

For a project location without a pre-listed weather station, users can choose the radio button "Interpolate climatic data for a given location" and the application will provide six weather stations nearby for the user to select for interpolation. Figure 2-15 presents the user input screen for climate data interpolation. The lines and numbers such as "#1, #2…" in the graph show the relative positions and distances from the location defined by the coordinates. The interpolated hourly data information is listed in the right part of the screen.

Figure 2-15. Climatic Data Interpolation Input Screen.

2.4 RELIABILITY RELATED INPUT

Figure 2-16 presents the reliability related input screen for a three-layer conventional pavement. Two input categories are displayed in this screen. On the left side are the performance criteria inputs, and on the right side are the variability inputs. For the performance criteria inputs, the user supplies the analysis stop criteria (performance limit) and reliability level in terms of percentage. For variability inputs, the user checks the applicable checkboxes and modifies the coefficient of variation value.

Figure 2-16. Reliability Related Input Screen for a Three-Layer Conventional Pavement.

Both performance criteria and variability parameters are related to pavement structure and pavement type. Whenever the pavement structure or pavement type changes, these parameters are changed accordingly. For example, Figure 2-17 shows the reliability related input screen for a four-layer perpetual pavement. As can be seen in this figure, the endurance limit entry appears on the left side and more parameters are listed on the right side.

Figure 2-17. Reliability Related Input Screen for a Four-Layer Perpetual Pavement.

2.5 OUTPUT

The output of TxME is organized into an Excel® file, which is mainly composed of three parts: the summary of user's inputs, the analysis result table, and the distress plots. See Figure 2-18. The predicted distresses are keyed to the pavement structure and pavement type. The following information discusses and illustrates the output for each pavement type.
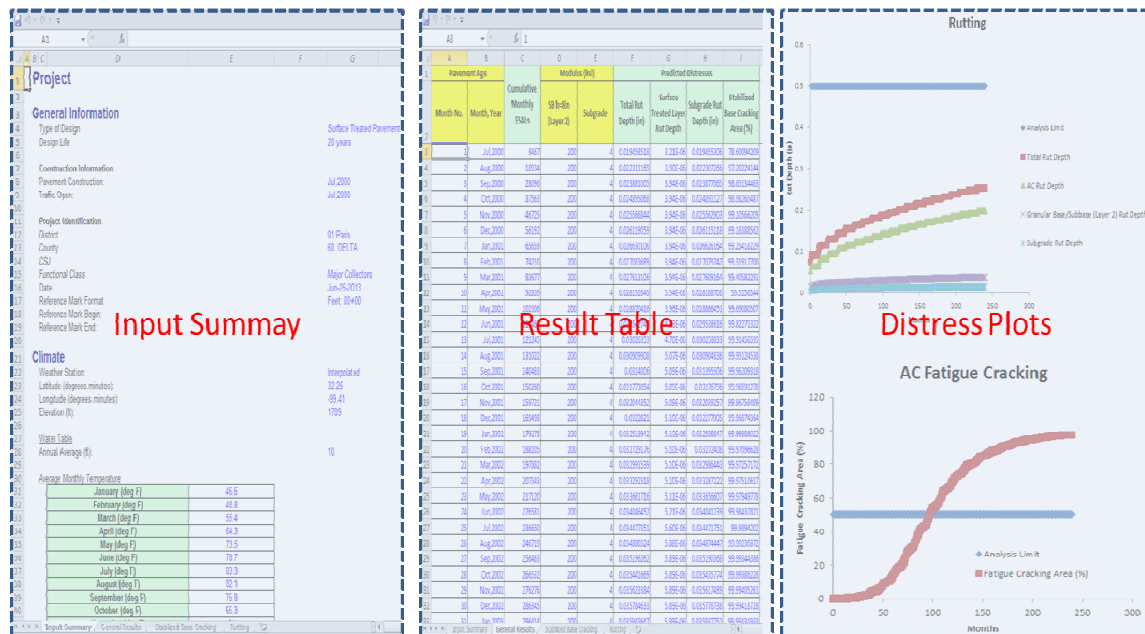
Figure 2-18. Output of TxME in Excel File Format.

2.5.1 Output of Surface Treated Pavement

For surface treated pavement with a flexible base, only rutting is predicted and plotted. See Figure 2-19. The premise is that rutting is rooted in failure in the unbound lower layers. Any fatiguing in the surface that may be manifested is directly caused by the over-extension of the surface due to the rutting.
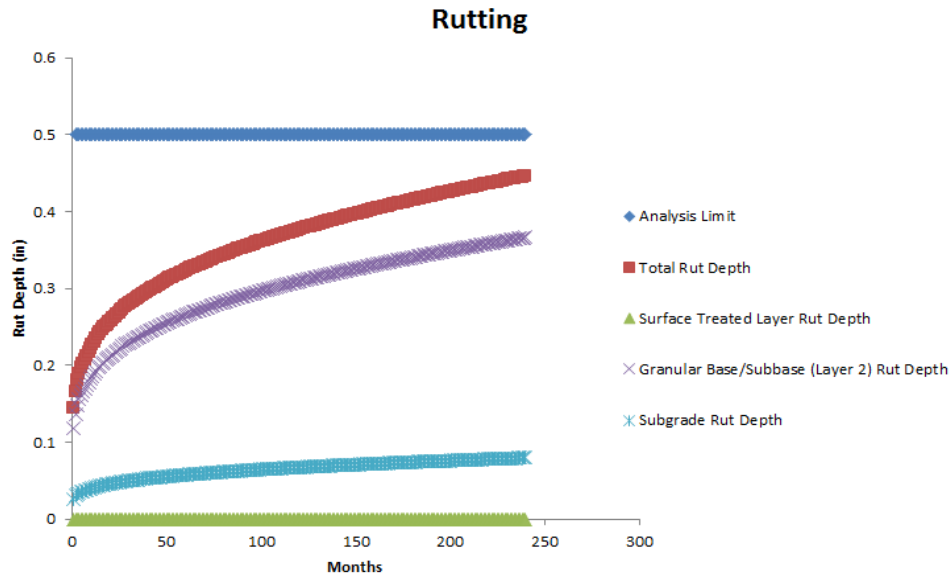
Figure 2-19. Output of Surface Treated Pavement with Flexible Base.

For surface treated pavement with stabilized base, both rutting and stabilized fatigue cracking are predicted and plotted. See Figure 2-20; note that the rut depth of stabilized base is ignored.
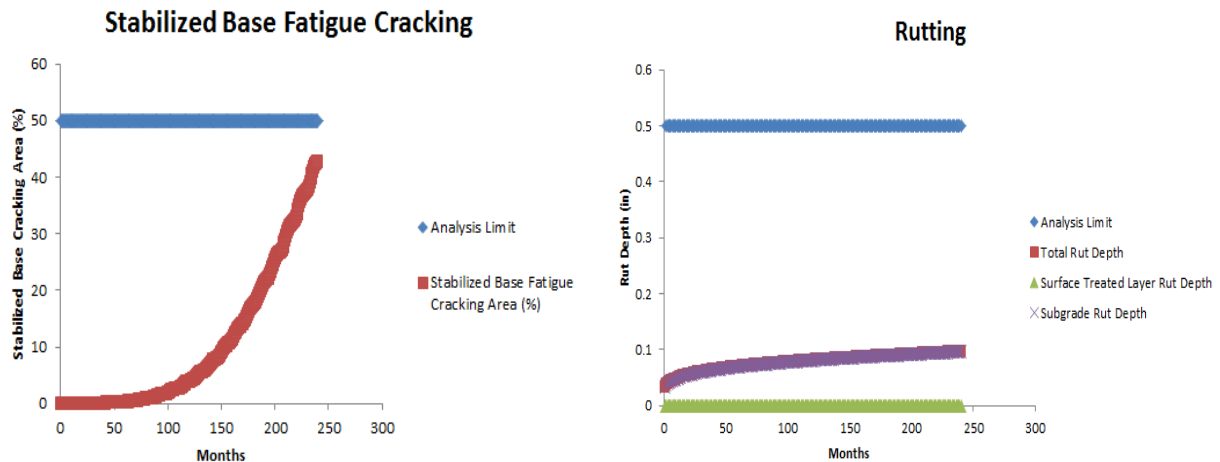
Figure 2-20. Output of Surface Treated Pavement with Stabilized Base.

16

If there are more than two base or subbase layers, of which some are flexible and the others are stabilized, TxME will predict the stabilized fatigue cracking only if the stabilized base layer is just under the surface layer. The rut depth of flexible base layer is always predicted no matter where the layer is.

2.5.2 Output of Conventional or Thin HMA Pavement

Figure 2-21 shows the typical output of conventional or thin HMA pavement with flexible base. rutting, AC fatigue cracking, and AC thermal cracking are predicted in the analysis.
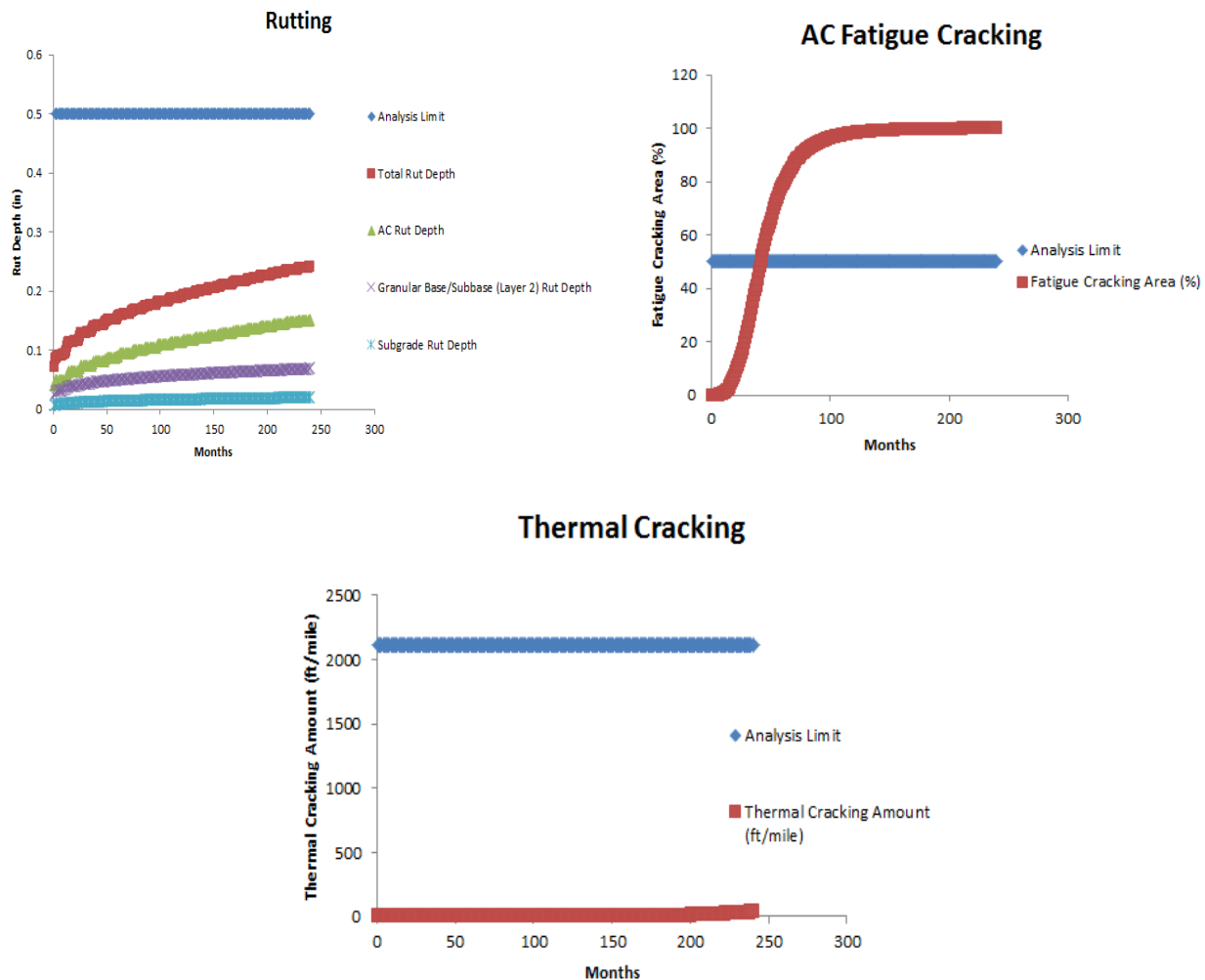
Figure 2-21. Output of Conventional or Thin HMA with Flexible Base.

Similar to surface treated pavement, if the first base layer (counted from top to bottom) is a stabilized layer, the stabilized base fatigue cracking is also predicted and plotted.

2.5.3 Output of Perpetual Pavement

For perpetual pavement analysis, the endurance limit is determined according to the traffic input level. For ESALs input (Level 2), the endurance limit is actually the maximum strain at the bottom of all HMA layers under the standard 18 kip single axle dual tire load. For load spectrum input (Level 1), the endurance limit is the frequency of HMA bottom layer strain distribution under the spectrum of axle load levels. Figure 2-22 shows the endurance limit output under the traffic load spectrum.

AC Bottom Strain Distribution
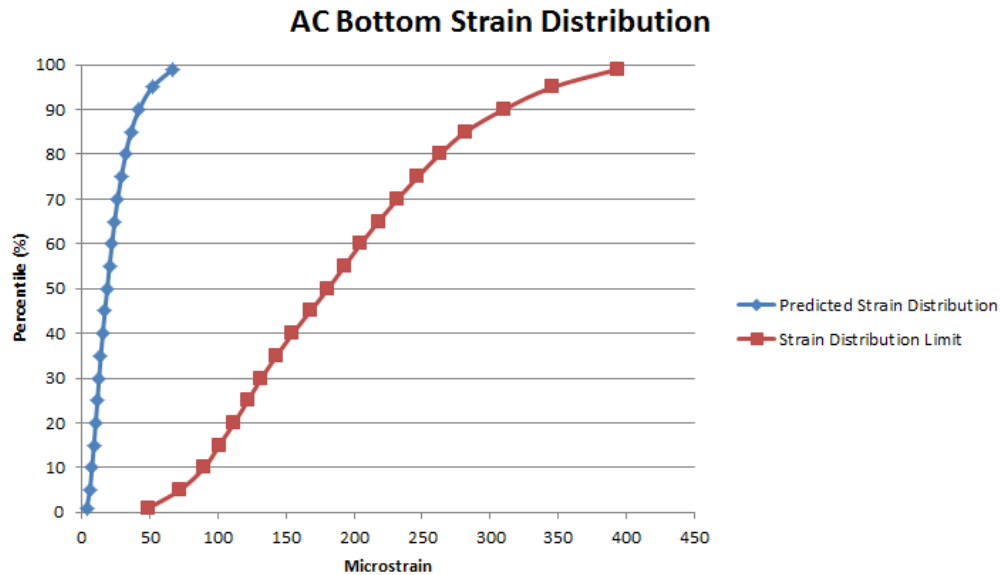
Figure 2-22. Output of Endurance Limit of Perpetual Pavement under Load Spectrum.

Other typical output of a perpetual pavement analysis is similar to conventional pavement, which includes rutting, AC fatigue cracking, and AC thermal cracking. There is no stabilized fatigue cracking analysis for perpetual pavement since normally the AC layers are thick enough to prevent the occurrence of fatigue cracking in the stabilized base layer.

2.6 CONNECTION WITH FPS 21

FPS 21 is the flexible pavement design system currently used by TxDOT. Figure 2-23 shows the program start screen.

Figure 2-23. Start Screen of FPS 21.

The users' input of FPS 21 includes pavement location, beginning and ending serviceability indices, traffic ESALs, elastic modulus (can be based on Falling Weight Deflectometer [FWD] backcalculation) of each layer, maximum and minimum thickness of each layer, etc. FPS 21 reports combinations of layer thicknesses that fulfill the performance equation as constrained by the inputs. Note that FPS 21 only uses FWD backcalculated/estimated elastic modulus, and Poisson's ratio to represent each layer's properties; it does not use any lab testing data so it is impossible to determine performance benefits from improved base materials or superior asphalt mixes. To evaluate these benefits, TxME is designed to import pertinent input and output information from FPS21, then to incorporate additional specific test results such as rutting properties or fracture properties, to conduct the performance check. Figure 2-24 shows the connection concept.

19
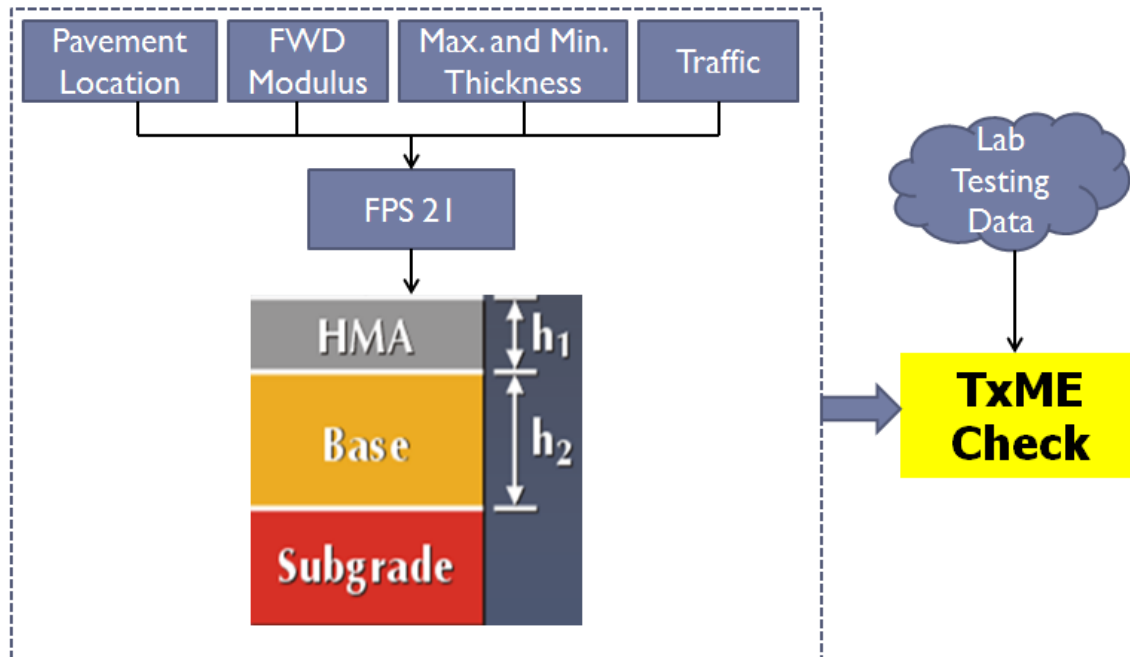
Figure 2-24. Connection Concept between FPS 21 and TxME.

Figure 2-25 shows an example of a TxME pavement structure imported from FPS 21 using a specially modified version of the program. By clicking the button "TxME Check" in the FPS 21 screen, the TxME will be launched and automatically import the related information, such as pavement location, layer type, layer thickness, ESALs, and so on. The left part of Figure 2-25 is the FPS 21 recommended design option, and the right part is the TxME pavement structure after importation. TxME also searches the embedded database and provides default values for lab testing data. Users can edit these values if specific lab test results are available.
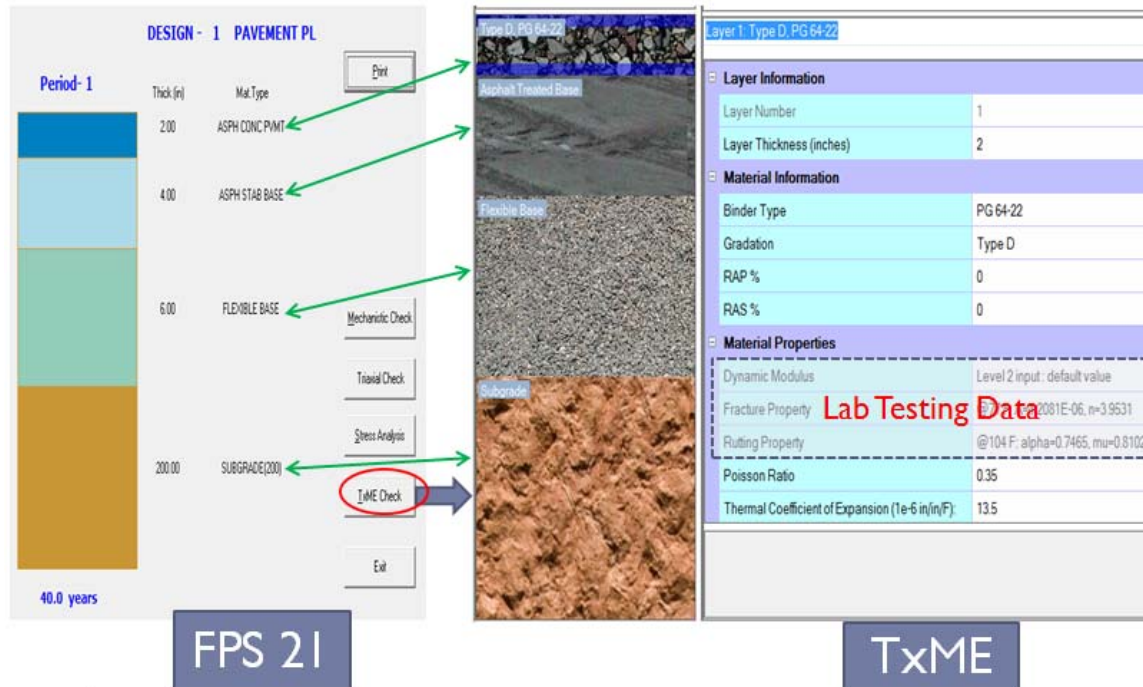
Figure 2-25. An Example of TxME Pavement Structure Imported from FPS 21.

CHAPTER 3.
IMPLEMENTATION OF MODELS

In the published year 1 Report 0-6622-1, performance models and related lab tests were evaluated. The six models listed below were recommended to be implemented into TxME.

- Asphalt layer rutting model.
- Asphalt layer fatigue cracking model.
- Granular base and subgrade rutting model.
- Asphalt layer thermal cracking model.
- Stabilized base fatigue cracking model.
- Perpetual pavement endurance limit model.

This chapter discusses how these models are implemented in the TxME design system.

3.1 IMPLEMENTATION OF ASPHALT LAYER RUTTING MODEL

The VESYS layer rutting model, originally developed by the Federal Highway Administration (FHWA) in the 1970s, was selected as the asphalt layer rutting model; see Equation 3-1. The Mechanistic-Empirical Pavement Design Guide (MEPDG) has used a similar conceptual rutting model (NCHRP 2004).

$$RD_{AC} = k_{AC} \int \Delta U \, \mu N^{-\alpha}$$

(3-1)

where

RD_{AC}	=	rut depth in the AC layer.
k_{AC}	=	calibration factor.
ΔU	=	deflection difference between the AC layer top and layer bottom.
N	=	load repetitions.
α & μ	=	rutting properties of the AC layer, determined by lab test.

In the TxME, the major feature is to characterize each layer's properties rather than global parameters for all layers used in the MEPDG (Zhou and Scullion, 2002). To implement this model, the key tasks are the determination of ΔU and the monthly accumulation of $RD_{AC.}$

3.1.1 ΔU Determination

Multi-layer linear elastic theory (MLET) solutions were employed to determine the ΔU. A major advantage of MLET solutions is the very quick computation times. It is suitable for cases in which all materials in the pavement structure can reasonably be approximated as behaving linearly elastically. Solutions for multiple wheel loads can be constructed from the fundamental axisymmetric single wheel solutions via superposition method.

Inputs to the MLET module include:

- Pavement geometry: Layer thickness.
- Traffic: a) Speed, b) ESALs or Load Spectrum.
- Material properties: a) Elastic modulus (considering the influence of temperature, moisture, and traffic speed), b) Poisson's Ratio.

Figure 3-1 shows the schematic of ΔU under the standard single axle with dual tires (18 kip) loading. Only one end of the axle load (dual tires) needs to be considered due to the long distance between the two ends of the axle. The shape of each tire-pavement contact area is assumed to be a circle and the contact pressure is assumed to be evenly distributed, thus the radius R of the circle can easily be calculated based on the load P and the tire pressure from users' input. X axis is the horizontal direction, which is parallel to the load axle; Y axis is also the horizontal direction, which is perpendicular to load axle but parallel to the vehicle moving direction; and Z axis is vertically downward.
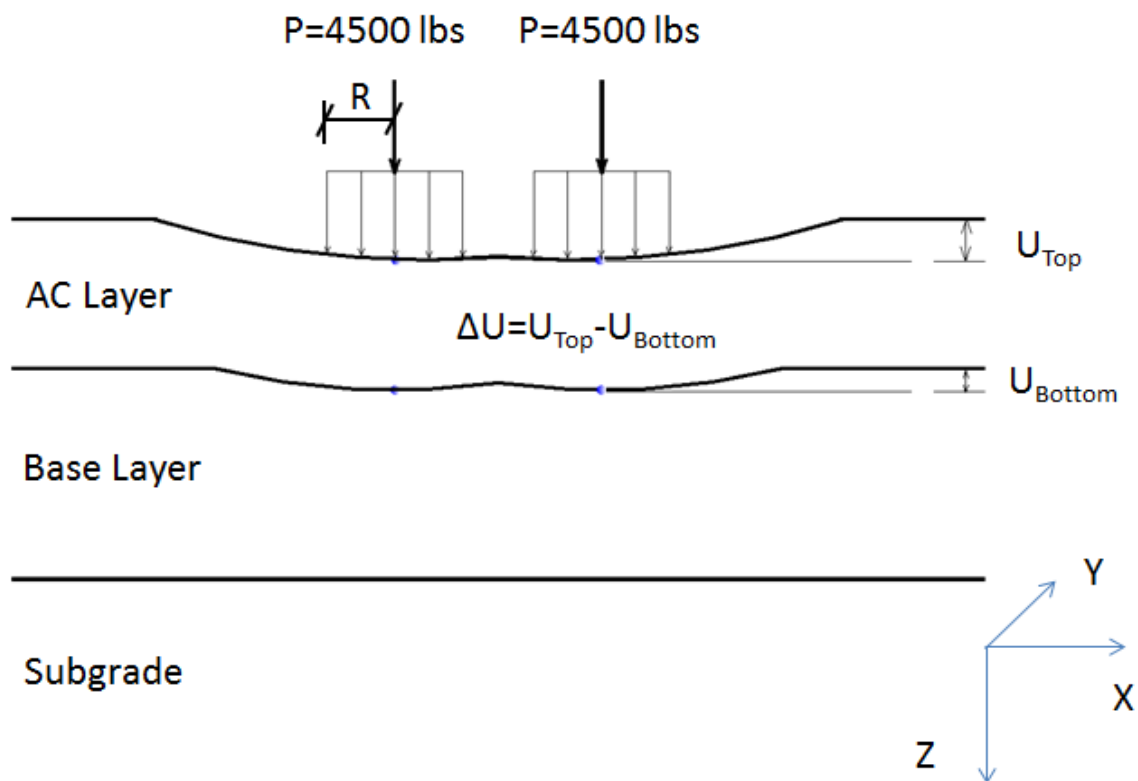
Figure 3-1. Schematic of ΔU Determination.

The MLET solution can determine the displacement, stress, and strain at any point (X, Y, Z) in the pavement. In the TxME, the displacements of both AC top and AC bottom at the tire center location are determined, represented as U_{Top} and U_{Bottom}, respectively. See Figure 3-1. ΔU is the difference between U_{Top} and U_{Bottom}.

24

3.1.2 Monthly Accumulation of RD_{AC}

Since α, μ, ΔU, and N for each month might vary because the monthly average temperature is different, the integral form of Equation 3-1 has to be expanded monthly and accumulated using the superposition method. The following describes this method by taking a three-month rut depth accumulation as an example.

Assume RD_1, RD_2, and RD_3 are the rut depths at the end of the first month, second month, and third month, respectively; N_1, N_2, and N_3 are the monthly ESALs of the first, second, and third month, respectively; α_1, μ_1, α_2, μ_2, α_3, and μ_3 are the rutting properties of the first, second, and third month, respectively. For the first month, the Equation 3-1 can be expanded into the Equation 3-2.

$$RD_1 = k_{AC}\Delta U_1 \mu_1 \frac{N_1^{1-\alpha_1}}{1-\alpha_1}$$

(3-2)

To determine RD_2, the equivalent ESASLs N_{eq1} (based on the RD_1 and the parameters of the second month) has to be determined first, using Equation 3-3.

$$N_{eq1} = \left(\frac{RD_1(1-\alpha_2)}{\Delta U_2 \mu_2 k_{AC}} \right)^{\frac{1}{1-\alpha_2}}$$

(3-3)

Then RD_2 can be calculated as follows:

$$RD_2 = k_{AC}\Delta U_2 \mu_2 \frac{\left(N_{eq1} + N_2\right)^{1-\alpha_2}}{1-\alpha_2}$$

(3-4)

Similarly, before determining RD_3, the equivalent ESASLs N_{eq2} (based on the RD_2 and the parameters of the third month) has to be determined; see Equation 3-5.

$$N_{eq2} = \left(\frac{RD_2(1-\alpha_3)}{\Delta U_3 \mu_3 k_{AC}} \right)^{\frac{1}{1-\alpha_3}}$$

(3-5)

Finally, RD_3 can be determined using Equation 3-6.

$$RD_3 = k_{AC}\Delta U_3 \mu_3 \frac{\left(N_{eq2} + N_3\right)^{1-\alpha_3}}{1-\alpha_3}$$

(3-6)

Figure 3-2 shows the schematic of this monthly rutting accumulation method.
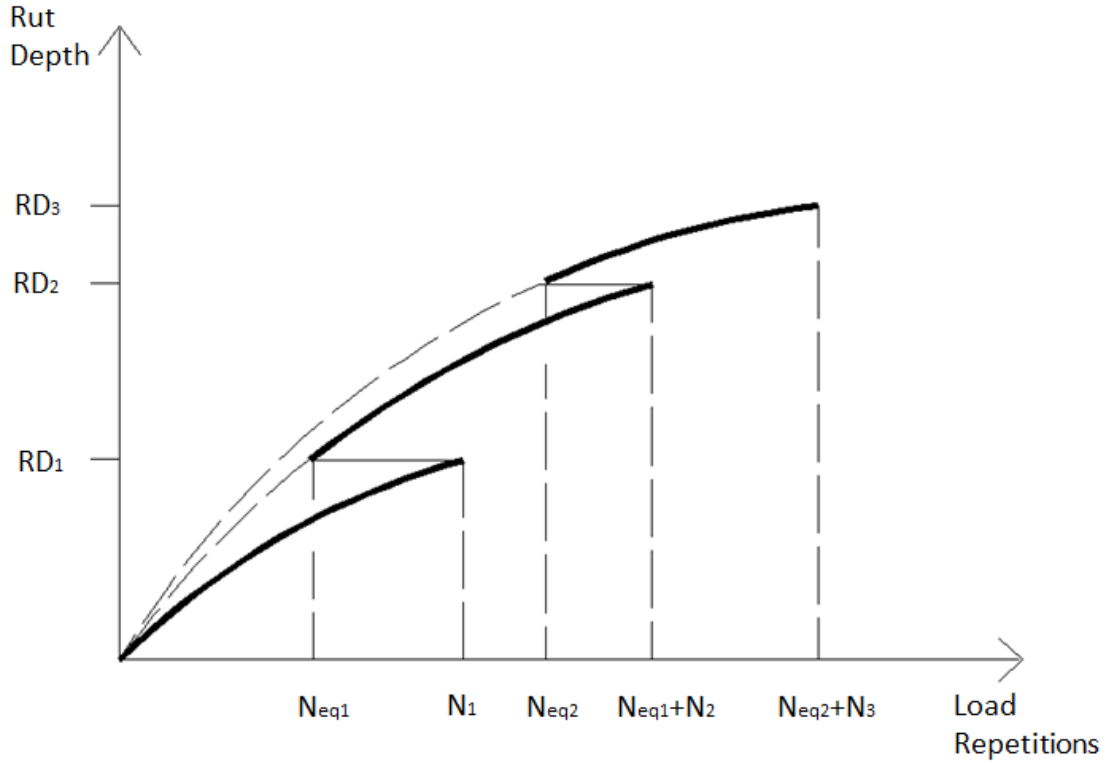
Figure 3-2. Schematic of Monthly Rut Accumulation Method.

This monthly rut accumulation method can be used not only when traffic input is in terms of ESALs, but also can be used when traffic input is axle load spectrum. In the case of load spectrum input, the rut has to be accumulated among different load levels and different axles before monthly accumulation. More details are discussed in Chapter 4: Methodology for Incorporating Axle Load Spectrum.

3.1.3 Preliminary Calibration of Asphalt Layer Rutting Model

The asphalt layer rutting model has been preliminarily calibrated using eight test sections of the 2006 National Center for Asphalt Technology (NCAT) test track program (Hu et al. 2011). k_{AC}, the calibration factor used in the above Equations 3-1 through 3-6, was calibrated as follows.

$$k_{AC} = f_1(T) \times f_2(E) \times f_3(h_{AC}) \qquad (3-7)$$

where

$f_1(T)$	=	the pavement temperature correction factor.
$f_2(E)$	=	the modulus correction factor to alternatively consider non-linear stress dependency of rutting development.
$f_3(h_{AC})$	=	the asphalt layer thickness correction factor.

The three adjustment factors, $f_1(T), f_2(E)$, and $f_3(h_{OL})$ for temperature, modulus, and layer thickness, have been separately determined and are presented in Equations 3-8, 3-9, and 3-10, respectively.

$$f_1(T) = 0.191112 + \frac{3.643124}{1 + e^{18.3009 - 0.204437\ T}}$$

(3-8)

$$f_2(E) = 0.37264 + \frac{1.18771}{1 + e^{-8.90208 + 0.09879\ E}}$$

(3-9)

$$f_3(h_{OL}) = \left(0.01445272\ h_1^3 - 0.12471319\ h_1^2 + 0.22193794\ h_1 + 1.37640722\right) \times$$
$$\left(0.00567302\ h_2^3 + 0.07104301\ h_2^2 - 0.49592553\ h_2 + 2.12378879\right) \times$$
$$\left(0.00199314 + \frac{0.54035153}{1 + e^{-2.61478586 + 0.58494148\ (h_1 + h_2)}}\right)$$

(3-10)

where

T =   the asphalt layer temperature, °F.

E =   the asphalt layer dynamic modulus value at 54°C (130°F) and 10 Hz, ksi.

h_1 and h_2 =   the representative layer thicknesses.

3.2 IMPLEMENTATION OF ASPHALT LAYER FATIGUE CRACKING MODEL

The proposed asphalt layer fatigue cracking model has three components: 1) Fatigue life model, 2) Fatigue damage model, and 3) Fatigue area model (Zhou et al. 2007 and Hu et al. 2010b).

The fatigue life model includes the following equations:

$$N_f = k_i N_i + k_p N_p$$

(3-11)

$$N_i = k_1 \left(\frac{1}{\varepsilon}\right)^{k_2}$$

(3-12)

$$k_1 = 10^{6.97001 - 3.20145 k_2 - 0.8366 1 \log E}$$

(3-13)

$$k_2 = n$$

(3-14)

$$N_p = \int_{c_0}^{h} \frac{1}{k_b AK_I^{\ n} + k_s AK_{II}^{\ n}}\ dc$$

(3-15)

where

N_f	=	fatigue life.
N_i	=	crack initiation life.
N_p	=	crack propagation life.
k_i, k_p, k_b, k_s	=	calibration factors.
ε	=	maximum tensile strain at the bottom of asphalt layer.
E	=	dynamic modulus.
A, n	=	fracture properties, determined from OT testing.
K_I, K_{II}	=	stress intensity factors (SIF) caused by bending and shearing stresses.

The fatigue damage model is estimated using Miner's Law:

$$D = \sum \frac{N}{N_f} \tag{3-16}$$

where

D = the accumulated fatigue damage.

N = the applied load repetitions.

The fatigue area model is proposed as a sigmoidal model:

$$fatigued\_area(\%) = \frac{100}{1 + e^{C \log D}} \tag{3-17}$$

where C is the field calibration factor.

Notice that in each month, pavement layers have different material properties (moduli or cracking properties) due to different temperature or different moisture content, thus the N_i and N_p of each month are different.

To determine the crack initiation life N_i for a given month, maximum tensile strain at the bottom of asphalt layer ε needs to be determined based on the MLET program. Equations 3-12, 3-13, and 3-14 can be used directly to calculate the N_i.

To determine the crack propagation life N_p for a given month, the SIFs K_I and K_{II} need to be determined at each crack length, and Equation 3-15 has to be expanded to achieve accumulation incrementally.

The following provides more details about the determination of K_I and K_{II} and monthly N_p, and model calibration.

3.2.1 Determination of K_I and K_{II}

Figure 3-3 shows the fracture mechanism of crack mode *I* (bending mode) and mode *II* (shearing mode), and corresponding axle load modes in the pavement. K_I and K_{II} are the SIFs at the crack tip under the bending mode and shearing mode, respectively.

(a)   (b)

(c)

(d)
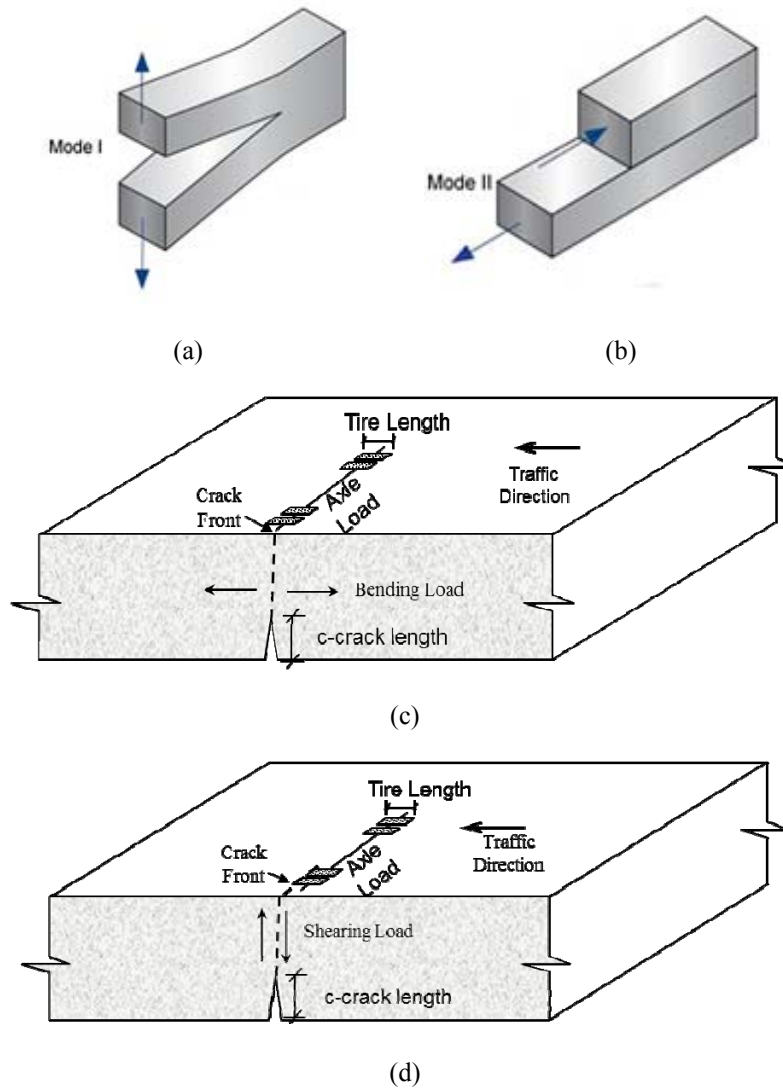
Figure 3-3. (a) Bending Mode in Fracture Mechanics, (b) Shearing Mode in Fracture Mechanics, (c) Pavement Loading Type in Bending Mode, and (d) Pavement Loading Type in Shearing Mode.

Only the finite element method (FEM) can determine the SIFs K_I and K_{II}, MLET analysis cannot do the job. However, directly incorporating the finite element calculation module into TxME is not practical due to the running time issue. To address this, the research team selected 147,000 combinations in terms of different pavement layer thickness, layer modulus, crack length, axle

29

load level (tire length), etc., to determine the corresponding SIFs. Table 3-1 lists the parameters' range used for the calculation.

Table 3-1. Range of Parameters in Fatigue Cracking SIF Calculations.

Parameters	Min.	Max.	Values Picked
AC Modulus (ksi)	150	4500	5
AC Thickness (inches)	1	64	7
Base Modulus (ksi)	7.5	3000	7
Base Thickness (inches)	4	64	5
Subgrade Modulus (ksi)	3	27	3
Ratio of Crack Length over AC Thickness	0.05	0.95	10
Tire Length (inches)	1.6	10	4

Note: Total combination number is $5 \times 7 \times 7 \times 5 \times 3 \times 10 \times 4$, which equals 147,000.

It should be mentioned that one SIF calculation takes about 20–30 minutes for a normal computer with 3D FE package such as ANSYS or ABAQUS, which implies more than 10 years of time is needed to complete 147,000 SIF calculations. With the help of *SA-CrackPro*, a specifically developed pavement SIF calculation tool (Hu et al. 2008), this work was done in a couple of months.

To use these pre-determined SIFs data in the TxME, the research team explored the neural network (NN) technique to fit the relationship between SIFs and the structure and loading parameters (White 1992). For each dataset, the researchers randomly divided it into training and validating parts at the ratio of 80 percent over 20 percent. The training data set is used to build/calibrate NN models, and the validating data set is for validating against over-fitting. To achieve this, the researchers used the MATLAB® function of "dividevec," which supports random partition of original data to avoid the over-fitting on the final results. The validation data is completely different from the training data, but can represent all features contained in the trained NN model. The fatigue SIF prediction models were successfully developed and summarized in Figure 3-4. The overall R^2 of NN prediction models for K_I and K_{II} are 0.993 and 0.997, respectively. More details about fatigue cracking SIF NN modeling can be found in the reference (Wu et al. 2013).
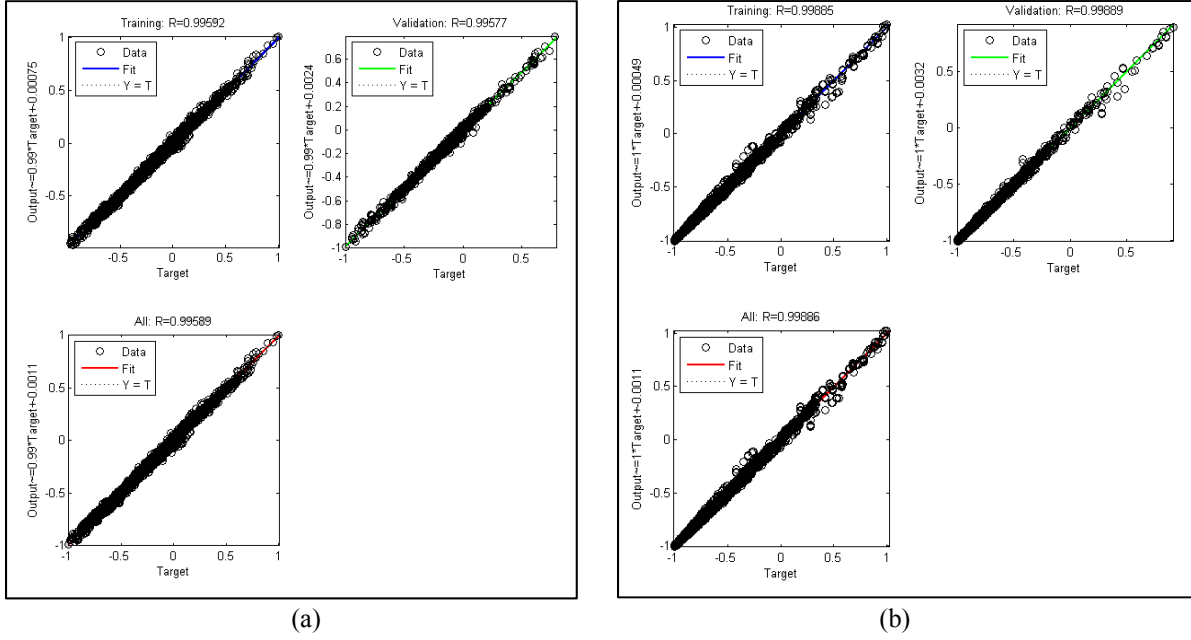
Figure 3-4. Fatigue Cracking Bending (a) and Shearing (b) NN SIF Prediction Performance.

After incorporating the NN SIF prediction model into TxME, the K_I ans K_{II} values of any pavement structure at any crack length can be determined instantly.

3.2.2 Determination of Monthly N_p

Rewrite Equation 3-15 into incremental form, as follows:

$$\sum \Delta N_{pi} = \frac{\sum \Delta c_{pi}}{k_b A K_I{}^n + k_s A K_{II}{}^n}$$

(3-18)

where
ΔN_{pi} = a load repetition incremental number.
Δc_{pi} = the crack propagation length caused by ΔN_{pi}.

With Equation 3-18, the monthly N_p determination steps are described below.

Step 1: Determine the K_I and K_{II} at the initiated crack length using NN SIF models.

Step 2: Assume a load repetition incremental number ΔN_{pi}, calculate the crack length increment Δc_{pi}, which equals $\Delta N_{pi}*(k_b A K_I{}^n + k_s A K_{II}{}^n)$.

Step 3: Determine the K_I and K_{II} at the new crack length (initiated crack length plus Δc_{pi}) using NN SIF models.

Step 4: Repeat Step 2 and Step 3 until $\Sigma \Delta c_{pi}$ equals or is larger than the asphalt layer thickness.

Step 5: Sum all the ΔN_{pi} to obtain N_p.

31

After the determination of monthly N_p, the monthly N_f is obtained by adding monthly N_p and N_i together. Then the fatigue damage and fatigue area at the given month can be calculated by Equation 3-16 and 3-17.

When the traffic input is load spectrum, the ΔN_{pi} has to be calculated separately for each axle load level and each axle type. More details are discussed in Chapter 4: Methodology for Incorporating Axle Load Spectrum.

3.2.3 Preliminary Calibration of Asphalt Layer Fatigue Cracking Model

The researchers used measured fatigue cracking data from the seven test sections of the 2006 test cycle at the NCAT Test Track to preliminarily calibrate this asphalt fatigue cracking model. Then the calibrated model was further validated using the fatigue cracking data of two test sections of the 2003 test cycle at the NCAT Test Track. The final values of the calibration factors k_b and k_s are k_b=2 and k_s=4. It is obvious that further calibration and validation are needed, especially for Texas materials and environmental conditions.

3.3 IMPLEMENTATION OF GRANULAR BASE/SUBGRADE RUTTING MODEL

After reviewing all existing rutting models for unbound materials, Project 0-5798 (Zhou et al. 2010) identified that the VESYS layer rutting model presented in Equation 3-1 is also a good candidate for unbound materials, as shown in Equations 3-19 and 3-20.

$$RD_{granularba\,se} = k_{granularba\,se} \int \Delta U \mu N^{-\alpha}$$
(3-19)

$$RD_{subgrade} = k_{subgrade} \int \Delta U \mu N^{-\alpha}$$
(3-20)

where
$RD_{granularbase}$ and $RD_{subgrade}$ = rut depth of granular base and subgrade, respectively.
$k_{granularbase}$ and $k_{subgrade}$ = calibration factors.

The general implementation of the granular base/subgrade rutting model is similar to that of the AC layer rutting model. One major difference between the AC layer rutting model and the granular base/subgrade layer rutting model is that the moisture impact on layer modulus is considered for these unbound materials.

The following discusses the implementation of the moisture impact model and the preliminary calibration of the granular base/subgrade rutting model.

3.3.1 Moisture Impact on M_r

Seven granular bases have been tested by Dr. Nazarian's UTEP group (Navarro et al. 2012). As shown below in Figure 3-5 (Navarro et al. 2012), MEPDG *Mr* ratio model (Equation 3-21) fits

better for Texas material. After reviewing the test results, the PMC members and research team agreed to use Equation 3-19 to adjust impact of moisture on Mr.

$$\log \frac{M_r}{M_{ropt}} = a + \frac{b-a}{1+e^{(\ln\frac{-b}{a}+K_s(S-S_{opt}))}}$$

(3-21)

where

M_r	=	representative resilient modulus at a degree of saturation S.
M_{ropt}	=	representative resilient modulus at the optimum moisture content, (in decimals).
S	=	degree of saturation.
S_{opt}	=	degree of saturation at the optimum moisture content.
a, b, and k_S	=	regression parameters listed in Table 3-2.
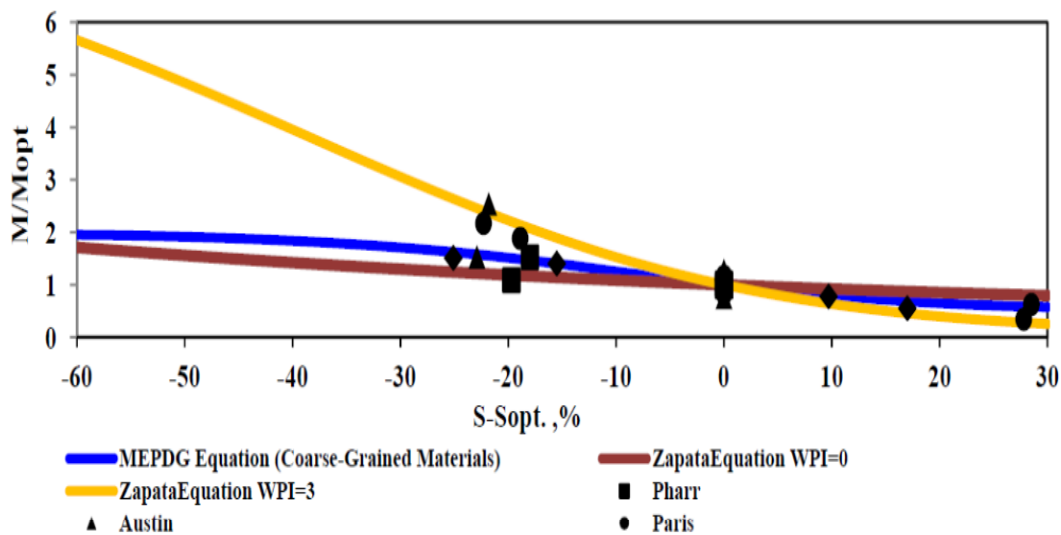
Figure 3-5. Variations of Normalized Representative Modulus with Degree of Saturation.

Table 3-2. Regression Parameters Proposed by MEPDG.

Type of Material	a	b	k_S
Coarse-Grained	−0.3123	0.3010	6.8157
Fine-Grained	−0.5934	0.3979	6.1324

3.3.2 Implementation of Moisture Impact Model

Notice that in Equation 3-21, S_{opt} is a material property, which can be calculated by the following equation (NCHRP 2004):

$$S_{opt} = \frac{\dfrac{w_{opt}\,\gamma_{d\,max}}{\gamma_{water}}}{1 - \dfrac{\gamma_{d\,max}}{\gamma_{water}\,G_s}} \tag{3-22}$$

where

w_{opt}	=	optimum gravimetric moisture content.
γ_{dmax}	=	maximum dry density of the unbound material.
γ_{water}	=	unit weight of the water (in consistent units of γ_{dmax}).
G_s	=	specific gravity of the unbound material.

The properties G_s, w_{opt}, and γ_{dmax} can be directly measured using AASHTO T100 (AASHTO 2010a), T180 (AASHTO 2004) for base layers, and T99 (AASHTO 2010b) for other layers. Thus the only unknown parameter in Equation 3-21 is degree of saturation S, which depends on the moisture content of the base or subgrade layer.

Figure 3-6 illustrates the moisture-related input and output. In this figure, the left side shows the TxME user inputs such as depth of water table values, M_{ropt}, G_s, w_{opt}, and γ_{dmax}. After processing, these data are transferred into the Enhanced Integrated Climatic Model (EICM), and the EICM output is shown in the right side of the Figure 3-6, which includes the sublayer number, sublayer thickness, and sublayer volumetric moisture content, for each month.

Figure 3-6. Moisture Related Input and Output.
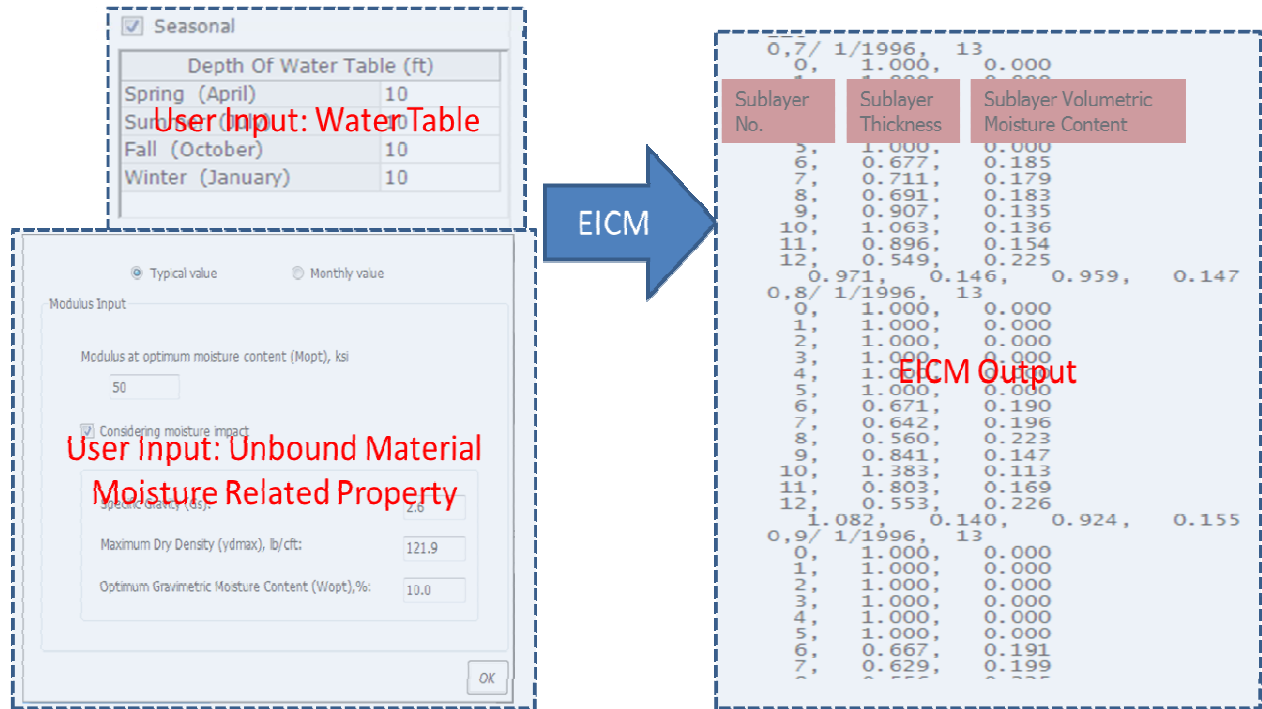
Based on the EICM output, TxME determined the monthly average volumetric moisture content θ for each layer (granular base layer or subgrade layer). Then the monthly degree of saturation S is determined by the following equation:

$$S = \frac{\theta}{w_{opt}} \frac{\gamma_{water}}{\gamma_{d\max}} S_{opt} \qquad (3\text{-}23)$$

where

θ = the volumetric moisture content.

$w_{opt}, \gamma_{dmax}, \gamma_{water},$ and S_{opt} = the same parameters as those defined previously.

After the monthly S value of the base layer or subgrade layer is determined, the monthly modulus Mr can be obtained through Equation 3-21. For the users' convenience, TxME provides three options for Mr of granular base or subgrade:

Option 1: Users input typical Mr value for all seasons and all analysis periods without any adjustment. No information about moisture related properties of granular base or subgrade is needed.

Option 2: Users input M_{ropt}, G_s, w_{opt}, and γ_{dmax} values. Monthly moisture impacted Mr is determined internally by TxME.

Option 3: Users input monthly Mr values directly.

Each option has its pros and cons, depending on the availability of test data.

3.3.3 Preliminary Calibration of Granular Base/Subgrade Rutting Model

The researchers reviewed several Accelerated Pavement Testing (APT) test results and trench studies on a variety of asphalt pavements, such as:

- FHWA-ALF test results at intermediate temperatures.
- FHWA-ALF test results at high temperatures.
- Lake Wales test road results.
- National Center for Asphalt Technology (NCAT) study.
- Rutting study in Alabama.
- TxDOT's trench study on SPS1-US281 sections.
- MnRoad mainline trench study.
- Mississippi (SH302E, SH28E) trench study.
- Cold Regions Research & Engineering Laboratory (CRREL) subgrade test results.

Based on the above information, the researchers made the following recommendations on rutting distribution in an individual layer, as indicated in Table 3-3. The details of these test results and trench studies are summarized in Appendix C.

Table 3-3. Average Rutting Distribution in Individual Layers.

Layer	Surface Treated	Asphalt Layer Thickness			
		1–2 inches	2–4 inches	4–6 inches	>6 inches
Asphalt concrete	0	10	60	80	100
Granular base	60	55	25	15	0
Subgrade	40	35	15	5	0

Using Table 3-3 as a reference, the researchers used TxME to analyze hundreds of rutting cases based on different pavement structures, different pavement type (surface treated, conventional/thin HMA, and perpetual), and different material types. The preliminarily calibrated factors $k_{granular}$ and $k_{subgrade}$ are presented below.

$$k_{granularbase} = 1.0871 + \frac{9.4879}{e^{0.6483*h_{AC}}} \tag{3-24}$$

$$k_{subgrade} = \frac{8.9494}{e^{(4.346+0.2304*h_{AC})}} \tag{3-25}$$

where h_{AC} is the asphalt layer thickness (inches). The calibration factors still need validation or fine tuning by Texas field test section rutting results.

3.4 IMPLEMENTATION OF STABILIZED BASE FATIGUE CRACKING MODEL

Accurate characterization of the fatigue behavior of stabilized mixtures is a very complex technical issue. The fact that fatigue cracking in the material layer is not directly observed in the pavement surface further complicated the situation. Similar to the AC fatigue cracking model, the stabilized base fatigue cracking model implemented in the TxME includes three components as well: 1) Equation 3-26 the fatigue life model, 2) Equation 3-27 the fatigue damage model, and 3) Equation 3-28 the fatigue area model. Notice that the fatigue life model is the same as that in MEPDG (NCHRP 2004).

$$N_{f-SB} = 10^{\frac{k_1 B_1 - \left(\frac{\sigma_t}{M_R}\right)}{k_2 B_2}} \tag{3-26}$$

$$D = \sum \frac{N}{N_{f-SB}} \tag{3-27}$$

$$fatigued\_area(\%) = \frac{100}{1+e^{C\log D}} \tag{3-28}$$

where

$N_{f\text{-}SB}$ =   fatigue cracking life (number of load repetitions) of the stabilized layer.

σ_t =   maximum traffic-induced tensile stress at the bottom of the stabilized layer, psi.

M_R =   28-day modulus of rupture (Flexural Strength), psi.

k_1, k_2 =   calibration factors.

B_1, B_2 =   stabilized layer fatigue cracking properties.

C =   field calibration factors.

N =   applied load repetitions.

D =   accumulated fatigue damage.

In TxME, stabilized base layer fatigue cracking analysis is needed only if 1) the pavement type is surface treated or conventional/thin HMA, and 2) the stabilized layer lies directly underneath the HMA/surface treated layers. If a crack relief layer (e.g., unbound granular base/subbase layer) is placed between the HMA and stabilized layer, pavement failure by fatigue cracking of the stabilized layer is presumed implausible.

The implementation of the stabilized base fatigue cracking model is similar to that of the AC fatigue cracking model after the monthly $N_{f\text{-}SB}$ is determined. The following provides more details about the determination of monthly $N_{f\text{-}SB}$ and model calibration issues.

3.4.1 Determination of Monthly $N_{f\text{-}SB}$

In Equation 3-26, only the monthly maximum tensile stress σ_t at the bottom of the stabilized layer needs to be determined in the TxME; the other parameters are from users' input. Figure 3-7 shows the schematic of σ_t determination. As mentioned previously, an MLET solution is used to determine the displacement, stress, and strain at any point (X, Y, Z) in the pavement. Since the fatigue cracking can happen in both X and Y directions, the stresses σ_{XX} and σ_{YY} were compared and the larger one is used as σ_t.
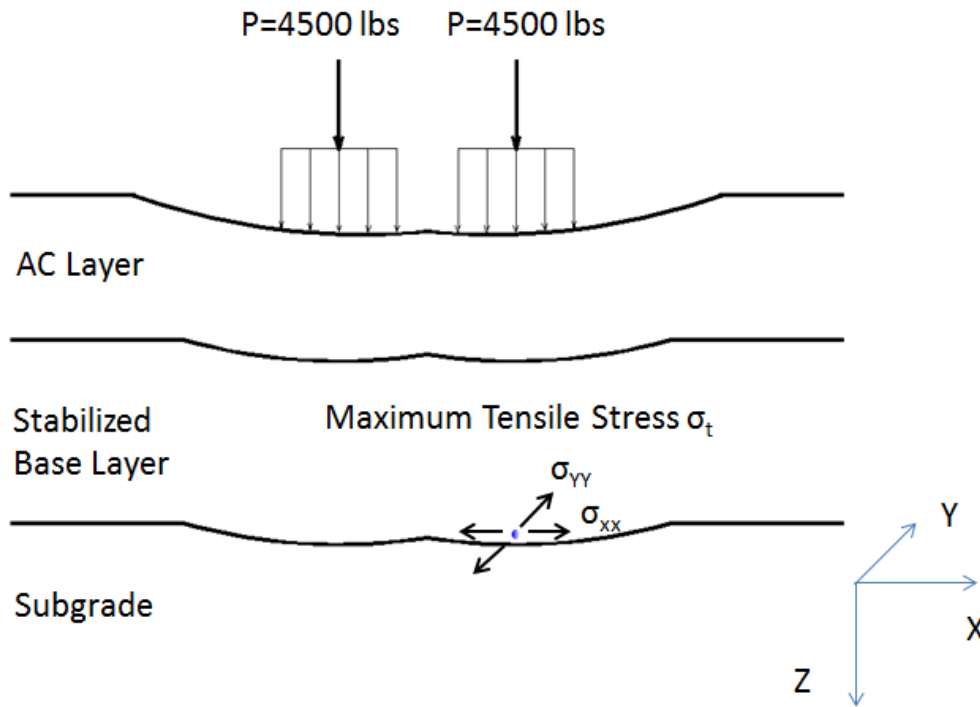
Figure 3-7. Schematic of σ_t Determination.

After the monthly maximum tensile stress σ_t is calculated, the monthly $N_{f\text{-}SB}$ can be easily determined by Equation 3-26. Note that when the traffic input is load spectrum, the $N_{f\text{-}SB}$ has to be calculated separately for each axle load level and each axle type. More details are discussed in Chapter 4: Methodology for Incorporating Axle Load Spectrum.

3.4.2 Stabilized Base Fatigue Cracking Model Calibration and Issues

In MEPDG the stabilized base fatigue cracking has not been field calibrated due to the complexity and requirements of field section design input and performance data. As a result, the field calibration factors, k1 and k2 are both defined to be 1.0. In a recently completed research study, Dr. Jacob Uzan calibrated these two models using the accelerated pavement test data from an earlier PCA study (Scullion et al. 2006). He developed factors for two materials types: cement treated base and fine-grained soil cement subbase type material. The final calibration factors for these two types of cement treated materials are presented below:

- For cement treated base: k1=1.0645, k2=0.9003.
- For fine-grained soil cement: k1=1.8985, k2=2.5580.

TxME adopted these factors and found this model is very sensitive to layer modulus E and modulus of rupture M_R, since the ratio of σ_t (impacted by the layer modulus E) over M_R has a very big influence on the cracking life $N_{f\text{-}SB}$. One big issue is that when applying this model to

the traffic load spectrum scenario, some heavy axle loads often, if not always, cause the σ_t to be larger than M_R, which leads $N_{f\text{-SB}}$ to be less than 1and the fatigue area to be 100 percent in the first month.

It is envisioned that more research needs to be done in this area. Currently TxDOT is in the process of initiating a new project "Updated Testing Procedure for Long Life Heavy Duty Stabilized Bases." The main objective of the project is to identify or develop new test procedures to better characterize stabilized base materials and to better model the long-term performance. The accomplishments of this project will be incorporated into TxME.

3.5 IMPLEMENTATION OF THERMAL CRACKING MODEL

The proposed thermal cracking model is presented below (Hu et al. 2012a and Hu et al. 2013).

$$\Delta C = kA(\Delta K)^n \qquad (3\text{-}29)$$

$$CA = \frac{100 * B}{e^{0.693147*(\rho/m)^\beta}} \qquad (3\text{-}30)$$

where
ΔC = daily crack length increment in the asphalt concrete pavement layer.
A, n = fracture properties, determined by OT test.
ΔK = stress intensity factor caused by thermal load.
k = calibration factor for daily crack length increment model.
ρ = time point (months) when $\Sigma\Delta C$ equals the asphalt concrete pavement layer thickness.
m = month number.
CA = low temperature cracking amount, ft/mile.
β, B = calibration factors.

In Equation 3-29, the thermal stress intensity factor ΔK is the key parameter that considers the HMA viscoelastic behavior under thermal load. The following provides more details about the determination of the thermal SIF ΔK and preliminary calibration of the model.

3.5.1 Determination of the Thermal SIF ΔK

Theoretically, the thermal SIF ΔK has to be determined by FEM. However, it is not practical to directly incorporate FEM into TxME due to the running time issue. Based on theoretical FEM studies and results (Witczak et al. 2000), a simplified relationship was developed between the thermal SIF and thermal stress due to a cooling cycle, as follows:

$$\Delta K = \sigma(0.45 + 1.99C^{0.56}) \qquad (3\text{-}31)$$

where

C = *the* crack length.

σ = the daily maximum thermal stress due to cooling cycles.

The thermal stress calculating point is at the depth of the crack tip, but far from the crack tip in the horizontal direction. Figure 3-8 (Hu et al. 2009) shows an example of pavement temperature profiles at different depths. To obtain the daily maximum thermal stress σ, the hourly thermal stress $\sigma(t)$ corresponding to the hourly temperature variation has to be determined.
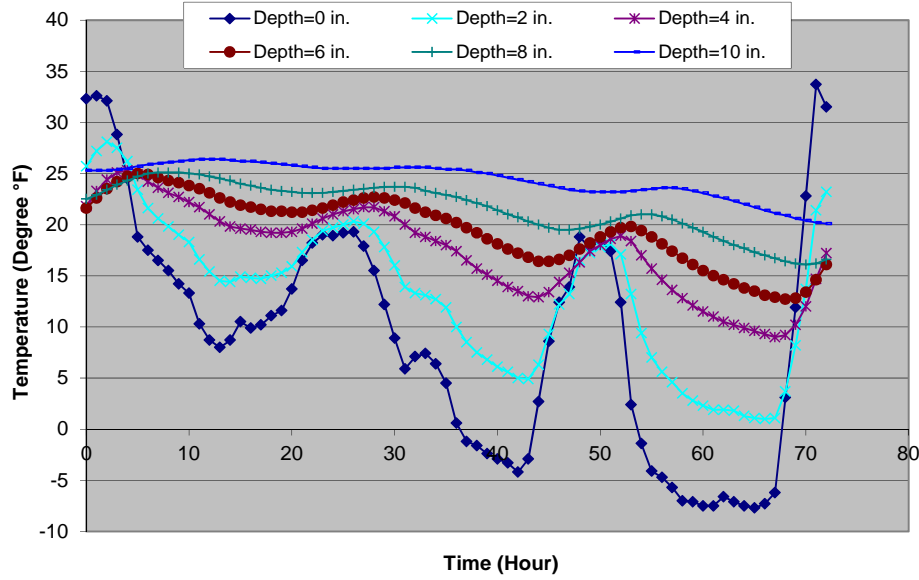
Figure 3-8. An Example of Pavement Temperature Profiles at Different Depths.

Due to the viscoelastic behavior exhibited by HMA under thermal load, $\sigma(t)$ can be determined by the Boltzmann superposition integral:

$$\sigma(t)=\int_{0}^{t} E(t-\tau)\frac{d\varepsilon(\tau)}{d\tau}\,d\tau$$

(3-32)

where

$E(t\text{-}\tau)$ = the relaxation modulus at time $t\text{-}\tau$.

$\varepsilon(\tau)$ = the strain at time τ.

τ = the variable of integration.

Note that the E in Equation 3-32 is the relaxation modulus while in TxME the accepted input is dynamic modulus (or complex modulus); the conversion between them is necessary. Theoretically this conversion can be achieved by the following relationships (Park and Schapery 1999):

$$E'(\varpi) = E_e + \sum_{i=1}^{m} \frac{\varpi^2 \rho_i^2 E_i}{\varpi^2 \rho_i^2 + 1}$$

(3-33)

$$E(t) = E_e + \sum_{i=1}^{m} E_i e^{-(t/\rho_i)}$$

(3-34)

where

ω	=	frequency, Hz.
t	=	time, second.
$E'(\omega)$	=	the real part of complex modulus $E^*(\omega)$.
$E(t)$	=	relaxation modulus.
E_e	=	the equilibrium modulus.
E_i	=	constants representing the relaxation strengths.
ρ_i	=	constants representing the relaxation times.
m	=	number of E_i or ρ_i.

Parameters E_e, E_i, and ρ_i are referred to as Prony coefficients as well. The number m is also called the Prony series mode number. Thus the key of the conversion is to determine these Prony coefficients according to Equation 3-33 based on dynamic modulus data, and then calculate the relaxation modulus based on Equation 3-34. Using numerical methods and the Levenberg-Marquardt algorithm (Levenberg 1944 and Marquardt 1963), the researchers developed a specific tool to accomplish this conversion (Hu et al. 2010a). Figure 3-9 illustrates some results of these conversions at different Prony mode numbers.
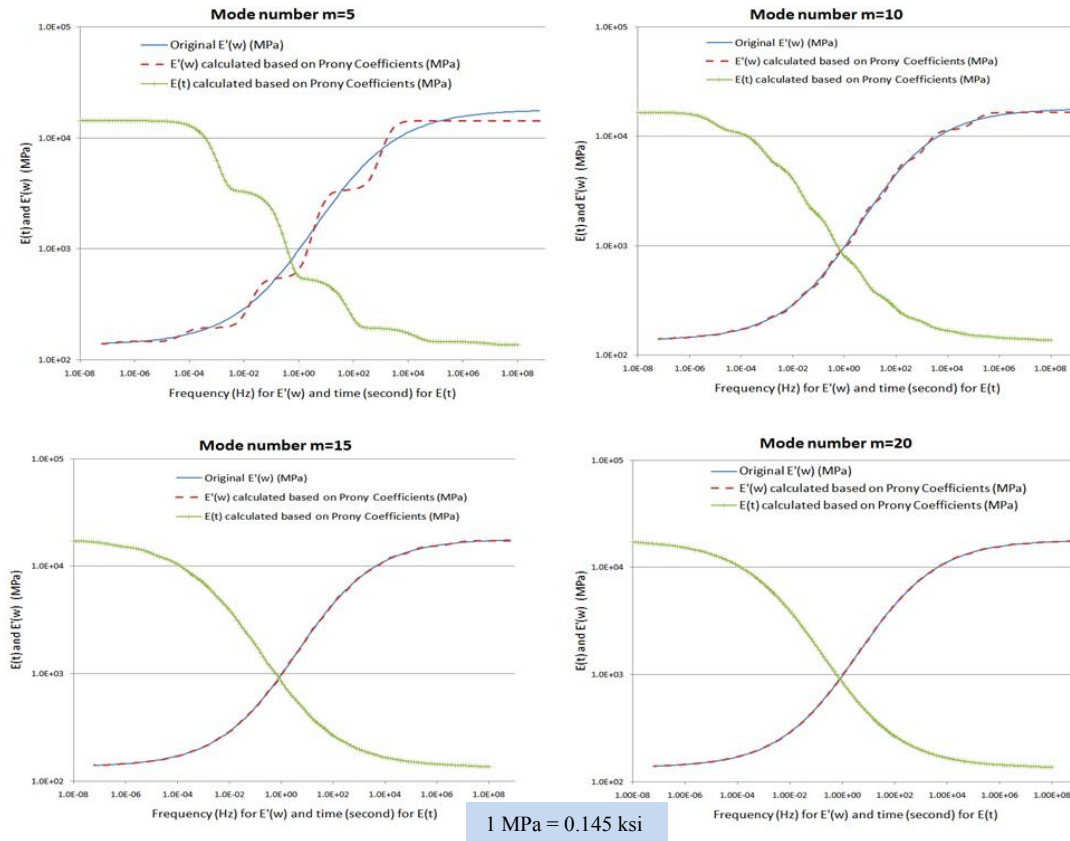
Figure 3-9. Conversions from Dynamic Modulus to Relaxation Modulus at Different Prony Mode Numbers.

This conversion tool has been incorporated into TxME. The preferred mode number *m* is preferred to be larger than 15 to obtain an accurate conversion. With that, the viscoelastic thermal stress $\sigma(t)$ at each hour can be determined according to Equation 3-32, and the daily maximum thermal stress and daily thermal SIF ΔK can be obtained.

3.5.2 Preliminary Calibration of the Thermal Cracking Model

Based on field observation (Witczak et al. 2000), a maximum amount of 400 ft of cracking per 500 ft of pavement, corresponding to a crack frequency of one crack per 15 ft of pavement, was selected as the maximum amount of thermal cracking that would typically develop in a pavement. Thus, the maximum thermal cracking amount CA is 4224 ft/mile, with the assumptions that the pavement lane width is 12 ft and each thermal crack covers the whole lane width.

Therefore the calibration factor B in Equation 3-30 is currently assigned as 42.24, which assures that when thermal crack length equals the pavement layer thickness, the cracking amount CA equals 2112 ft/mile, which is 50 percent of the maximum. Another calibration factor β controls the CA curve shape; see Figure 3-10 (Hu et al. 2013).

42
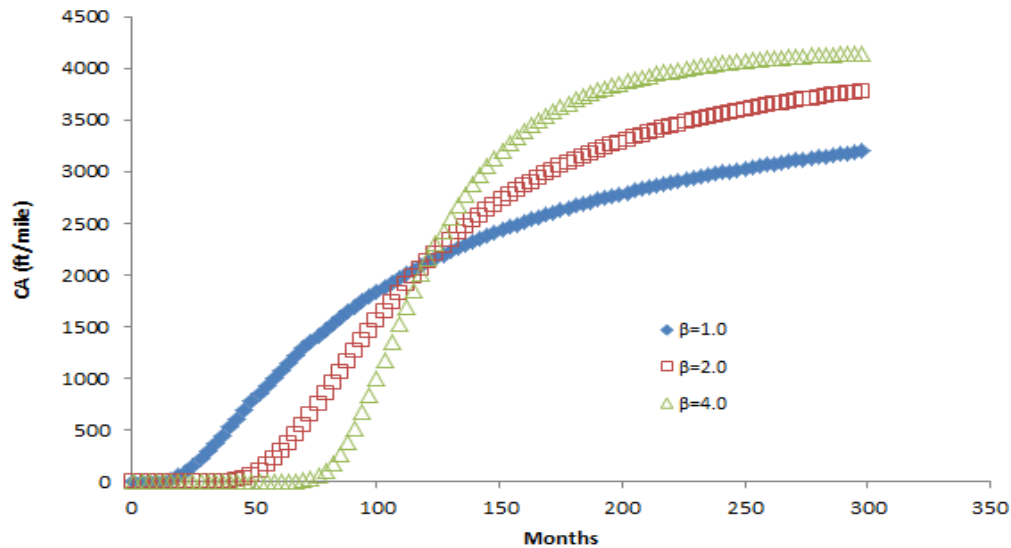
Figure 3-10. Thermal Cracking Amount Curves of Different β.

To calibrate the β value, the observed thermal cracking data for the Lamount test road (Dunn and Gavin 1997) were employed and analyzed. Table 3-4 (Dunn and Gavin 1997) lists the number of thermal cracks observed in the test sections (two lanes, each lane 500 m long).

Table 3-4. Number of Thermal Cracks.

Test Section	1st Year	2nd Year	3rd Year	4th Year	5th Year
1	0	24	60	74	83
2	0	100	120	126	144
4	0	108	128	136	137
5	0	2	13	17	33

Note: Other test section data are ignored since very few cracks were observed.

By interpreting the crack number in terms of cracking amount (ft/mile), and survey period in terms of month, Table 3-5 is obtained.

Table 3-5. Thermal Crack Amount (ft/mile).

Test Section	Months				
	12	24	36	48	60
1	0	460.8	1152	1420.8	1593.6
2	0	1920	2304	2419.2	2764.8
4	0	2073.6	2457.6	2611.2	2630.4
5	0	38.4	249.6	326.4	633.6

43

According to Table 3-5, test section data were fitted using the thermal cracking amount model. The results are presented in Figure 3-11.
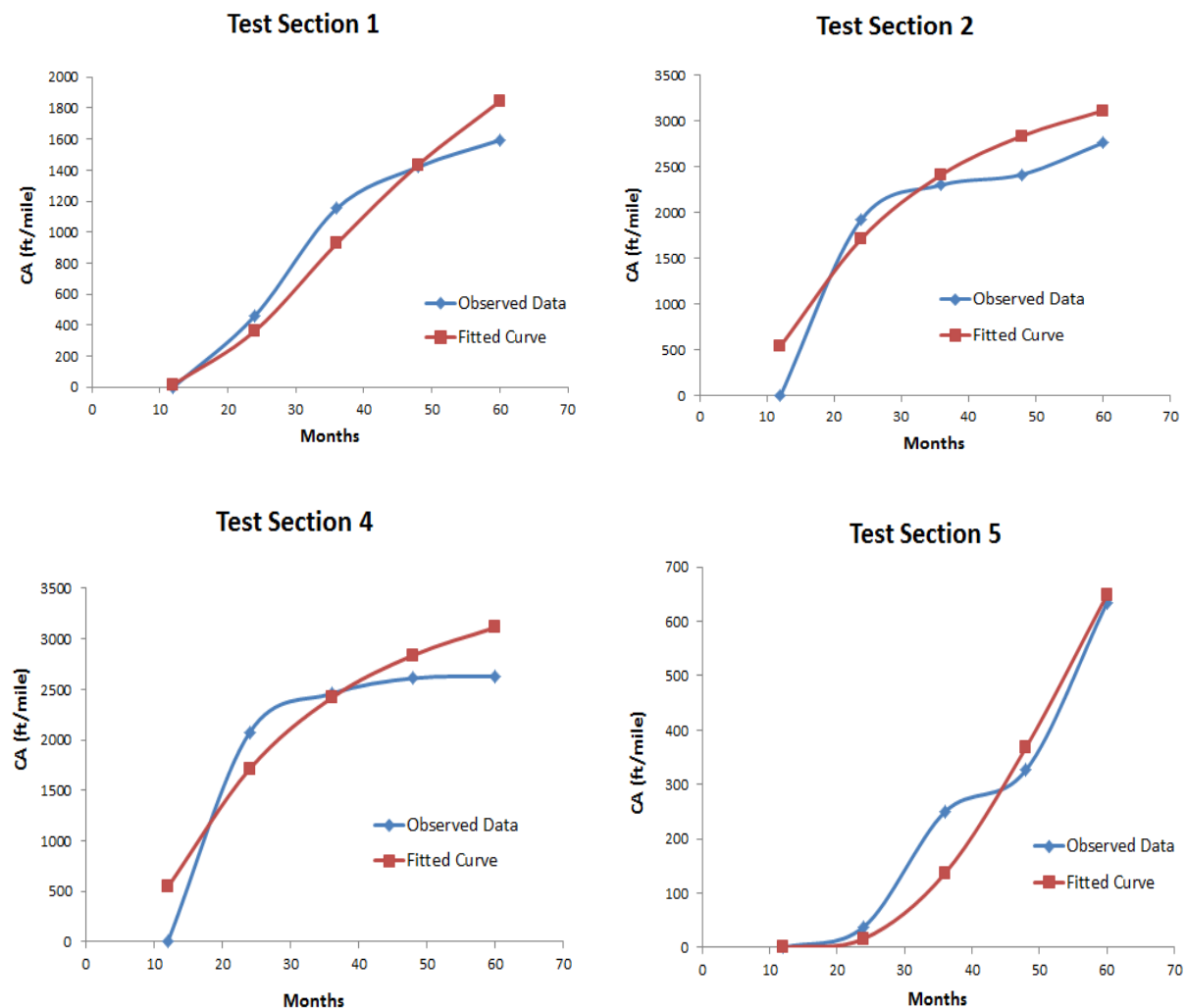
Figure 3-11. Thermal Cracking Amount Model Fitting Curves.

Based on the fitting results, the β value (CA curve shape factor) is preliminary calibrated as 1.185. This factor and other thermal cracking calibration factors need to be further validated and refined based on Texas field data.

3.6 IMPLEMENTATION OF THE ENDURANCE LIMIT MODEL

The concept of an endurance limit is widely recognized in many areas of material science, especially that of metals. However, relatively less work was done for HMA, a typical viscoelastic material. Currently the MEPDG does not fully incorporate the endurance limit concept.

3.6.1 Previous Research Findings of the Pavement Endurance Limit Model

Monismith and McLean (1972) first demonstrated the existence of a fatigue endurance limit below which asphalt mixtures tend to have an extraordinarily long fatigue life, and proposed an endurance limit of 70 $\mu\varepsilon$ for asphalt pavements. The log-log relationship between strain and bending cycles converged below 70 $\mu\varepsilon$ at approximately 5 million cycles (Figure 3-12). Maupin and Freeman (1976) noted a similar convergence. Nunn (1997) in the United Kingdom (UK) and Nishizawa et al. (1997) in Japan proposed concepts for long-life pavements where classical bottom-up fatigue cracking would not occur. Nishizawa et al. (1997) reported an endurance limit of 200 $\mu\varepsilon$ based on the analysis of in-service pavements in Japan. Similarly, strain levels at the bottom of the asphalt layer of between 96 and 158 $\mu\varepsilon$ were calculated based on backcalculated stiffness data from the falling weight deflectometer for a long-life pavement in Kansas (Wu et al. 2004). Other engineers propose that one should limit the strain anywhere from 60 to 100 $\mu\varepsilon$ based on laboratory testing (Romanoschi et al. 2008). Another experimental pavement project in China allowed perpetual pavement design to reach the less conservative value of 125 $\mu\varepsilon$ (Yang et al. 2005).
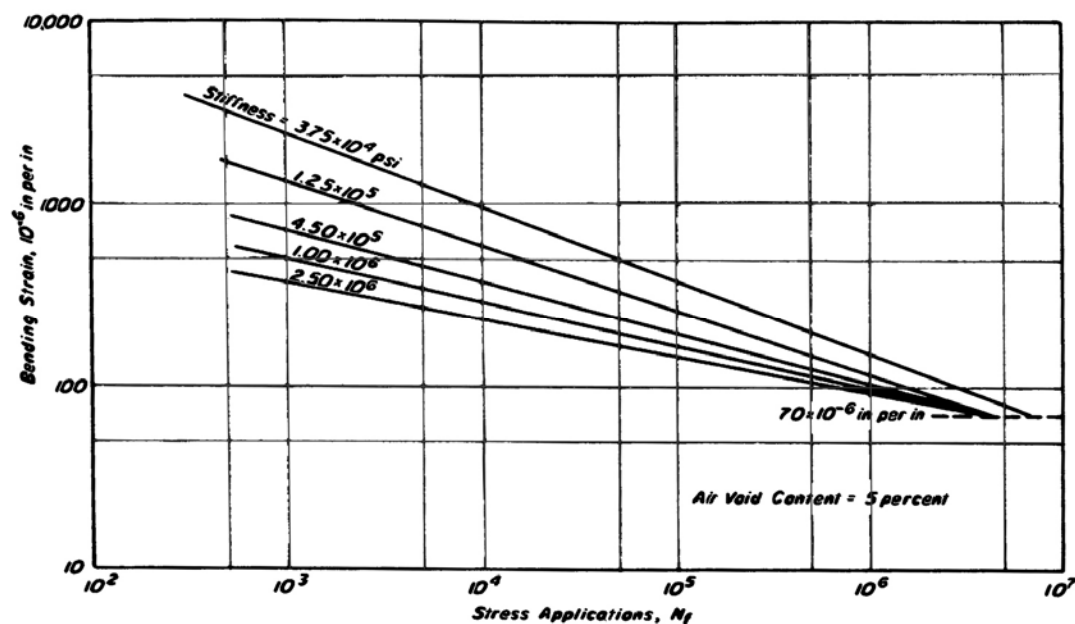
Figure 3-12. Strain vs. Stress Applications to Failure Relationships (Monismith and McLean 1972).

Most recently, NCAT has led a research effort for NCHRP Project 9-38 to investigate the endurance limit for HMA (Prowell et al. 2010). This study involves conducting fatigue tests for a number of mixtures over a wide range of strain levels. Tests requiring up to 50 million cycles to failure were conducted. The Asphalt Institute has also been involved in the portion of the work to test samples having fatigue lives up to 50 million cycles. The primary objectives of that study were to determine if HMA mixtures do have an endurance limit and to provide guidance on

45

determining this limit for various mixture types. The results indicated that HMA mixtures appeared to have an endurance limit that varies with mix type, so there is not just one limit that can be used for all mixes.

Based on measured strains from the NCAT Test Track from sections that have not experienced fatigue cracking (Figure 3-13), Willis (2008) proposed a cumulative frequency distribution of allowable strains for perpetual pavements design; see Table 3-6. Priest (2005) initially proposed a similar concept.
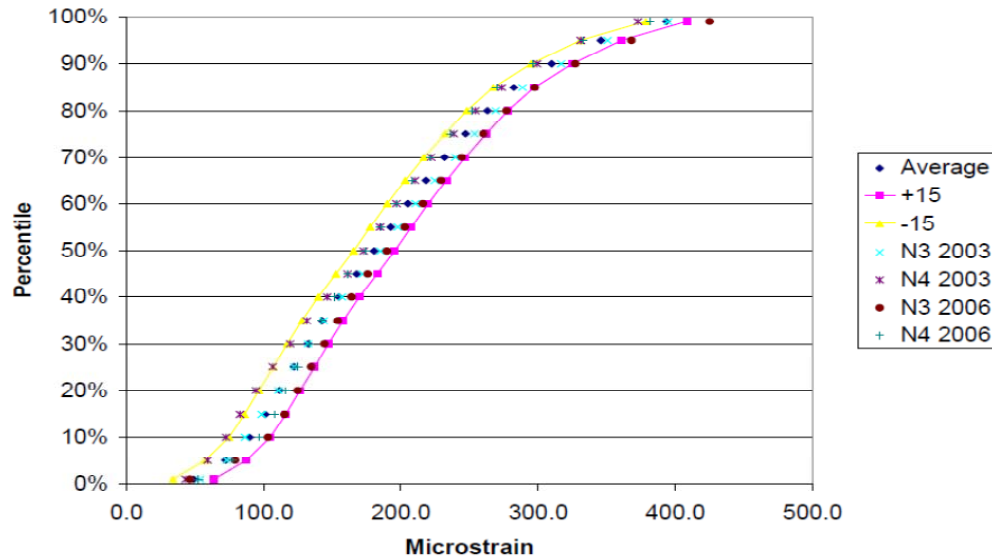
Figure 3-13. Average Strain Distribution with Confidence Bands (Willis 2008).

Table 3-6. Strain Criteria for Perpetual Pavements (Willis 2008).

Percentile	Fatigue Limit
99	394
95	346
90	310
85	282
80	263
75	247
70	232
65	218
60	205
55	193
50	181
45	168
40	155
35	143
30	132
25	122
20	112
15	101
10	90
5	72
1	49

According to the preceding discussion, TxME implements two levels of the endurance limit model: one is for traffic loading inputs in ESALs and the other is for load spectrum input. Only perpetual pavement needs endurance limit analysis. The following discusses the details of model implementation.

3.6.2 TxME Endurance Limit Model Implementation for Traffic ESALs Input

When traffic input is ESALs, the equivalent standard 18 kip axle load is assumed to be applied on the pavement structure. The maximum tensile strain at the bottom of the last asphalt layer is determined and compared to the single endurance limit value. Figure 3-14 shows the schematic of maximum tensile strain determination using the MLET solution. The monthly average temperature profile is used to determine each AC layer modulus. The monthly tensile strains in both X and Y directions, ε_{XX} and ε_{YY}, are calculated and the larger one is used as the monthly tensile strain. The final maximum tensile strain ε_{max} is selected among these monthly tensile strains.
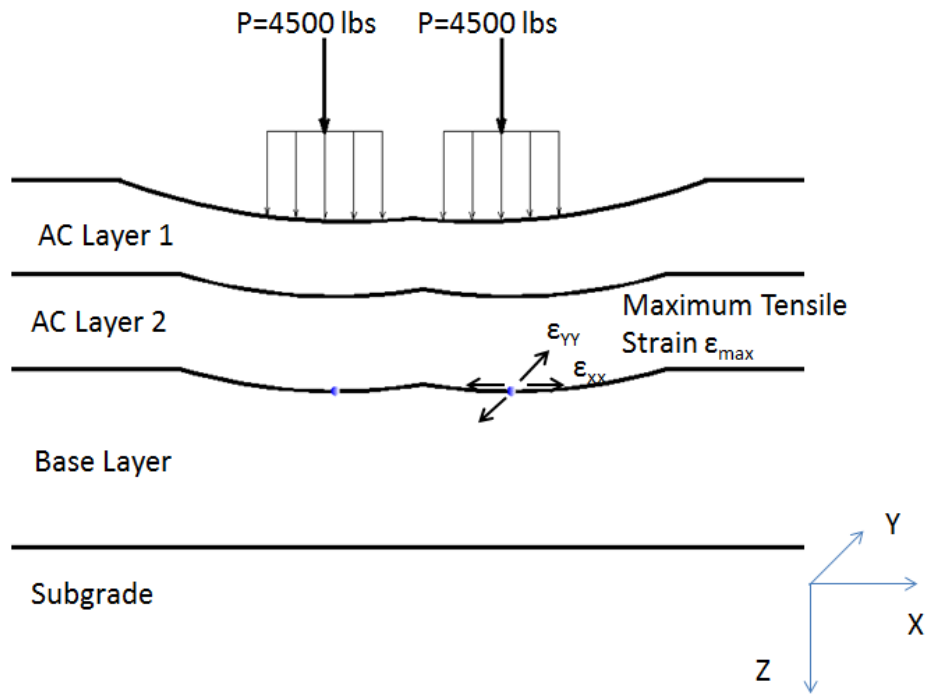
Figure 3-14. Schematic of Maximum of Tensile Strain Determination.

A single endurance limit value EL is assigned for comparison with the maximum tensile strain: if $\varepsilon_{max} < EL$, the pavement is considered to be perpetual; otherwise, it is considered to be non-perpetual. Currently TxME adopts 70 $\mu\varepsilon$ as the default single EL value and this value can be a users' input. Definitely this is a very arbitrary value and further study is needed in this area.

One main objective of the active research NCHRP 9-44A "Validating an Endurance Limit for HMA Pavements: Laboratory Experiment and Algorithm Development" is to further identify the endurance limit as a potential function of mixture composition, binder rheology, pavement temperature, etc. The publication in the NCHRP 9-44A Report series is anticipated in the end of 2013. It is envisioned that the newest findings of NCHRP 9-44A potentially can be used to validate and refine the EL value and calibrations.

3.6.3 TxME Endurance Limit Model Implementation for Axle Load Spectrum

When traffic input is load spectrum, the maximum tensile strain under each axle load is determined; the corresponding strain distribution is evaluated based upon the number of repetitions of each axle load. The following steps describe how the strain distribution curve is determined.

Step 1: Process the load spectrum data into monthly repetition numbers for each axle type (single, tandem, tridem, or quad), and for each load level (3 kips, 4 kips, 5 kips,…etc.). More details about this step are described in Chapter 4: Methodology for Incorporating Axle Load Spectrum.

48

Step 2: Determine the monthly average pavement temperature profile.

Step 3: Determine each AC layer modulus (monthly) based upon the layer temperature at mid-depth of each HMA layer and loading time (depends on the traffic speed).

Step 4: Determine the monthly maximum tensile strains at the bottom of the last AC layer, for each axle type and each load level.

Step 5: Replicate these strains according to their repetition numbers determined by Step 1. For example, if the monthly repetition number of a single axle with load level 3 kips is 200, and the maximum strain of that is 0.5, then 0.5 should be replicated 200 times.

Step 6: Sort all these strains and divide them into groups (bins). For each group, use the median strain value as the representative strain.

Step 7: Count the strain numbers of each group and calculate the frequencies of each representative strain.

Step 8: Accumulate these frequencies and obtain the strain distribution curve.

As a reference to compare the TxME determined strain distribution curve against, a pre-defined strain distribution limit has to be provided. Currently TxME adopts the strain criteria listed in Table 3-6 as the strain distribution limit.

Figure 3-15 shows an example generated by TxME. Note that if the predicted strain distribution curve is to the left side of the strain distribution limit curve, the pavement is deemed as perpetual; otherwise the pavement is non-perpetual. Again, this model has not been calibrated and further study is defnitely needed in this area.
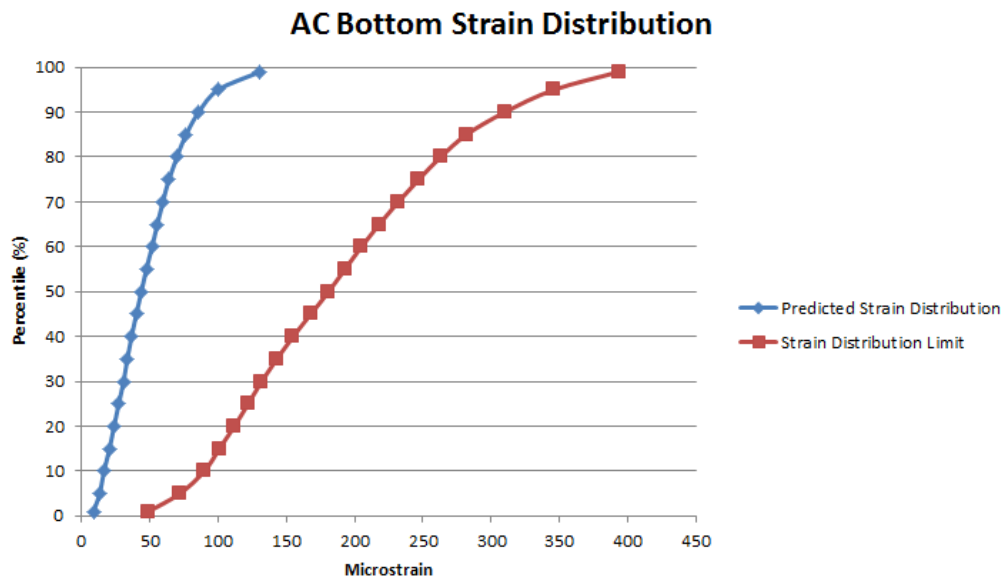
Figure 3-15. Example of Endurance Limit Output for Axle Load Spectrum Input.

CHAPTER 4.
METHODOLOGY FOR INCORPORATING AXLE LOAD SPECTRUM
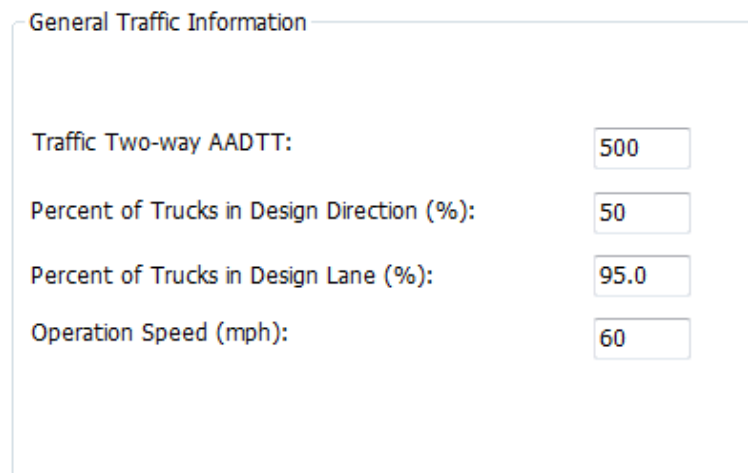
Traffic data is one of the key data elements required for the pavement structural design/analysis. Axle load spectrum input provides the opportunity of evaluating the pavement response under the real traffic loads throughout the pavement design life. This chapter describes the methodology for incorporating axle load spectrum into the TxME, which includes how to determine the monthly axle applications and how to apply these axle applications in performance predictions. The discussed load spectrum related performance measures are AC fatigue cracking, rutting (AC rutting, granular base/subgrade rutting), and stabilized fatigue cracking.

4.1 DETERMINATION OF MONTHLY AXLE APPLICATIONS

To determine monthly axle applications, three types of data are required for load spectrum inputs: 1) basic traffic volume information, 2) traffic volume adjustment factors, and 3) axle load information. These inputs in the TxME are generally consistent with MEPDG load spectrum inputs (NCHRP 2004). The details about these inputs and corresponding calculations are described below.

4.1.1 Basic Traffic Volume Information

Figure 4-1 shows the basic traffic volume information inputs in the TxME.

Figure 4-1. Basic Traffic Volume Information Inputs.

Two-Way Annual Average Daily Truck Traffic (AADTT)

Two-way AADTT is the total volume of truck traffic (the total number of heavy vehicles [classes 4 to 13] in the traffic stream) passing a point or segment of a road facility to be designed, during a 24-hour period.

Percent of Trucks in Design Direction (%)

Percent trucks in the design direction, or the directional distribution factor (DDF), is used to quantify any difference in the overall volume of trucks in each direction.

Percent of Trucks in Design Lane (%)

Percent trucks in the design lane, or truck lane distribution factor (LDF), accounts for the distribution of truck traffic between the lanes in one direction. For two-lane, two-way highways (one lane in one direction), this factor is 1.0 because all truck traffic in any one direction must use the same lane. For multiple lanes in one direction, it depends on the AADTT and other geometric and site-specific conditions.

Thus, the Daily Total Truck Numbers in the Design Lane for the first month of the first year, denoted by $DTTN_1$, can be calculated using the following equation:

$$DTTN_1 = AADTT*DDF*LDF \tag{4-1}$$

4.1.2 Traffic Volume Adjustment Factors

Traffic volume adjustment factors include vehicle class distribution factors, traffic growth factors, and monthly adjustment factors.

Vehicle Class Distribution Factors

Vehicle class distribution factors are the pecentages of each type of truck within the total truck volume. The class distribution factors for truck class k is denoted by CDF_k.

Traffic Growth Factors

Traffic growth factors are the yearly growth rates for each truck class. The growth function can be either linear growth or compound growth. Figure 4-2 shows an example of the vehicle class distribution factors and the growth rates in the TxME. The growth rate for the truck class k is denoted by GR_k.
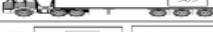
Figure 4-2. Vehicle Class Distribution Factors and Growth Rates.

Monthly Adjustment Factors

Truck traffic monthly adjustment factors (MAF) simply represent the proportion of the annual truck traffic for a given truck class that occurs in a specific month. In other words, the monthly distribution factor for a specific month is equal to the monthly truck traffic for the given class for the month divided by the total truck traffic for that truck class for the entire year. Truck traffic monthly adjustment factors depend on factors such as adjacent land use, the location of industries in the area, and roadway location (urban or rural). For each truck class, the sum of the MAF of all months must equal 12.

Pavement designs can be sensitive to MAF. If no information is available, it is recommended that designers assume an even or equal distribution (i.e., 1.0 for all months for all vehicle classes) as shown in Table 4-1.

The mth monthly adjusting factor for truck class k is denoted by $MAF_{k,m}$.

Table 4-1. Monthly Adjustment Factors for Each Truck Class.

Month	Truck Classification									
	4	5	6	7	8	9	10	11	12	13
January	1	1	1	1	1	1	1	1	1	1
February	1	1	1	1	1	1	1	1	1	1
March	1	1	1	1	1	1	1	1	1	1
April	1	1	1	1	1	1	1	1	1	1
May	1	1	1	1	1	1	1	1	1	1
June	1	1	1	1	1	1	1	1	1	1
July	1	1	1	1	1	1	1	1	1	1
August	1	1	1	1	1	1	1	1	1	1
September	1	1	1	1	1	1	1	1	1	1
October	1	1	1	1	1	1	1	1	1	1
November	1	1	1	1	1	1	1	1	1	1
December	1	1	1	1	1	1	1	1	1	1

Based on these traffic volume adjustment factors, $MTTN_{y,m,k}$, the Monthly Total Truck Numbers of Design Lane for the yth year, m^{th} month, and truck class k, can be determined by the equations below.

For compound growth,

$$MTTN_{y,m,k}=DTTN_1*(No\ of\ Days)_m*CDF_k*(1+GR_k)^{y-1}*MAF_{m,k} \qquad (4\text{-}2)$$

For linear growth,

$$MTTN_{y,m,k}=DTTN_1**(No\ of\ Days)_m*CDF_k*[1+(y\text{-}1)*GR_k]\ *MAF_{m,k} \qquad (4\text{-}3)$$

4.1.3 Axle Load Information

Axle load information includes axle configurations, number of axles per truck, and axle load distribution factors.

Axle Configuration

Figure 4-3 shows the axle configuration information, such as tire pressure, tire spacing, and axle spacing, etc. These data are needed when using MLET evaluations to determine pavement responses under different axle loads.

Figure 4-3. Axle Configuration Information.

Number of Axles per Truck

This input represents the average number of axles for each truck class (classes 4 to 13) for each axle type (single , tandem, tridem, and quad). Currently, TxME adopted the MEPDG-suggested default values, which are listed in Table 4-2. Additionally, TxME allows for dividing the single axle category into steering single axle (single tire) and other single axle (dual tire). The default values need to be further refined based on Texas traffic data.

Table 4-2. Default Values for Each Axle Type per Truck Class.

Truck Classification	Number of Steering Axles per Truck	Number of Other Single Axles per Truck	Number of Tandem Axles per Truck	Number of Tridem Axles per Truck	Number of Quad Axles per Truck
4	0.00	1.62	0.39	0.00	0.00
5	0.00	2.00	0.00	0.00	0.00
6	0.00	1.02	0.99	0.00	0.00
7	0.00	1.00	0.26	0.83	0.00
8	0.00	2.38	0.67	0.00	0.00
9	0.00	1.13	1.93	0.00	0.00
10	0.00	1.19	1.09	0.89	0.00
11	0.00	4.29	0.26	0.06	0.00
12	0.00	3.52	1.14	0.06	0.00
13	0.00	2.15	2.13	0.35	0.00

Note: The number of quad axles per truck class is 0.00, because there were too few counted in the LTPP traffic database.

Using $NA_{k,\ axletype}$ (*axletype* can be *Steering Single*, *Other Single*, *Tandem, Tridem,* or *Quad*) to represent the Number of Axles for truck class *k* and specific axle type, the Monthly Axle Number can be determined as follows:

$$MAN_{y,m,k,axletype}=MTTN_{y,m,k} * NA_{k,\ axletype} \tag{4-4}$$

where

$MAN_{y,m,k,axletype}$ = the Monthly Axle Number in the design lane for the yth year, m^{th} month, truck class *k*, and specific axle type.

MTTN = the Monthly Total Truck Number, determined by Equation 4-2 or 4-3.

Axle Load Distribution Factors

The axle load distribution factors simply represent the percentage of the total axle applications within each load interval for a specific axle type (single, tandem, tridem, and quad) and vehicle class (classes 4 through 13). A definition of load intervals for each axle type is provided below:

- Single (Steering Single or Other Single) – 3,000 lb. to 40,000 lb. at 1,000-lb intervals.
- Tandem – 6,000 lb. to 80,000 lb. at 2,000-lb intervals.
- Tridem and Quad – 12,000 lb. to 102,000 lb. at 3,000-lb intervals.

Table 4-3 shows an example of tandem axle load distribution factors (NCHRP 2004). Note that these factors might be different for each month. The Axle Load Distribution Factor for m^{th} month, truck class k, specific axle type, and load group g is denoted by $ALDF_{m, k, axletype, g}$.

Table 4-3. Tandem Axle Load Distribution Factors for Each Truck Class.

Load Group	Axle Load (lb.)	Truck Classification									
		4	5	6	7	8	9	10	11	12	13
1	6000	5.88	7.06	5.28	13.74	18.95	2.78	2.45	7.93	5.23	6.41
2	8000	1.44	35.42	8.42	6.71	8.05	3.92	2.19	3.15	1.75	3.85
3	10000	1.94	13.23	10.81	6.49	11.15	6.51	3.65	5.21	3.35	5.58
4	12000	2.73	6.32	8.99	3.46	11.92	7.61	5.4	8.24	5.89	5.66
5	14000	3.63	4.33	7.71	7.06	10.51	7.74	6.9	8.88	8.72	5.73
6	16000	4.96	5.09	7.5	4.83	8.25	7	7.51	8.45	8.37	5.53
7	18000	7.95	5.05	6.76	4.97	6.77	5.82	6.99	7.08	9.76	4.9
8	20000	11.58	4.39	6.06	4.58	5.32	5.59	6.61	5.49	10.85	4.54
9	22000	14.2	2.31	5.71	4.26	4.13	5.16	6.26	5.14	10.78	6.45
10	24000	13.14	2.28	5.17	3.85	3.12	5.05	5.95	5.99	7.24	4.77
11	26000	10.75	1.53	4.52	3.44	2.34	5.28	6.16	5.73	6.14	4.34
12	28000	7.47	1.96	3.96	6.06	1.82	5.53	6.54	4.37	4.93	5.63
13	30000	5.08	1.89	3.21	3.68	1.58	6.13	6.24	6.57	3.93	7.24
14	32000	3.12	2.19	3.91	2.98	1.2	6.34	5.92	4.61	3.09	4.69
15	34000	1.87	1.74	2.12	2.89	1.05	5.67	4.99	4.48	2.74	4.51
16	36000	1.3	1.78	1.74	2.54	0.94	4.46	3.63	2.91	1.73	3.93
17	38000	0.76	1.67	1.44	2.66	0.56	3.16	2.79	1.83	1.32	4.2
18	40000	0.53	0.38	1.26	2.5	0.64	2.13	2.24	1.12	1.07	3.22
19	42000	0.52	0.36	1.01	1.57	0.28	1.41	1.69	0.84	0.58	2.28
20	44000	0.3	0.19	0.83	1.53	0.28	0.91	1.26	0.68	0.51	1.77
21	46000	0.21	0.13	0.71	2.13	0.41	0.59	1.54	0.32	0.43	1.23
22	48000	0.18	0.13	0.63	1.89	0.2	0.39	0.73	0.21	0.22	0.85
23	50000	0.11	0.14	0.49	1.17	0.14	0.26	0.57	0.21	0.22	0.64
24	52000	0.06	0.2	0.39	1.07	0.11	0.17	0.4	0.07	0.23	0.39
25	54000	0.04	0.06	0.32	0.87	0.06	0.11	0.38	0.13	0.2	0.6
26	56000	0.08	0.06	0.26	0.81	0.05	0.08	0.25	0.15	0.12	0.26
27	58000	0.01	0.02	0.19	0.47	0.03	0.05	0.16	0.09	0.07	0.18
28	60000	0.02	0.02	0.17	0.49	0.02	0.03	0.15	0.03	0.19	0.08
29	62000	0.1	0.01	0.13	0.38	0.06	0.02	0.09	0.06	0.09	0.14
30	64000	0.01	0.01	0.08	0.24	0.02	0.02	0.08	0.01	0.04	0.07
31	66000	0.02	0.01	0.06	0.15	0.02	0.02	0.06	0.01	0.02	0.08
32	68000	0.01	0	0.07	0.16	0	0.02	0.05	0.01	0.04	0.03
33	70000	0.01	0.02	0.04	0.06	0	0.01	0.11	0	0.12	0.01
34	72000	0	0.01	0.04	0.13	0	0.01	0.04	0	0.01	0.04
35	74000	0	0	0.02	0.06	0	0.01	0.01	0	0.01	0.02
36	76000	0	0	0.01	0.06	0	0	0.01	0	0.01	0.04
37	78000	0	0	0	0.02	0	0	0.01	0	0.01	0.02
38	80000	0	0	0	0.02	0	0	0	0	0	0.08
39	82000	0	0	0	0	0	0	0	0	0	0

4.1.4 Calculation of Monthly Axle Applications for Each Axle Type and Load Group

Based on previous equations, $N_{g, y, m, k, axletype}$, the monthly axle applications of yth year, m^{th} month, truck class k, axle type (*Steering Single*, *Other Single*, *Tandem, Tridem,* or *Quad*), and load group g, can be determined by the following equation:

$$N_{g, y, m, k, axletype} = MAN_{y, m, k, axletype} * ALDF_{k, m, axletype, g} \tag{4-5}$$

where
$ALDF$ =   the Axle Load Distribution Factor.
MAN =   the Monthly Axle Number.

The axle applications for each axle type are then summed for all truck classes to obtain the total number of axle applications within each time increment (the yth year and m^{th} month), axle type, and load group g, as follows:

$$N_{g,y,m,axletype} = \sum_{k=4}^{13} N_{g,y,m,k,axletype} \tag{4-6}$$

where $N_{g, y, m, axletype}$ is the monthly axle applications for each axle type and each load group that will be used in all the load spectrum based performance predictions.

4.2 LOAD SPECTRUM-BASED AC FATIGUE CRACKING

AC fatigue cracking model in the TxME considers both crack initiation and crack propagation. The crack initiation life depends on the AC bottom tensile strain, and the crack propagation life depends on the stress intensity factor. These pavement responses have to be determined for each axle type and each axle load level throughout the design period. The method for treating multiple axles in crack initiation is different from that in crack propagation. The details are discussed below.

4.2.1 Method for Treating Multiple Axles in Crack Initiation

Equation 3-12 shows that to determine the crack initiation life, the maximum AC bottom tensile strains under the multiple axles have to be analyzed. Figure 4-4 (Zhao et al. 2012) shows the examples of tensile strain comparisons between single axle and tridem axle. Note that sometimes the maximum tensile strain of multiple axles is even smaller than that of the single axle, as shown in Figure 4-4b.

(a)   (b)
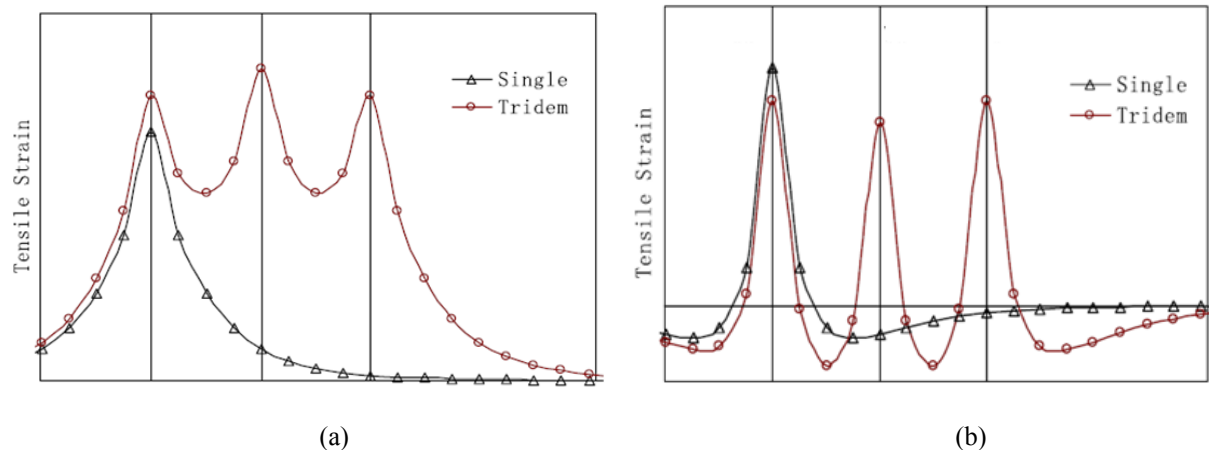
**Figure 4-4. Tensile Strain Comparisons between Single and Tridem Axle Load
(Zhao et al. 2012).**

As Huang (2004) stated, "Due to the large spacing between two axles, the critical tensile and
compressive strains under multiple axles are only slightly different from those under a single axle.
If one passage of each set of multiple axles is assumed to be one repetition, the damage caused by
an 80 kN (18 kips) single axle is nearly the same as that caused by a 160 kN (36 kips) tandem axle
or a 240 kN (54 kips) tridem axle; if one passage of a tandem axle is assumed to be two repetitions
and that of the tridem axle to be three repetitions, the damage caused by a 160 kN (36 kips) tandem
and a 240 kN (54 kips) tridem axle are two and three times greater than that by an 80 kN (18 kips)
single axle, respectively. Both assumptions are apparently incorrect."

One approach Huang proposed is demonstrated in Figure 4-5. This figure shows a tandem axle load
and associated tensile strain responses at different locations. Due to symmetry, the strain under the
2nd axle is the same as that of the 1st axle, denoted by ε_1. The strain between 1st and 2nd axle is
denoted by ε_2. The effect of this tandem axle load on fatigue damage and associated crack initiation
is taken into account by using ε_1 for the 1st axle and ε_1-ε_2 for the 2nd axle. In other words, to
determine the crack initiation life, each set of tandem axles is assumed to be two repetitions; and the
maximum strain caused by each repetition is different: the strain caused by the 1st axle is ε_1 and the
strain caused by the 2nd axle is ε_1-ε_2. This method might be appropriate since the AASHTO 1993
Guide (AASHTO 1993) recommended equivalent axle load factor for tandem (36 kip) is 1.38,
which is much larger than 1 but far less than 2.

59
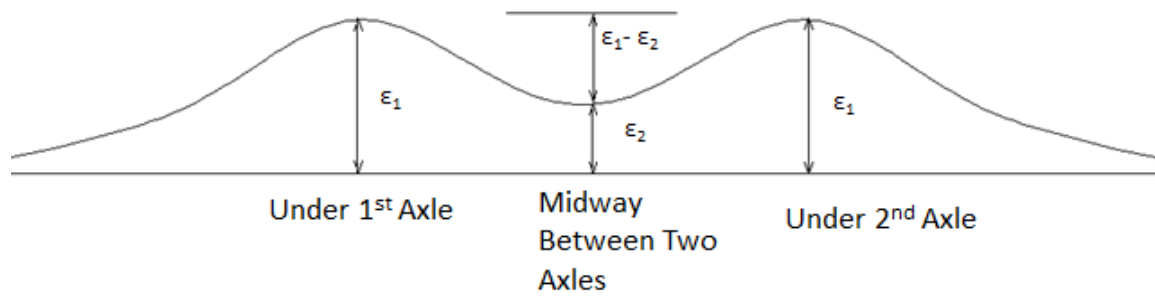
Figure 4-5. AC Bottom Tensile Strain Caused by a Tandem Axle.

Similarly, Figure 4-6 shows a tridem axle load and associated tensile strain responses at different locations. The strains under the 1st axle, midway between the 1st and 2nd axles, and 2nd axle are denoted by ε_1, ε_2, and ε_3, respectively. Due to symmetry, the strain under the 3rd axle is the same as that of the 1st axle, and the strain between the 1st and 2nd axles is the same as that between the 2nd and 3rd axles. Thus the effect of this tridem axle load on fatigue damage and associated crack initiation is taken into account by using ε_1 for the 1st axle, $\varepsilon_3 - \varepsilon_2$ for the 2nd axle, and $\varepsilon_1 - \varepsilon_2$ for the 3rd axle, respectively.
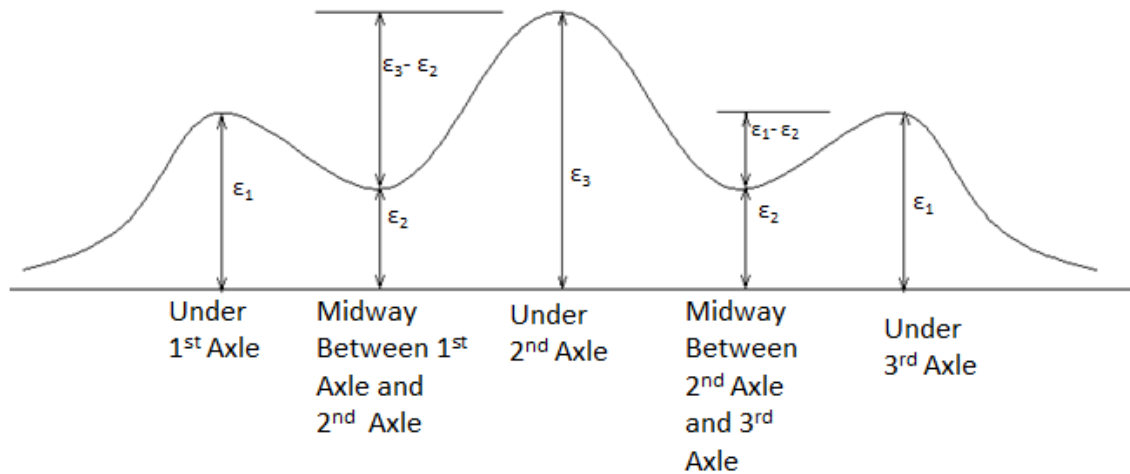
Figure 4-6. AC Bottom Tensile Strain Caused by a Tridem Axle.

Then Figure 4-7 shows a quad axle load and associated tensile strain responses at different locations. The strains under the 1st axle, midway between the 1st and 2nd axles, 2nd axle, and midway between the 2nd and 3rd axles are denoted by ε_1, ε_2, ε_3, and ε_4, respectively. The strains at other locations are also marked in the figure according to the symmetric principle. The effect of this quad axle load on fatigue damage and associated crack initiation is taken into account by using ε_1 for the 1st axle, $\varepsilon_3 - \varepsilon_2$ for the 2nd axle, $\varepsilon_3 - \varepsilon_4$ for the 3rd axle, and $\varepsilon_1 - \varepsilon_2$ for the 4th axle, respectively.
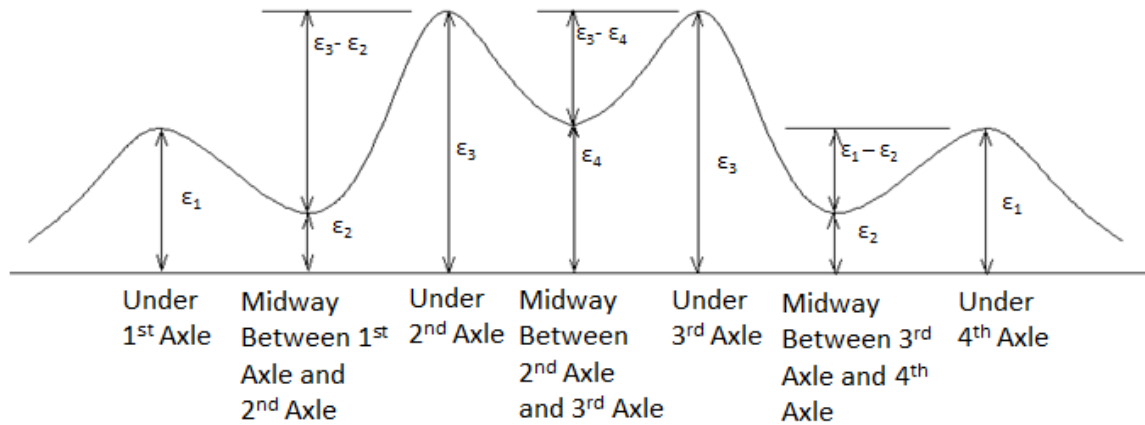
Figure 4-7. AC Bottom Tensile Strain Caused by a Quad Axle.

4.2.2 Method of Treating Multiple Axles for Crack Propagation

To determine the crack propagation life, the stress intensity factors under the multiple axles have to be analyzed. In the stage of crack propagation, a macro-crack in the direction perpendicular to traffic exists and ideally propagates in the vertical direction toward the pavement surface. Thus the method of treating multiple axles for crack initiation may not be applicable to crack propagation because of the existence of a macro-crack.

The main contributions to the crack propagation are from the SIF K_I and K_{II} in the traffic direction. As an example, a pavement structure consisting of two HMA layers, a base layer, and the subgrade was used for investigating the K_I and K_{II} values corresponding to different crack lengths under a moving tridem-axle load passing over a crack. Figure 4-8 shows the K_I and K_{II} development at different crack lengths under a 240 kN tridem-axle load with a tire pressure of 100 psi (0.689 MPa). For comparison purposes, the K_I and K_{II} development at different crack lengths (mm) is also presented in this figure.

61
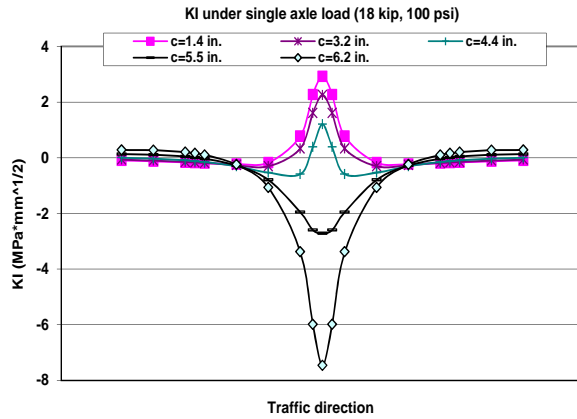
(a) K_I under Single Axle Load   (b) K_I under Tridem Axle Load
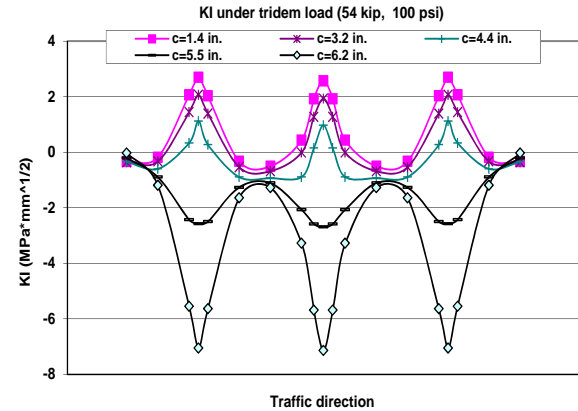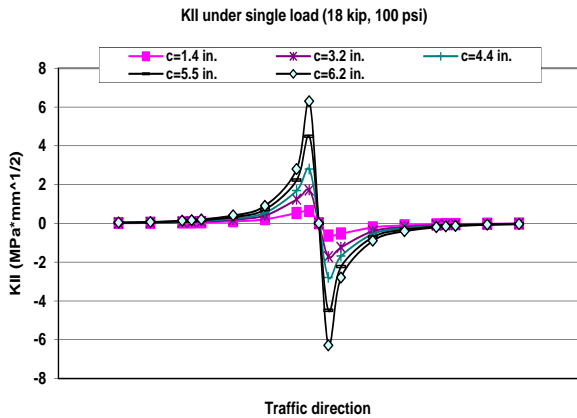
(c) K_{II} under Single Axle Load   (d) K_{II} under Tridem Axle Load
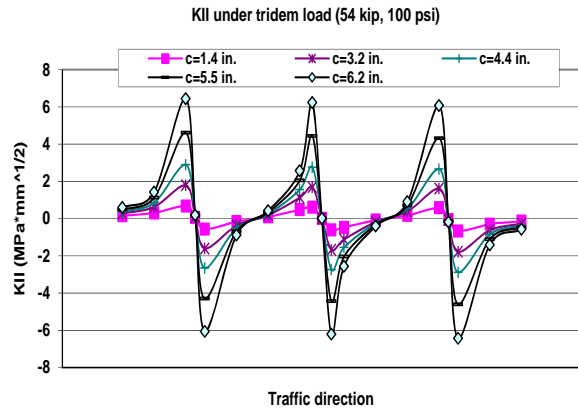
Figure 4-8. K_I and K_{II} Comparisons between Single and Tridem Axle Load.

As show in Figure 4-8, the maximum K_I and K_{II} values under the tridem axle load are almost the same as those under the single axle load. Meanwhile, the K_I and K_{II} values at midway between the axles are very close to 0, which implies there is little overlapped response between axles. Extensive analysis results show that this observation is also true for other pavement structures under different types of multi-axle loads. Therefore, multi-axle loads, for simplicity, can be handled through multiple applications of the single axle load. Thus, the varied traffic loading spectrum for crack propagation purposes can be analyzed as a single axle multi-repetitions issue.

The single axle loading may range between 3,000 and 40,000 lb. (standard MEPDG analysis range), and may be further influenced by varying tire pressures, contact areas, or both. It is well known that both K_I and K_{II} are linearly proportional to the tire pressure for the same contact area. Thus, only one tire pressure of 100 psi (0.689 MPa) was used in this analysis. K_I and K_{II} under the other tire pressures can be readily determined proportionally. In the case of varying contact area but keeping constant tire pressure, K_I and K_{II} must be specifically calculated for each contact area (the product of

effective tire width and tire length). The tire length and associated contact area increases with an increase in tire load level keeping constant tire pressure, but the effective tire width hardly varies with tire load (Fernando et al. 2006).

Therefore, the increasing contact area is actually equal to an increase in the tire length, since the effective tire width does not vary with the load level. After reviewing the default load spectrum in the MEPDG (NCHRP 2004), four levels of single axle loads were recommended for developing SIF regression equations, as listed in Table 4-4. Note that a constant effective tire width of 6.22 in (158 mm) was chosen based on the textbook *Pavement Analysis and Design* by Huang (2004). The SIF values corresponding to another load level (or contact area/tire length) can be interpolated or extrapolated based on these SIF values.

Table 4-4. Four Single Axle Loads Recommended for SIF Analysis.

Axle Load (lb)	Tire Pressure (psi)	Effective Tire Width (inches)	Tire Length (inches)
4000	100	6.22	1.6
11000	100	6.22	4.4
18000	100	6.22	7.2
25000	100	6.22	10

Note: A standard single axle consists of two sets of dual tires.

4.2.3 Load Spectrum-Based Fatigue Cracking Area Determination

Based on the previous discussion, the steps and equations for determining load spectrum-based fatigue cracking area are described below.

Step 1: Determine the AC bottom strain for a specific axle according to the section 4.2.1.

This specific axle depends on the *axletype* (*Steering Single*, *Other Single*, *Tandem*, *Tridem* or *Quad),* *axleOrder (*1st for a single axle, 1st or 2nd for a tandem…, 1st or 2nd or 3rd for a tridem…etc.), load group *g (*e.g., g=1 for a tandem axle means the axle load is 6000 lb., g=2 means the axle load is 8000 lb.,…etc.).

For a given month (m^{th} month, y^{th} year), this determined strain is represented by $\varepsilon_{y,m,g,axletype,axleOrder}$.

Step 2: Determine the initial cracking life for that specific axle, as follows:

$$N_i(y,m,g,axletype,axleOrder) = k_1 \left(\frac{1}{\varepsilon_{y,m,g,axletype,axleOrder}} \right)^{k_2} \tag{4-7}$$

Step 3: Determine the crack propagation life for that specific axle, as follows:

$$N_p(y,m,g,axletype) = \int_{c_0}^{h} \frac{1}{AK_{I,y,m,g,axletype}^n + AK_{II,y,m,g,axletype}^n} dc \tag{4-8}$$

To complete this step, the steps in the section 3.2.2 Determination of Monthly N_p should be followed. Note that the crack propagation life is not influenced by *axleOrder*.

Step 4: Determine total crack life for that specific axle, as follows:

$$N_f(y,m,g,axletype,axleOrder) = N_i(y,m,g,axletype,axleOrder) + N_p(y,m,g,axletype) \qquad (4\text{-}9)$$

Step 5: Determine the damage for that specific axle, as follows:

$$D_{y,m,g,axletype,axleOrder} = \frac{N_{g,y,m,axletype}}{N_f(y,m,g,axletype,axleOrder)} \qquad (4\text{-}10)$$

where $N_{g,y,m,axletype}$ is the monthly axle applications for each axle type and each load group; see Equation 4-6.

Step 6: Repeat Steps 1 to 5 for all the *axleOrder*, *axletype,* and load group *g*. Sum all the damage values for a given month and year, as follows:

$$D_{y,m} = \sum_g \sum_{axletype} \sum_{axleOrder} D_{y,m,g,axletype,axleOrder} \qquad (4\text{-}11)$$

where $D_{y,m}$ is the monthly AC fatigue damage at the given month (m^{th} month, y^{th} year).

Step 7: Calculate the fatigue cracking area for a given month, as follows:

$$fatigued\_area(\%) = \frac{100}{1 + e^{C \log D_{y,m}}} \qquad (4\text{-}12)$$

4.3 LOAD SPECTRUM-BASED RUTTING (AC/GRANULAR BASE/SUBGRADE)

Since both the AC layer rutting model and unbound material layer (granular base/subgrade) rutting model use the VESYS layer rutting model principles, there is no difference between them in terms of the load spectrum methodology. The following describes the load spectrum-based rut depth accumulation method and multiple axles treatment method.

4.3.1 Load Spectrum-Based Rut Depth Accumulation Method

As shown in Equation 4-13, the layer rut depth depends on the layer deflection difference ΔU caused by each axle load.

$$RD = k \int \Delta U \, \mu N^{-\alpha} \qquad (4\text{-}13)$$

where
RD = layer rut depth.
k = calibration factor.

ΔU = deflection difference between the layer top and layer bottom.
N = load repetitions
α & μ = layer rutting properties, determined by lab test.

The monthly accumulation method of the rut depth RD is the same as that discussed in Section 3.1.2 "Monthly Accumulation of RDAC." The following discusses the rut accumulation method during the same month but among different axle load groups.

The example below takes a single axle with load group 1 (g=1, axle load =3000 lb.) and load group 2 (g=2, axle load =4000 lb.) to demonstrate the accumulation.

Since the accumulation is conducted during the same month, the layer rutting properties α and μ do not change. Thus the Equation 4-13 can be converted into Equation 4-14 to determine the rut depth under the first group of axle loads.

$$RD_{g1} = k\,\Delta U_{g1}\,\mu\,\frac{(N_{g1})^{1-\alpha}}{1-\alpha} \tag{4-14}$$

where
ΔU_{g1} = the layer deflection difference under the axle load of group 1.
N_{g1} = the number of repetitions of this load group.
RD_{g1} = the rut depth under this load group.

To accumulate the rut depth with that caused by load group 2, the equivalent axle repetition number N_{g1eq} has to be determined first, using Equation 4-15.

$$N_{g1eq} = \left(\frac{RD_{g1}\,(1-\alpha)}{\Delta U_{g2}\,\mu k}\right)^{\frac{1}{1-\alpha}} \tag{4-15}$$

where ΔU_{g2} is the layer deflection difference under the axle load of group 2.

Then the accumulated rut depth $RD_{g1,g2}$ can be calculated as follows:

$$RD_{g1,g2} = k\,\Delta U_{g2}\,\mu\,\frac{\left(N_{g1eq} + N_{g2}\right)^{1-\alpha}}{1-\alpha} \tag{4-16}$$

where N_{g2} is the number of repetitions of load group 2.

Combining Equations 4-15 and 4-16, Equation 4-17 can be achieved.

$$RD_{g1,g2} = k\,\mu\,\frac{\left(N_{g1}\left(\Delta U_{g1}\right)^{\frac{1}{1-\alpha}} + N_{g2}\left(\Delta U_{g2}\right)^{\frac{1}{1-\alpha}}\right)^{1-\alpha}}{1-\alpha} \tag{4-17}$$

Equation 4-17 implies that the accumulated rut depth does not depend on the load group applying sequence. For example, if applying load group 2 first and then applying load group 1, the final accumulated rut depth will be exactly the same. This is a very important feature, which assures the success of implementing the rutting model for load spectrum. If the load group applying sequence matters, the predicted rut depth will be unstable and inconsistent.

Thus, the equation of load spectrum-based rutting accumulation for a given month is as follows:

$$RD = \frac{k\ \mu}{1-\alpha}\left(\sum N_{axle}\left(\Delta U_{axle}\right)^{\frac{1}{1-\alpha}}\right)^{1-\alpha} \tag{4-18}$$

where
RD = the accumulated rut depth for a given month.
N_{axle} = the repetitions of each axle load.
ΔU_{axle} = the layer deflection difference cause by the axle load.

Combining the monthly accumulation method discussed in Section 3.1.2, the generalized load spectrum-based rutting can be determined by:

$$RD_m = \frac{k\ \mu_m}{1-\alpha_m}\left(\left[\frac{RD_{m-1}(1-\alpha_m)}{\mu_m}\right]^{\frac{1}{1-\alpha_m}} + \sum N_{axle}\left(\Delta U_{axle}\right)^{\frac{1}{1-\alpha_m}}\right)^{1-\alpha_m} \tag{4-19}$$

where m is the month number.

4.3.2 Method of Treating Rutting for Multiple Axle Groups

As discussed in Section 4.2 "Load Spectrum Based AC Fatigue Cracking," it is deemed as inappropriate for assuming each set of multiple axles to be one repetition or multiple repetitions (each repetition is of the same single axle load and causes the same ΔU). Thus TxME proposes the similar multiple axles treatment method to that of fatigue cracking initiation. The details about tandem, tridem, and quad axles are demonstrated below.

Tandem Axle

Figure 4-9 illustrates the layer deflection difference ΔU under a moving tandem axle load. In Figure 4-9a, the X axis is the horizontal direction which is parallel to the axles and the Y axis is also in the horizontal direction but parallel to traffic movement. The broken line indicates the cross section of interest (or calculating section). The numbers 1, 2, and 3 show the deflection calculating points. Figure 4-9b shows the layer deflection differences ΔU_1, ΔU_2, and ΔU_3 at the cross section of interest when points 1, 2, and 3 arrive at this cross section, respectively.

According to this figure, each set of tandem axle is assumed to be two load repetitions; and the layer deflection difference ΔU caused by each repetition is different: the ΔU caused by the 1st axle is ΔU_1 and the ΔU caused by the 2nd axle is $\Delta U_3 - \Delta U_2$.

(a)

(b)
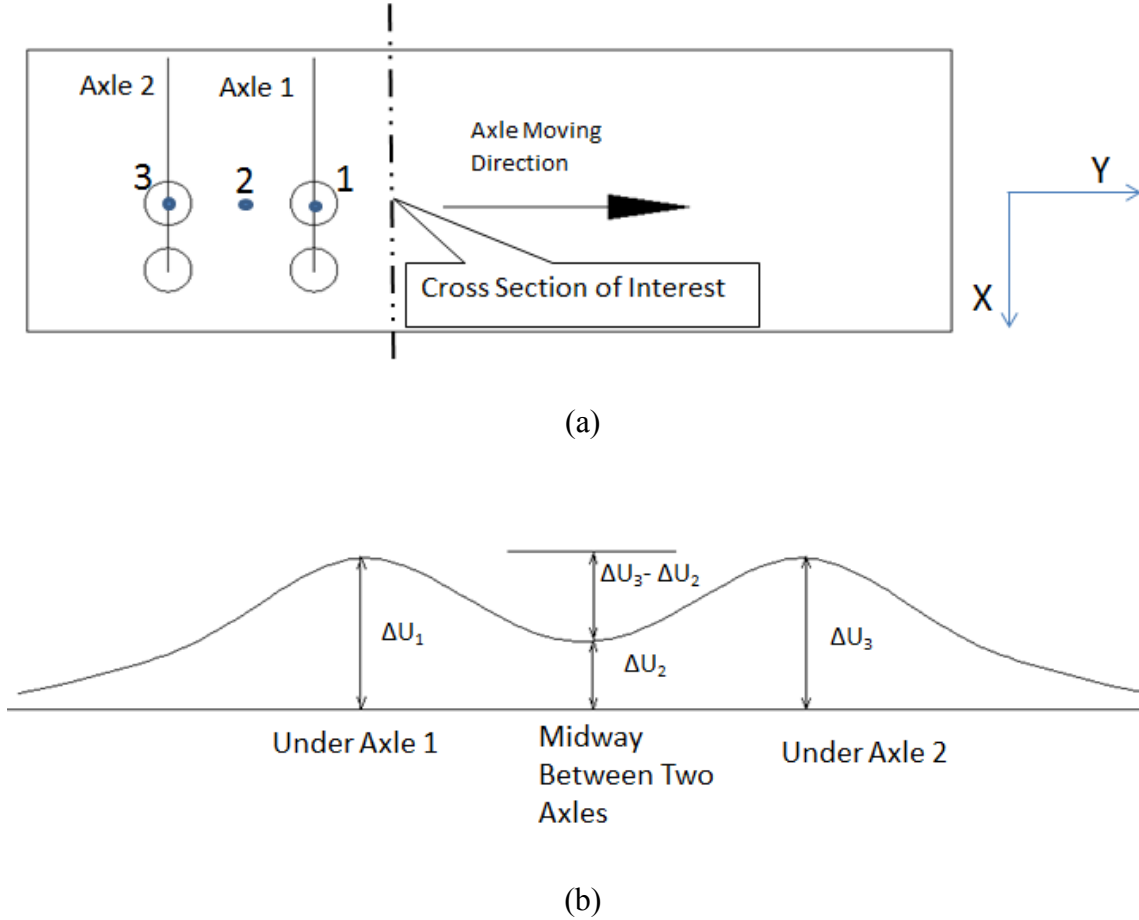
Figure 4-9. Schematic of (a) Tandem Axle Load Top View and (b) Layer Deflection Difference ΔU.

By similar formula derivations, the 'Σ' part in Equation 4-18 for tandem axles can be written in the following form.

$$\sum_{Tandem} = \sum_{g} N_{Tandem}{}^{g} \left[\left(\Delta U_{1}{}^{g}\right)^{\frac{1}{1-\alpha}} + \left(\Delta U_{3}{}^{g} - \Delta U_{2}{}^{g}\right)^{\frac{1}{1-\alpha}} \right] \qquad (4\text{-}20)$$

where

$N_{Tandem}{}^{g}$ = the monthly axle applications for the tandem axle and load group g.

$\Delta U_1{}^g$, $\Delta U_2{}^g$, and $\Delta U_3{}^g$ = the layer deflection differences caused by axle load group g corresponding to points 1, 2, and 3, respectively.

Note that due to symmetry, $\Delta U_3{}^g$ equals $\Delta U_1{}^g$. $N_{Tandem}{}^g$ at the mth month and y^{th} year equals $N_{g, y, m, axletype}$(*axletype=Tandem*), determined by Equation 4-6.

Tridem Axle

By analogy, Figure 4-10 illustrates the layer deflection difference ΔU under a moving tridem axle load. According to this figure, each set of tridem axles is assumed to be three load repetitions: the ΔU caused by the 1st axle is ΔU_1, the ΔU caused by the 2nd axle is $\Delta U_3 - \Delta U_2$, and the ΔU caused by the 3rd axle is $\Delta U_5 - \Delta U_4$.
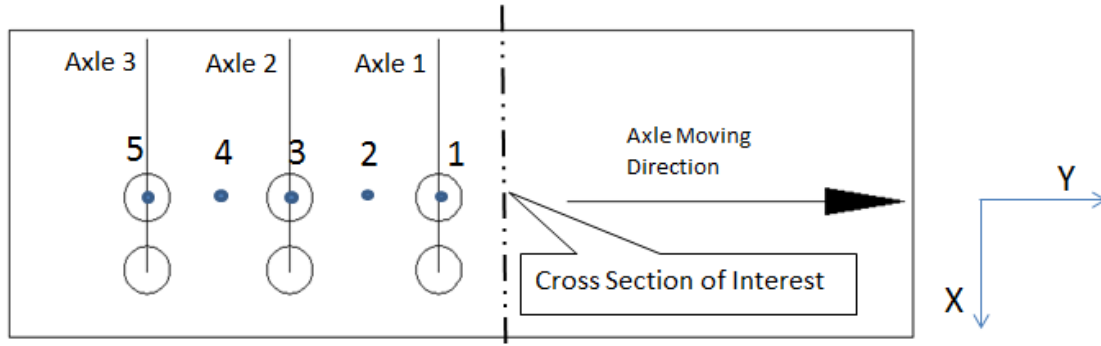
(a)
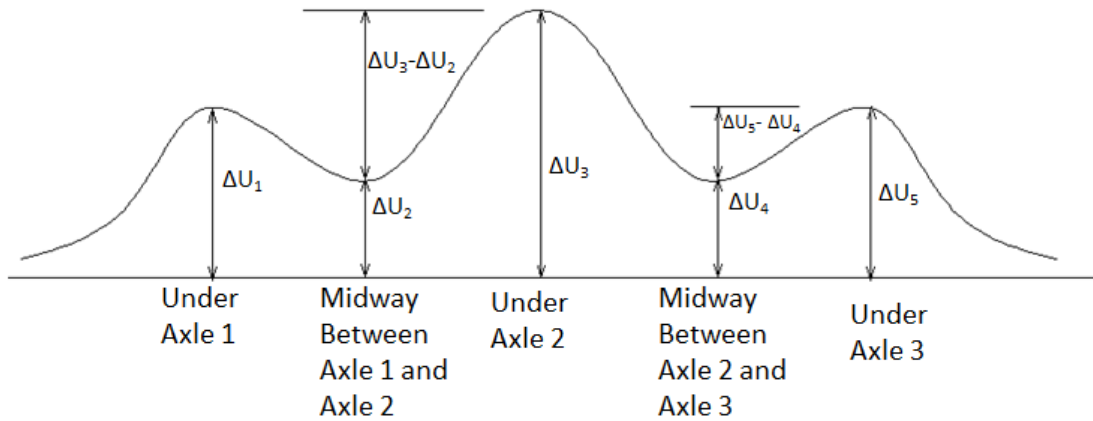
(b)

Figure 4-10. Schematic of (a) Tridem Axle Load Top View and (b) Layer Deflection Difference ΔU.

The 'Σ' part in Equation 4-18 for the tridem axle can be written in the following form:

$$\sum_{Tridem} = \sum_{g} N_{Tridem}{}^{g} \left[\begin{array}{l} \left(\Delta U_{1,}{}^{g} \right)^{\frac{1}{1-\alpha}} + \left(\Delta U_{3}{}^{g} - \Delta U_{2}{}^{g} \right)^{\frac{1}{1-\alpha}} \\ + \left(\Delta U_{5}{}^{g} - \Delta U_{4}{}^{g} \right)^{\frac{1}{1-\alpha}} \end{array} \right] \qquad (4\text{-}21)$$

where

$N_{Tridem}{}^g$ =   the monthly axle applications for the tridem axle and load group g.

$\Delta U_1{}^g$, $\Delta U_2{}^g$, $\Delta U_3{}^g$, $\Delta U_4{}^g$, and $\Delta U_5{}^g$ = the layer deflection differences caused by axle load group g corresponding to points 1, 2, 3, 4, and 5, respectively.

Note that due to symmetry, $\Delta U_4{}^g$ equals $\Delta U_2{}^g$ and $\Delta U_5{}^g$ equals $\Delta U_1{}^g$. $N_{Tridem}{}^g$ at the mth month and y^{th} year equals $N_{g,\,y,\,m,\,axletype}$ (*axletype=Tridem*), determined by Equation 4-6.

Quad Axle

Similarly, Figure 4-11 illustrates the layer deflection difference ΔU under a moving quad axle load. According to this figure, each set of quad axles is assumed to be four load repetitions: the ΔU caused by the 1st axle is ΔU_1, the ΔU caused by the 2nd axle is $\Delta U_3 - \Delta U_2$, and the ΔU caused by the 3rd axle is $\Delta U_5 - \Delta U_4$, and the ΔU caused by the 4th axle is $\Delta U_7 - \Delta U_6$.
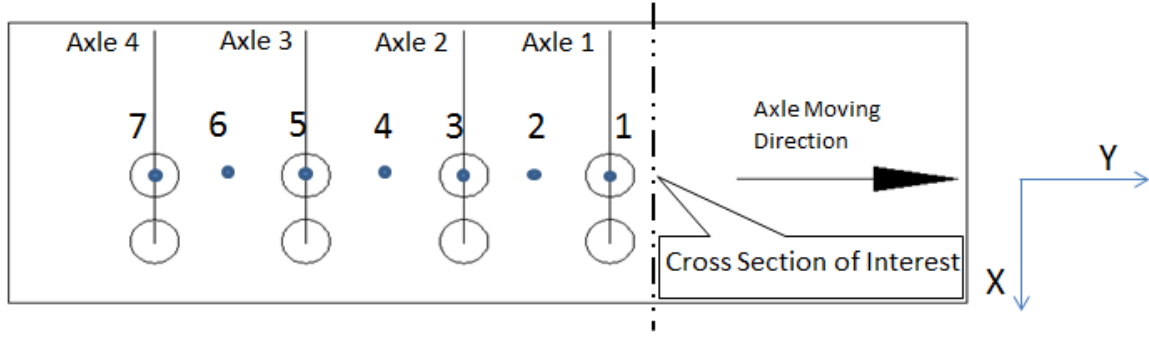
(a)
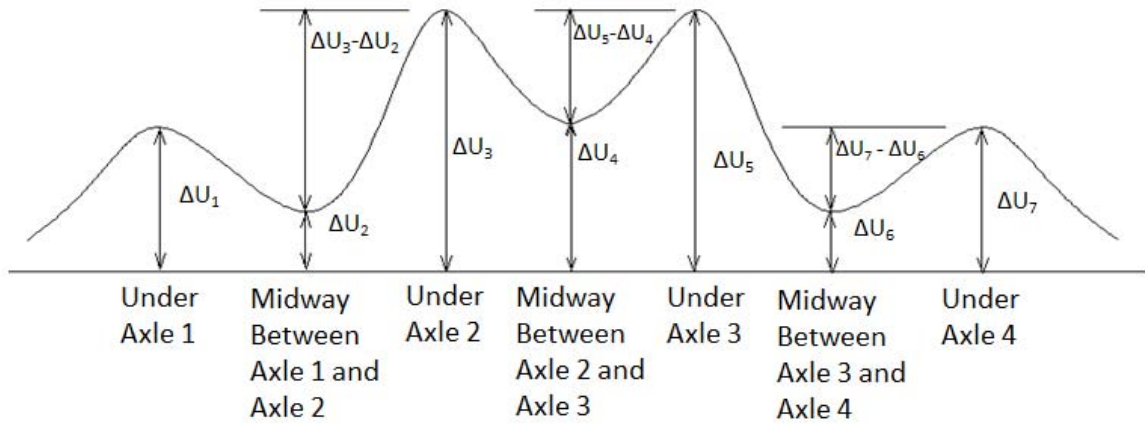
(b)

Figure 4-11. Schematic of (a) Quad Axle Load Top View and (b) Layer Deflection Difference ΔU.

The 'Σ' part in Equation 4-18 for the quad axle can be written in the following form.

$$\sum_{Quad} = \sum_{g} N_{Quad}{}^{g} \left[\begin{array}{l} \left(\Delta U_{1,}{}^{g}\right)^{\frac{1}{1-\alpha}} + \left(\Delta U_{3}{}^{g} - \Delta U_{2}{}^{g}\right)^{\frac{1}{1-\alpha}} \\ + \left(\Delta U_{5}{}^{g} - \Delta U_{4}{}^{g}\right)^{\frac{1}{1-\alpha}} \\ + \left(\Delta U_{7}{}^{g} - \Delta U_{6}{}^{g}\right)^{\frac{1}{1-\alpha}} \end{array} \right] \qquad (4\text{-}22)$$

where

$N_{Quad}{}^{g}$ = the monthly axle applications for the quad axle and load group g.

$\Delta U_1{}^{g}, \Delta U_2{}^{g}, \Delta U_3{}^{g}, \Delta U_4{}^{g}, \Delta U_5{}^{g}, \Delta U_6{}^{g},$ and $\Delta U_7{}^{g}$ = the layer deflection differences caused by axle load group g corresponding to points 1, 2, 3, 4, 5, 6, and 7, respectively.

Again, due to symmetry, $\Delta U_5{}^g$ equals $\Delta U_3{}^g$, $\Delta U_6{}^g$ equals $\Delta U_2{}^g$, and $\Delta U_7{}^g$ equals $\Delta U_1{}^g$. $N_{Quad}{}^g$ at the mth month and y^{th} year equals $N_{g,\,y,\,m,\,axletype}$ (*axletype=Quad*), determined by Equation 4-6.

Finally, Equation 4-19 can be further expanded to Equation 4-23 to determine the load-spectrum based rutting.

$$
RD_m = \frac{k\,\mu_m}{1-\alpha_m}\left(
\begin{array}{l}
\left[\dfrac{RD_{m-1}(1-\alpha_m)}{\mu_m}\right]^{\frac{1}{1-\alpha_m}} + \sum_{Tandem} + \sum_{Tridem} \\[2em]
+ \sum_{Quad} + \sum_{Steering\ Single} + \sum_{Other\ Single}
\end{array}
\right)^{1-\alpha_m}
\tag{4-23}
$$

where

$$
\sum_{Steering\ Single} = \sum_g N_{Steering\ Single}{}^g\left[\left(\Delta U_{Steering\ Single}{}^g\right)^{\frac{1}{1-\alpha}}\right]
\tag{4-24}
$$

$$
\sum_{Other\ Single} = \sum_g N_{Other\ Single}{}^g\left[\left(\Delta U_{Other\ Single}{}^g\right)^{\frac{1}{1-\alpha}}\right]
\tag{4-25}
$$

where

$N_{Steering\ Single}{}^g$	=	monthly axle applications for the steering single axle and load group *g*.
$\Delta U_{Steering\ Single}{}^g$	=	ΔU caused by the steering single axle of load group *g*.
$N_{Other\ Single}{}^g$	=	monthly axle applications for the other single axle and load group *g*.
$\Delta U_{Other\ Single}{}^g$	=	ΔU caused by the other single axle of load group *g*.

To be consistent, all the parameters in the 'Σ' parts correspond to the mth month.

4.4 LOAD SPECTRUM-BASED STABILIZED BASE FATIGUE CRACKING

The crack initiation life depends on the induced maximum tensile stress at the bottom of the stabilized layer. For load spectrum input, these tensile stresses have to be determined for each axle type and each axle load level throughout the design period.

TxME adopted the same method as that of AC Fatigue cracking initiation to analyze the influence of multiple axles. Taking a tandem axle load as an example, if the induced tensile stress under the 1st axle is σ_1 and the stress at midway between the 1st axle and 2nd axle is σ_2, the effect of this tandem axle load is taken into account by using σ_1 for the 1st axle and $\sigma_1\text{-}\sigma_2$ for the 2nd axle. Similar rules apply for the tridem and quad axles in terms of a multiple axle treatment method for stabilized base fatigue cracking.

71

Using $\sigma_t(y,m,g,axletype,axleOrder)$ to represent the maximum tensile stress at the bottom of the stabilized layer, for a given month (m^{th} month, y^{th} year), load group g, *axletype,* and *axleOrder,* the fatigue cracking life equation (Equation 3-26) can be rewritten in the following form:

$$N_{f-SB}(y,m,g,axletype,axleOrder) = 10^{\frac{k_1 B_1 - \left(\frac{\sigma_t(y,m,g,axletype,axleOrder)}{M_R}\right)}{k_2 B_2}} \qquad (4\text{-}26)$$

where $N_{f\text{-}SB}(y,m,g,axletype,axleOrder)$ is the fatigue life under that specific axle load (depends on the load group g, *axletype*, and *axleOrder*) for the given month (m^{th} month, y^{th} year). M_R, k_1, k_2, B_1, and B_2 are the same parameters as those defined previously.

Then the fatigue damage of that specific axle and the given month is:

$$D_{y,m,g,axletype,axleOrder} = \frac{N_{g,y,m,axletype}}{N_{f-SB}(y,m,g,axletype,axleOrder)} \qquad (4\text{-}27)$$

where $N_{g, y, m, axletype}$ is the monthly axle applications for each axle type and each load group, determined by Equation 4-6.

Sum all the damage values according to the load group g, *axleOrder*, and *axletype* for the given month, as follows:

$$D_{y,m} = \sum_{g} \sum_{axletype} \sum_{axleOrder} D_{y,m,g,axletype,axleOrder} \qquad (4\text{-}28)$$

where $D_{y,m}$ is the monthly stabilized base fatigue damage at the given month (m^{th} month, y^{th} year).

Finally, the stabilized base fatigue cracking area for the given month can be calculated as follows:

$$fatigued\_area(\%) = \frac{100}{1 + e^{C \log D_{y,m}}} \qquad (4\text{-}29)$$

CHAPTER 5.
IMPLEMENTATION OF RELIABILITY APPROACH

It is well known that pavement design and analysis involve a lot of uncertainties and variations from the specified design and as-constructed parameters. To address this issue, a reliability concept is often incorporated into the pavement design and analysis process. This chapter provides the background information of reliability approaches used in existing pavement design systems and presents the implementation of the recommended approach in the TxME.

5.1 BACKGROUND

In general, reliability is often defined as "the ability of a system or component to perform its required functions under stated conditions for a specified period of time" (Bagowsky 1961). Specifically for pavement design and analysis, the reliability is referred to as the probability that a pavement section designed using the process will perform satisfactorily in terms of pavement distress over the traffic and environmental conditions for the design period.

Even though mechanistic concepts provide a more accurate and realistic methodology for pavement design, a practical method to consider the uncertainties and variations in design and construction is still needed so that pavements can be designed for a desired level of reliability (i.e., pavement will perform as designed). The sources of variation and uncertainty include:

- Errors in estimating traffic loadings.
- Fluctuations in climate over many years.
- Variations in layer thicknesses, materials properties, and subgrade characteristics along the project.
- Differences between mean as-designed and as-built materials and other layer properties.
- Prediction model limitations and errors.

Different approaches have been employed to consider reliability in a variety of pavement design and analysis systems. Researchers reviewed the following pavement design and analysis systems:

- TxDOT's FPS 21 and AASHTO 1993 Guide.
- MEPDG.
- VESYS design system.
- CalME.

The reliability approach in each system is summarized below.

TxDOT FPS21 and AASHTO 1993 Guide

Both TxDOT's FPS 21 (Liu and Scullion 2006) and the AASHTO 1993 Guide (AASHTO 1993) incorporate reliability through simply adjusting estimated traffic (or ESALs) in the design period. The standard deviation of traffic was preset or assumed. With that, higher reliability indicates a larger adjusting factor for estimated traffic and consequently results in thicker pavement.

MEPDG

Different from adjusting the estimated traffic in the FPS21 and the AASHTO 1993 Guide, the MEPDG design reliability is achieved through adjusting pavement distress using the following equation (NCHRP 2004):

$$Distress\_P = Distress\_mean + STD_{distress\_mea} \times Z_P \qquad (5\text{-}1)$$

where

Distress_P	=	distress level corresponding to the reliability level *P*.
Distress_mean	=	distress predicted using the deterministic model with mean inputs.
STD_{distress_mean}	=	standard deviation of distress.
Z_P	=	standardized normal deviate corresponding to reliability level *P*.

Figure 5-1 further demonstrates the MEPDG reliability concept (Darter et al. 2005). The key points (or assumptions) behind this concept are

- All predicted distresses are normally distributed.
- The standard deviation of each predicted distress (e.g., fatigue cracking) can be substituted by that of measured data, since the MEPDG itself is deterministic and cannot predict the standard deviation of each distress.
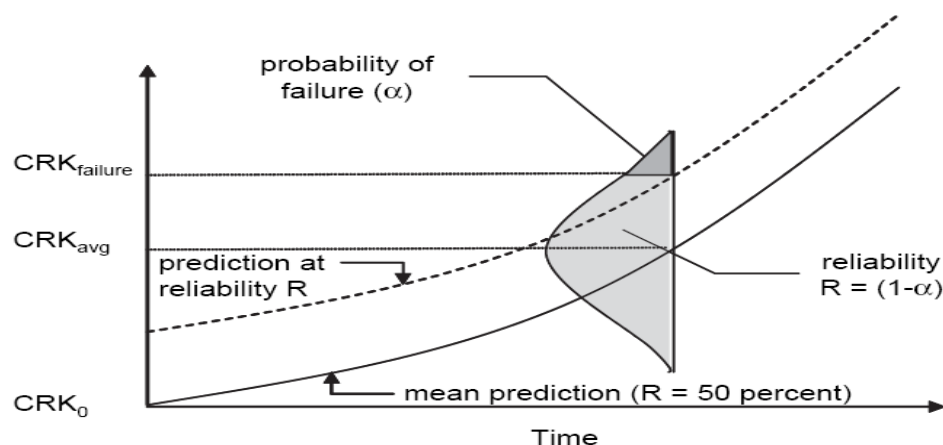
Figure 5-1. MEPDG Reliability Concept for a Given Distress (Darter et al. 2005).

VESYS Program

The Federal Highway Administration (FHWA) originally developed the VESYS program several decades ago (Kenis 1978). One of the main features of the program is that it considers the variability of pavement materials and traffic, and then evaluates the reliability of the pavement design. The VESYS program considers not only the reliability of pavement distresses (such as fatigue cracking, rutting, roughness, and low-temperature cracking) but also the pavement present serviceability index (PSI). Moavenzadeh and Elliott (1968) developed closed-form probabilistic solutions for this three-layer linear viscoelastic boundary value problem, and later Brademeyer (1975) refined and expanded the work. Therefore, the VESYS program, different from other design programs, evaluates reliability (or probability) of pavement distress using a closed-form function. Note that the closed-form solution is an analytical solution, which requires that the pavement response functions are quite simple and the partial derivative of which can be sought. For a more complicated pavement design system like mechanistic-empirical analysis, there are no such simple functions for pavement responses.

CalME

CalME is a program that the pavement research center at the University of California created for the California Department of Transportation (Caltrans). The program was developed to fill the need for a mechanistic-empirical analysis tool for designing new pavements and asphalt overlays (Ullidtz et al. 2010). CalME considers input variability and evaluates reliability of pavement distress through the Monte Carlo simulation. Currently, for nine uncertain variables, 1000 simulations may be needed. The beauty of the Monte Carlo simulation is that there is no need to assume the distribution of pavement distress. The major drawback of the Monte Carlo simulation is the running time: it often takes too long to tolerate for pavement design and analysis.

Table 5-1 presents a summary of all five existing pavement design programs in terms of reliability approach. More details about the reliability approaches in different pavement design systems can be found in the Report 0-6622-1 Appendix B (Hu et al. 2012a).

Table 5-1. Summary and Comparison among Different Reliability Approaches.

Reliability Approach	Advantages	Disadvantages	Iteration Number	Examples of Design System
Adjusting traffic	Simple	Cannot account for impact of the variability of other inputs on pavement design	1	▪ FPS21 ▪ AASHTO 1993
Adjusting prediction	Simple	Cannot account for variability of inputs directly	1	MEPDG
Monte Carlo simulation	▪ Accurate ▪ Accounts for all input variability ▪ Obtains the distribution of response	Has long computation time	>1000	CalME
Closed-form function	▪ Efficient ▪ Accounts for design input variability	▪ Very complicated to get a closed-form pavement response function (if not impossible) ▪ Requires partial derivatives	1	VESYS

Based on Table 5-1, there is no ideal practical approach to be used in the TxME. To further address this issue, the researchers reviewed the latest development in this area and found that the Rosenblueth $2n+1$ method (n is number of variables with uncertainty) has a high potential for evaluating pavement design reliability. Detailed information on this method is presented below.

5.2 ROSENBLUETH'S $2n+1$ METHOD

Rosenblueth (1975) developed a simple method known as the Point-Estimate method, which is similar to the finite difference procedure that can be used directly to determine the mean and variance of any function without knowing its formulation. The basic idea of the Point-Estimate method is to replace a continuous random variable with a discrete random variable. Specifically for reliability/probability, the continuous random variable (represented by a mean and standard deviation) is replaced by two masses representing the distribution of the function with the characteristic that the discrete distribution has the same mean and variance as the continuous

one. The following describes the Rosenblueth's $2n+1$ method using the function $y = f(X_1, X_2,..., X_n)$ as an example.

Define y_0 as the value of the function y when all input variables are equal to their mean values; that is,

$$y_0 = f(\mu_{X1}, \mu_{X2}, ..., \mu_{Xn}) \tag{5-2}$$

where μ_{Xi} is the mean value of each variable Xi, $i=1, 2...$, and n, respectively.

Assuming σ_{Xi} is the standard deviation of each variable Xi, $i=1, 2...$, and n, respectively, the values of the function y evaluated at an additional $2n$ points are presented below.

For each random variable Xi, evaluate the function at two values of Xi, which are shifted from the mean μ_{Xi} by $\pm\sigma_{Xi}$ while all other variables are assumed to be equal to their mean values. These values of the function will be referred to as y_i^+ and y_i^-. The subscript denotes the variable that is shifted, and the superscript indicates the direction of the shift. In mathematical notation,

$$y_i^+ = f(\mu_{X1}, \mu_{X2}, ..., \mu_{Xi} + \sigma_{Xi}, ..., \mu_{Xn}) \tag{5-3}$$

$$y_i^- = f(\mu_{X1}, \mu_{X2}, ..., \mu_{Xi} - \sigma_{Xi}, ..., \mu_{Xn}) \tag{5-4}$$

For each random variable, calculate the following two quantities based on y_i^+ and y_i^-:

$$\overline{y_i} = \frac{y_i^+ + y_i^-}{2} \tag{5-5}$$

$$V_{y_i} = \frac{y_i^+ + y_i^-}{y_i^+ - y_i^-} \tag{5-6}$$

Calculate the estimated mean and standard deviation of the function y as follows:

$$\mu_y = y_0 \prod_{i=1}^{n} \frac{\overline{y_i}}{y_0} \tag{5-7}$$

$$\sigma_y = \mu_y \sqrt{\{\prod_{i=1}^{n}(1 + V_{yi}^2)\} - 1} \tag{5-8}$$

Using the Rosenblueth's $2n+1$ simulation method, the number of simulations is substantially reduced compared to the Monte Carlo method, which is extremely beneficial to M-E pavement design and analysis. The Rosenblueth's $2n+1$ method is recommended as the reliability approach in the TxME program.

Examples and verifications for the Rosenblueth methods were demonstrated in the Report 0-6622-1 Appendix C: Examples and Comparisons among Closed-Form Method, Rosenblueth Method, and Monte Carlo Method (Hu et al. 2012). The accuracy and validity of the Rosenblueth 2n+1 method was verified by comparison with the closed-form method and the Monte Carlo method according to some simple functions. See Table 5-2.

Table 5-2. Comparison among Different Methods for $Y=X_1*X_2*X_3$.

	Mean Value of Y	Std. Dev. of Y
Closed-form method	200	87.7496
Rosenblueth 2n+1 method	200	90.4323
Monte Carlo method	199.57	90.4957

The mean value and standard deviation for each variable are listed in Table 5-3.

Table 5-3. Mean Value and Standard Deviation of Variables.

	Mean Value (μ)	Std. Dev. (σ)
X_1	10	2
X_2	4	1
X_3	5	1.5

Note that the results of the Monte Carlo method were based on 3000 simulations, which are relatively more repeatable than that of much fewer simulations, as shown in Figure 5-2.
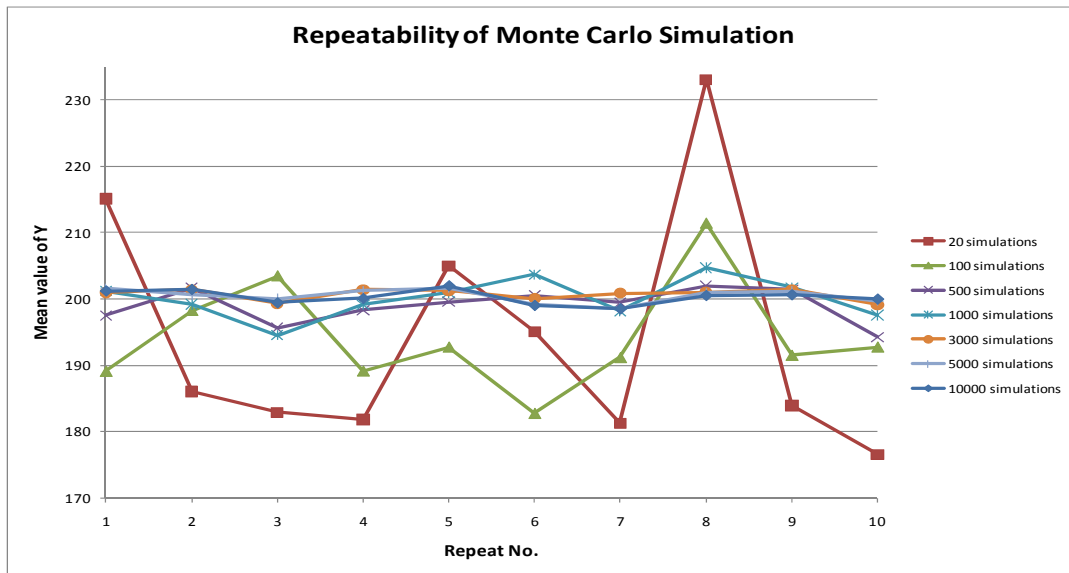
Figure 5-2. Repeatability of Monte Carlo Solution for Function $Y=X1*X2*X3$.

5.3 IMPLEMENTATION OF ROSENBLUETH'S METHOD

In the TxME, the desired level of reliability is specified along with the distress limit at the end of the design life in defining the performance requirements for a pavement design. For example, one criterion might be to limit rut depth to 0.5 inches at a design reliability of 90 percent. Thus, if a designer designed 100 projects, 90 of these projects would exhibit rut depths less than 0.5 inches at the end of the design life. Different reliability levels may be specified for different distresses in the same design. For example, the designer may choose to specify 95 percent reliability for rutting but 90 percent reliability for AC fatigue cracking.

Figure 5-3 shows an example of distress (or performance) limit and reliability level (in terms of percentage) inputs in the TxME.

Performance Criteria

Peformance	Limit	Reliability (%)
Rutting (inch)	0.5	90
Thermal cracking (ft./mile)	2112	85
Fatigue cracking of AC layer (percent)	50	95

Figure 5-3. TxME Inputs of Distress Limit and Reliability Level.

Note that the analyzed distress types depend on the pavement structure and pavement type. For Figure 5-3, the analyzed pavement is a conventional or thin HMA pavement with flexible base. The parameters of each layer which potentially have variability are listed in Figure 5-4. These parameters relate to pavement structure and pavement type as well; whenever the pavement structure or pavement type changes, these parameters change accordingly and automatically.

Variability of Input Parameters

Use	Parameter	Coefficient of Variation (%)
☑	Layer 1 (AC: DenseGraded) - Thickness	15
☑	Layer 1 (AC: DenseGraded) - Modulus	20
☐	Layer 1 (AC: DenseGraded) - Fracture Property A	
☐	Layer 1 (AC: DenseGraded) - Fracture Property n	
☐	Layer 1 (AC: DenseGraded) - Rutting Property Alpha	
☐	Layer 1 (AC: DenseGraded) - Rutting Property Mu	
☐	Layer 2 (Base: FlexibleBase) - Thickness	
☐	Layer 2 (Base: FlexibleBase) - Modulus	
☐	Layer 2 (Base: FlexibleBase) - Rutting Property Alpha	
☐	Layer 2 (Base: FlexibleBase) - Rutting Property Mu	
☑	Layer 3 (Subgrade) - Modulus	25
☐	Layer 3 (Subgrade) - Rutting Property Alpha	
☐	Layer 3 (Subgrade) - Rutting Property Mu	
☑	Traffic - ESALs or AADTT	30

Figure 5-4. TxME Inputs of Coefficients of Variation.

Users can provide the variability information by checking the checkboxes and modifying the coefficient of variation (CV) value in Figure 5-4. For example, if users check the checkbox and input "15" in the first row, the program will take the AC layer (Layer 1) thickness as an uncertain variable, and the CV of the thickness is 15 percent (CV is the ratio of the standard deviation over mean value).

With these inputs, the implementation of Rosenblueth's $2n+1$ method is described below.

The program will scan all the checkboxes in Figure 5-4 first. If none of these checkboxes are checked, the program will run analysis in the deterministic mode. Otherwise, the reliability analysis will be performed and the algorithm is presented by the following steps.

Step 1: Run analysis based on the input structure, traffic, and climate information. Save all the monthly distress (performance) results. These results corresponds to y_0 of Rosenblueth's method; see Equation 5-2.

Step 2: For each checked parameter in Figure 5-4, repeat the following sub steps.

Step 2.1: Adjust the parameter to the mean value plus one standard deviation and run analysis.
Step 2.2: Save all the monthly performance results, which corresponds to y^+ of Rosenblueth's method; see Equation 5-3.
Step 2.3: Change the parameter back to original value.
Step 2.4: Adjust the parameter to the mean value minus one standard deviation and run analysis.
Step 2.5: Save all the monthly performance results, which corresponds to y^- of Rosenblueth's method; see Equation 5-4.
Step 2.6: Change the parameter back to original value.
Step 2.7: For each monthly value, determine the two quantities ($\bar{y}$ and V_y) based on y^+ and y^-; see Equations 5-5 and 5-6.

Step 3: According to the two quantities ($\bar{y}$ and V_y) of each parameter, determine the μ and σ value for each month and for each distress type; see Equations 5-7 and 5-8. Note that the y_0 determined in Step 1 is needed in this step.

Step 4: Calculate the standardized normal deviate Z_p corresponding to reliability level P input in Figure 5-3.

Step 5: Determine the monthly distress value based on the μ, σ, and Z_p according to Equation 5-1.

The reliability analysis results are organized in Excel file format and are demonstrated in the following section.

5.4 TxME OUTPUT OF RELIABILITY ANALYSIS

Using the above pavement structure and reliability input information, TxME reliability analysis is performed to demonstrate the results. Note that most of the other user inputs such as material properties and traffic information are from default values, and the climate information (weather station) is randomly picked up.

Figure 5-5 shows the rutting reliablity analysis results. AC rut depth, granular base rut depth, and subgrade rut depth are plotted together in this figure. The total rut depth at 90 percent reliability is about 0.22 inches at the end of the design life (240 months or 20 years), which means 90 out 100 projects would exhibit rut depths less than 0.22 inches at the end of the design life.
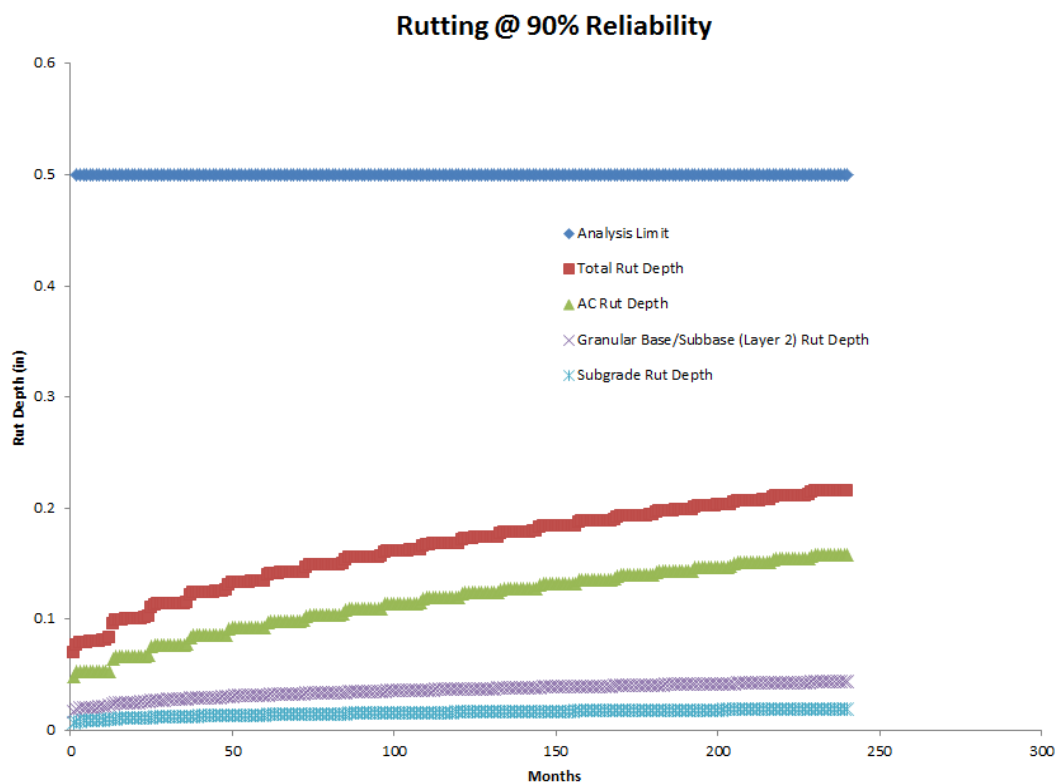
Figure 5-5. TxME Rutting Reliability Analysis Result.

Figure 5-6 shows the AC fatigue cracking analysis results. The results show that 95 out of 100 projects would exhibit AC fatigue cracking over 50 percent (the limit) of the wheel path area or less, before the 50th month. After the 75th month, 95 out of 100 projects would probably exhibit AC fatigue cracking over 100 percent or less of the wheel path area.
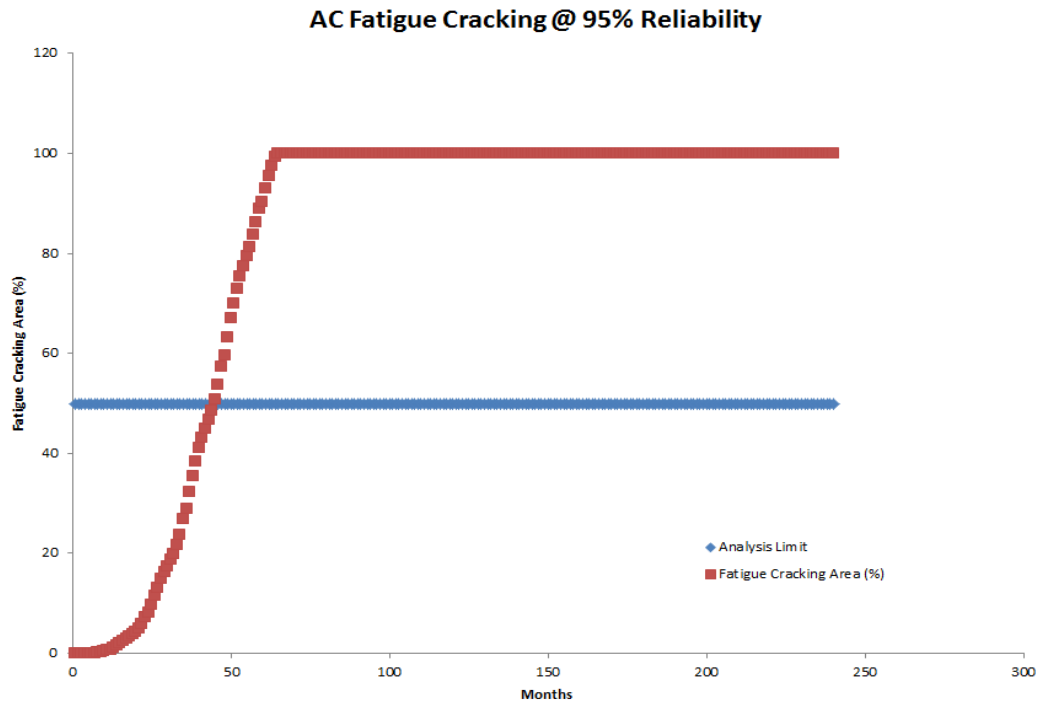
Figure 5-6. TxME AC Fatigue Cracking Analysis Result.

Figure 5-7 shows the AC thermal cracking analysis results. The results show that 85 out of 100 projects would exhibit thermal cracking at a level of 2112 ft/mile (the limit) or less before the 57th month; and exhibit 3700 ft/mile or less at the end of design life (240 month or 20 years).
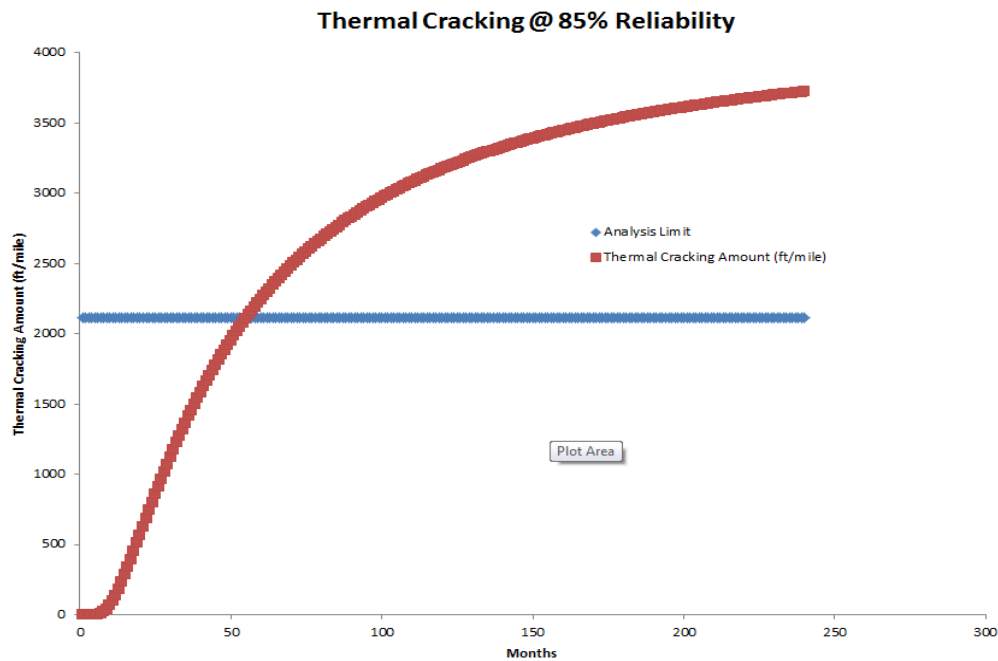
Figure 5-7. TxME Thermal Cracking Reliability Analysis Result.

82

Using different reliability levels or different input parameter variabilities (CV) will cause different prediction results. More details about these comparisons are discussed in Chapter 6: Sensitivity Analysis.

CHAPTER 6.
SENSITIVITY ANALYSIS

The objective of the sensitivity analysis is to investigate how the predicted distresses are influenced by changes in magnitude of several key input variables. This information will help to identify the input parameters that appear to substantially influence predicted performances. In this manner, users can focus efforts on those input parameters that will greatly influence the design.

To conduct the sensitivity analysis, TxME will run several factorial combinations of the input parameters and some pilot comparisons as well. In general, this sensitivity study was not intended to cover a complete full factorial matrix of all input parameters (that would involve millions of combinations). Rather, the intent was to investigate the effect of varying one parameter at a time, while keeping other variables as constant input parameters.

The sensitivity analysis conducted in this chapter includes:

- Factorial combinations of AC/Granular base/Subgrade, to evaluate sensitivity of rutting and AC fatigue/thermal cracking, for a conventional pavement with a flexible base.
- Pilot comparisons on the impact of performance predictions using alternate axle load spectrum, for the same conventional pavement structure as above.
- Pilot comparisons on endurance limit trends by varying the axle load spectra and resulting strain distributions for a perpetual pavement.
- Pilot comparisons on stabilized base fatigue cracking, based on a surface treated pavement with a stabilized base.
- Factorial combinations varying reliability inputs, using pavement structures described above.

The following presents the sensitivity analysis results in the listed order.

6.1 SENSITIVITY ANALYSIS ON AC/GRANULAR BASE/SUBGRADE RUTTING AND AC FATIGUE/THERMAL CRACKING

To study the effect of the sensitivity of input parameters on AC/Granular Base/Subgrade Rutting and AC Fatigue/Thermal Cracking, a three-layer conventional pavement structure is selected and the related parameters are listed below.

6.1.1 Design Parameters and Pavement Structure

For each input parameter, three or four values are assigned to ensure that an adequate range of the variable can be evaluated. The following lists the key input parameters and associated input values used in this study:

- Traffic (ESALs 20 YR, millions): 3, 5, **10**, 30.
- Climate: Amarillo (cold), **Austin** (intermediate), McAllen (hot).
- AC thickness: 1.5, **3**, 5, 7.
- Mix type: Type C, **Type D**, SMA D, SMA C.
- Binder type: PG64-22, PG70-22, **PG76-22.**
- Base modulus (ksi): 30, **50**, 100.
- Base thickness (inches): 8, **10**, 12.
- Subgrade modulus (ksi): 4, **8**, 16.

Note that the "median" value for each parameter above is marked in bold font. TxME will run analyses based on these median values–each time only the value of the investigated parameter varies, keeping median values for other parameters constant.

Figure 6-1 shows the selected pavement structure, labeled with all the "median" values.
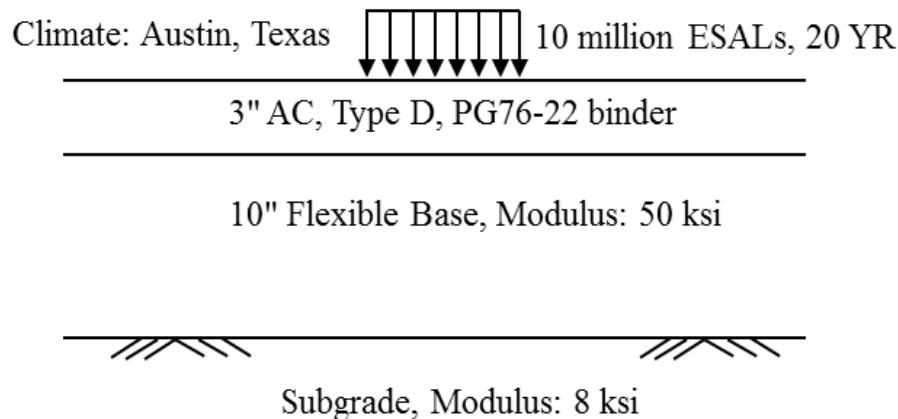
Figure 6-1. Conventional Pavement Structure for Sensitivity Analysis.

Detailed sensitivity analysis results are presented next.

6.1.2 Analysis Results

For each combination of the above parameters, five types of distresses are predicted and compared, such as 1) AC fatigue cracking, 2) AC rutting, 3) granular base rutting, 4) subgrade rutting, and 5) AC thermal cracking. These predictions are plotted in Figures 6-2 to 6-11.

Influence of Traffic Loading

Figure 6-2 shows the influence of traffic loading. It is clear that traffic level (ESALs over 20 YR) has significant influence on all the predicted distresses except the AC thermal cracking, since the thermal cracking model has nothing to do with traffic.

AC Fatigue Cracking

AC Rutting

Subgrade Rutting

Base Rutting

AC Thermal Cracking
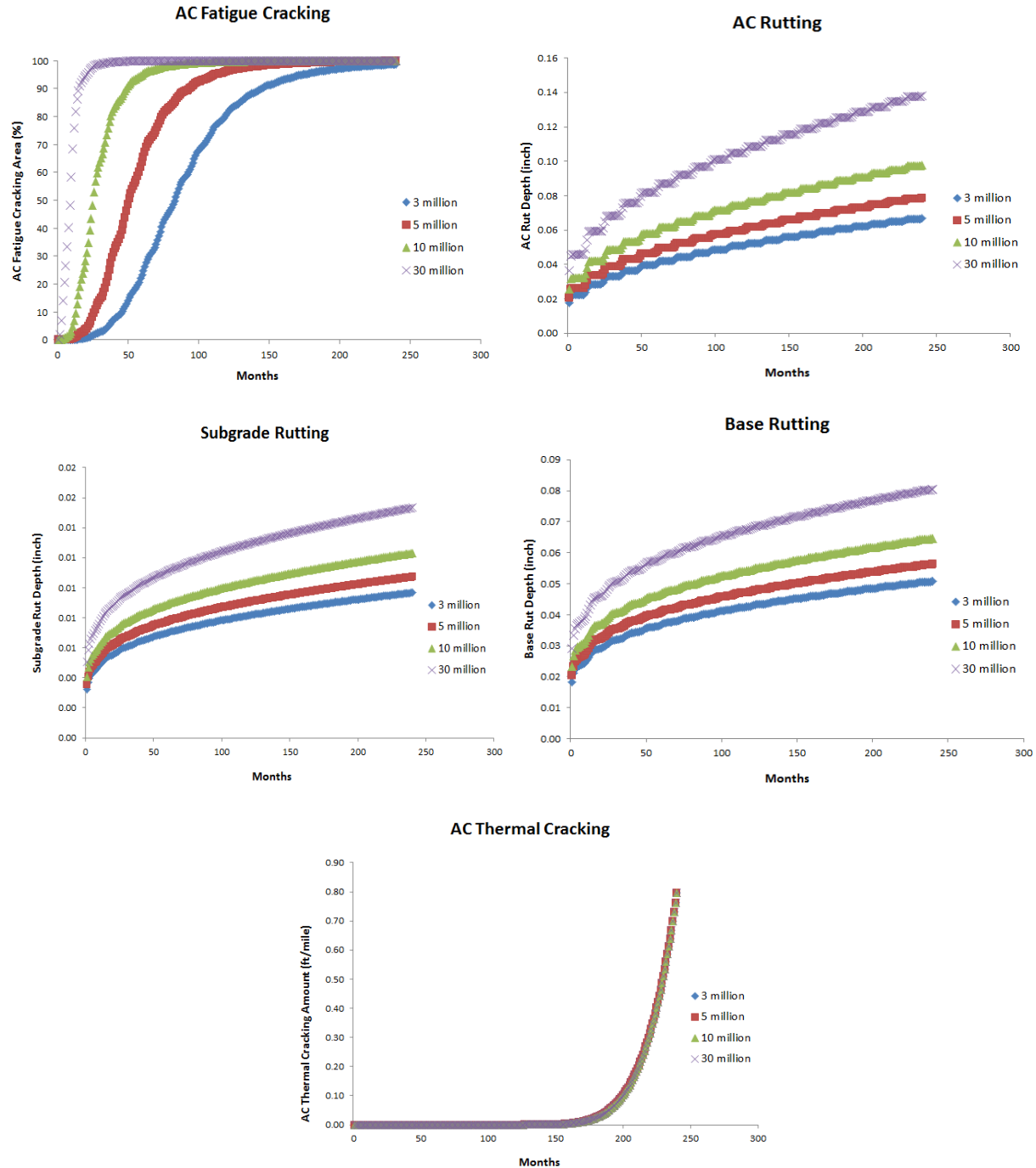
Figure 6-2. Influence of Traffic Loading.

Influence of Climate

Figure 6-3 shows the influence of climate. Note that climate has a significant influence on AC thermal cracking and AC rutting, but it has only a minor influence on base rutting and subgrade rutting. This is reasonable since climate mainly impacts AC layer modulus, which

87

has direct influence on the AC layer's performance but has indirect influence on the other layer's performance.

AC Fatigue Cracking

AC Rutting

Base Rutting

Subgrade Rutting

g

AC Thermal Cracking
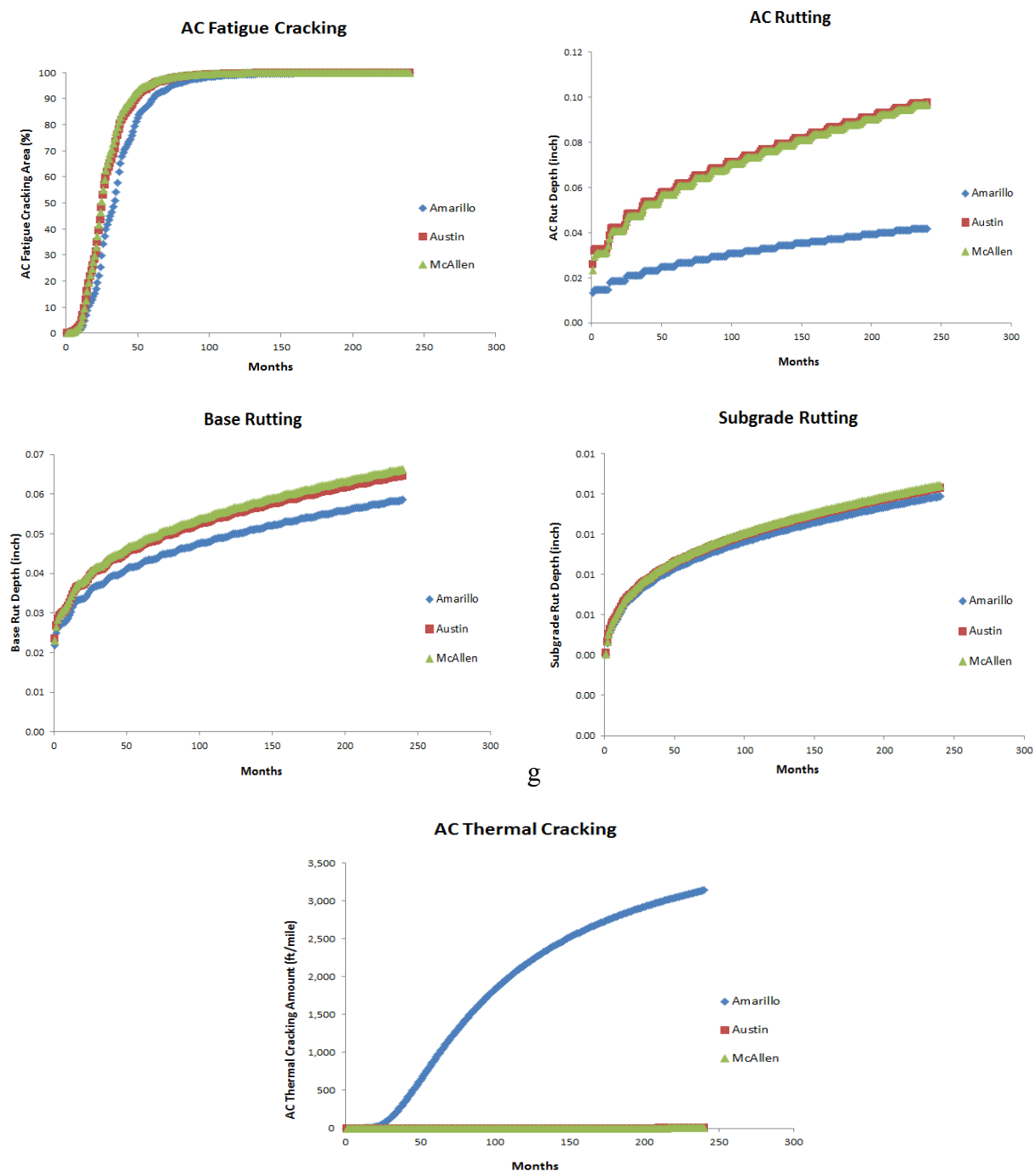
Figure 6-3. Influence of Climate.

In Figure 6-3, note that Amarillo (cold) area has less AC fatigue cracking than that of McAllen (hot) area, which is somewhat counterintuitive. The reason is that the AC fatigue cracking life depends on both the crack initiation life and the crack propagation life; stiff AC materials may

88

have shorter crack propagation life but longer crack initiation life than that of soft AC materials, since the AC bottom strain is smaller. By changing the AC material from 3 inches Type D to 2 inches SMA D, an opposite trend is observed in Figure 6-4, which shows Amarillo (cold) area has more AC fatigue cracking than that of the McAllen (hot) area.

AC Fatigue Cracking
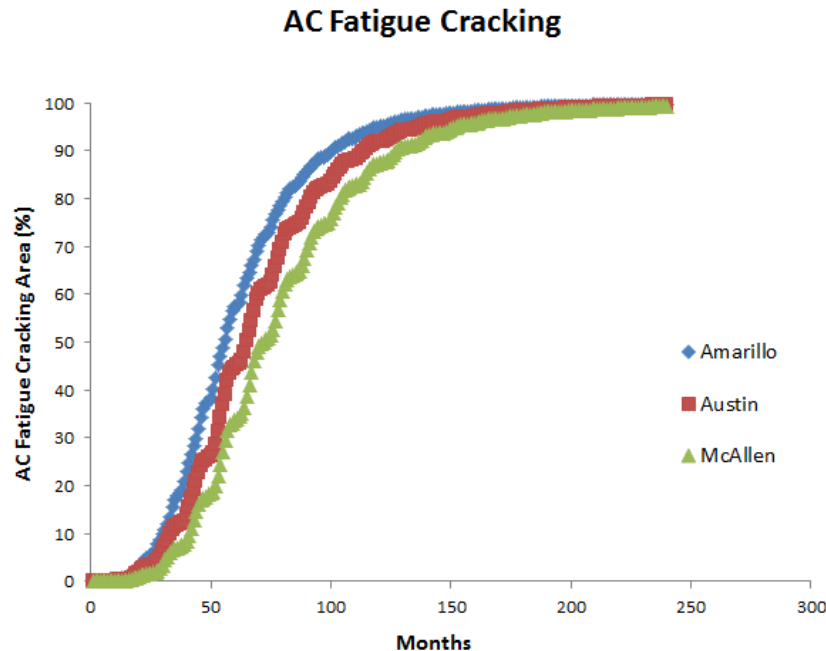
Figure 6-4. Influence of Climate on SMA D Fatigue Cracking.

This finding is consistent with the MEPDG (El-Basyouny and Witczak 2005), which points out that "It is observed that for very thick AC sections, fatigue damage (cracking) is increased for low stiffness AC mixtures. This is 180 degrees opposite to the findings of mix stiffness-fatigue damage for very thin AC layers. The influence of AC mix stiffness is more significant as the foundation support decreases. In general, for a very large AC thickness, low E* mixtures would tend to show more damage (cracking)." Note that the "very large AC thickness" used in this study is 10 inches.

Influence of AC Thickness

Figure 6-5 shows the influence of AC thickness. Note that AC thickness has a significant influence on all pavement performance predictions. It is also found that thicker AC layers may have larger AC rut depth than that of thinner AC layers, but may have smaller total rut depth since the thicker AC layers lead to smaller rut depth in the base and subgrade layers.
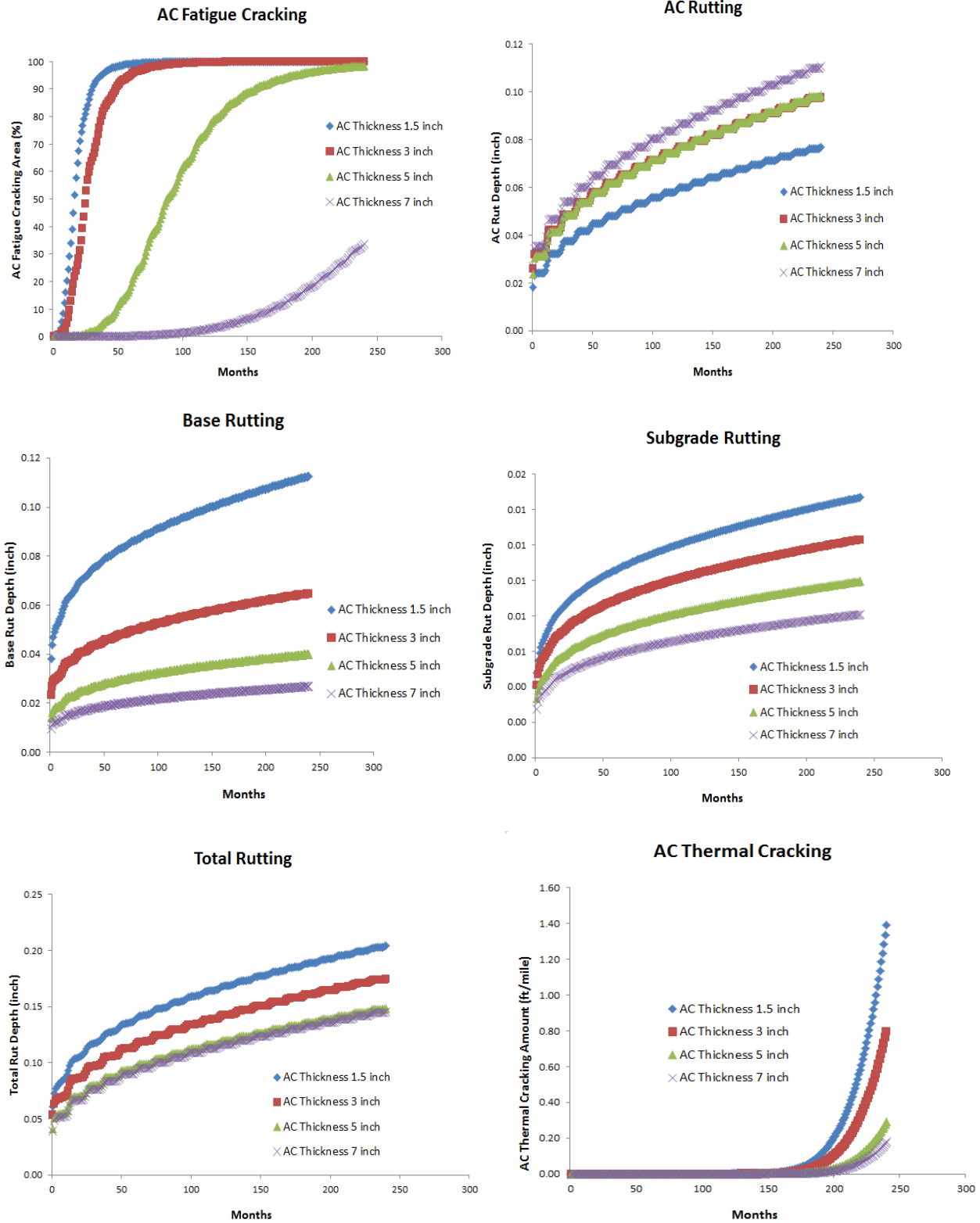
Figure 6-5. Influence of AC Thickness.

Influence of Mix Type

Figure 6-6 shows the influence of AC mix type. Note that AC mix type has significant influence on AC thermal cracking and AC rutting, but it has only a minor influence on base rutting and subgrade rutting. It is reasonable since AC mix type mainly impacts AC layer modulus, AC cracking properties, and AC rutting properties, which have a direct influence on the AC layer's performance but has indirect influence on the other layer's performance.
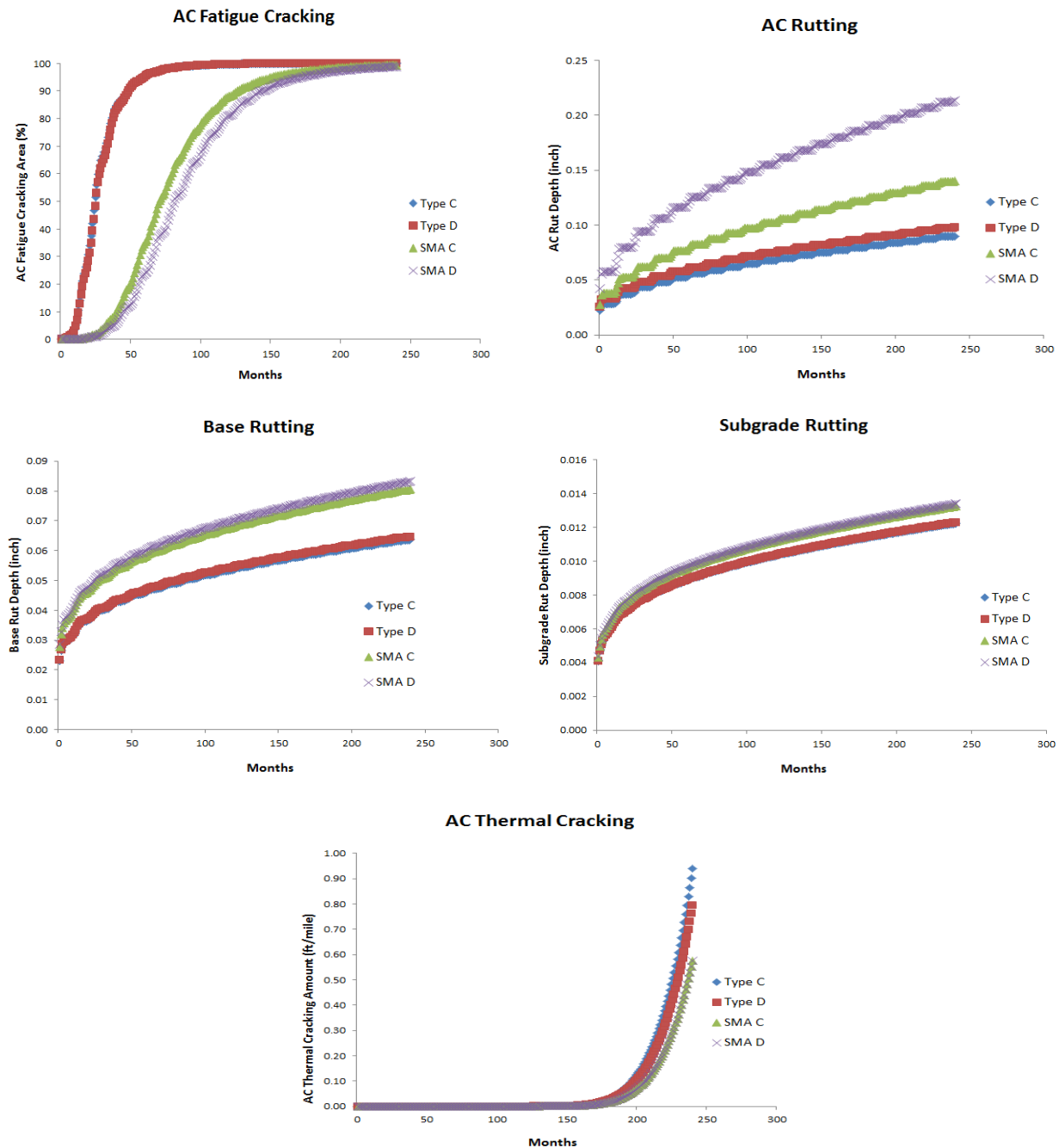
Figure 6-6. Influence of AC Mix Type.

91

Influence of Binder Type

Figure 6-7 shows the influence of AC binder type. Binder type mainly impacts AC layer modulus, AC cracking properties, and AC rutting properties, which have a direct influence on the AC layer's performance but an indirect influence on the other layer's performance. In Figure 6-7, both AC fatigue cracking curves and AC thermal cracking curves are little influenced by binder type; however, it is not always that way. Different pavement structures may show greater difference among different binder types on AC cracking.
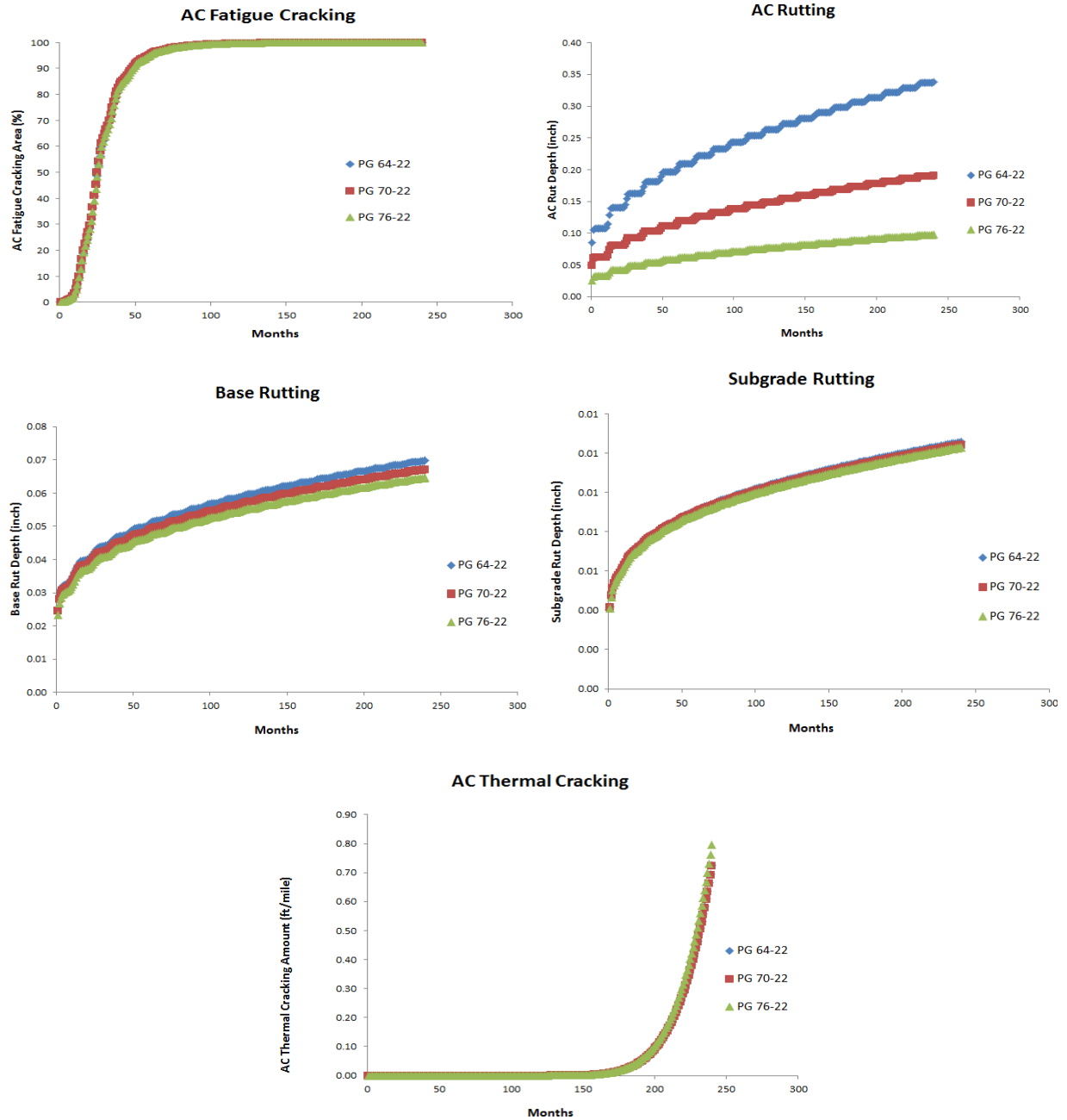
Figure 6-7. Influence of AC Binder Type.

Influence of Base Modulus

Figure 6-8 shows the influence of base modulus. Note that base modulus has significant influence on all pavement performance predictions, except the AC thermal cracking.
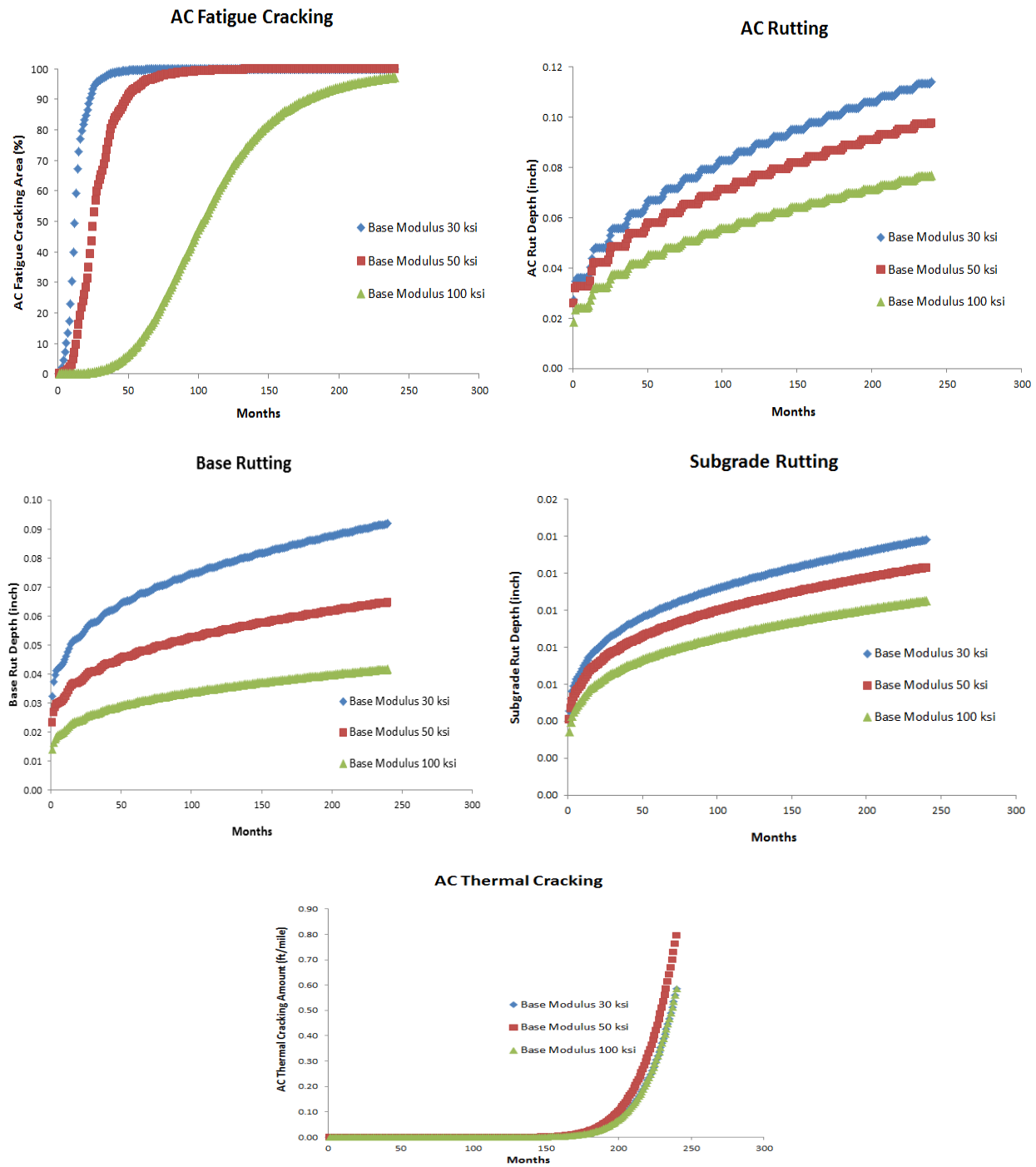
Figure 6-8. Influence of Base Modulus.

Influence of Base Thickness

Figure 6-9 shows the influence of base thickness. Note that base thickness mainly impacts base and subgrade rutting. It also has a minor influence on AC layer performance.
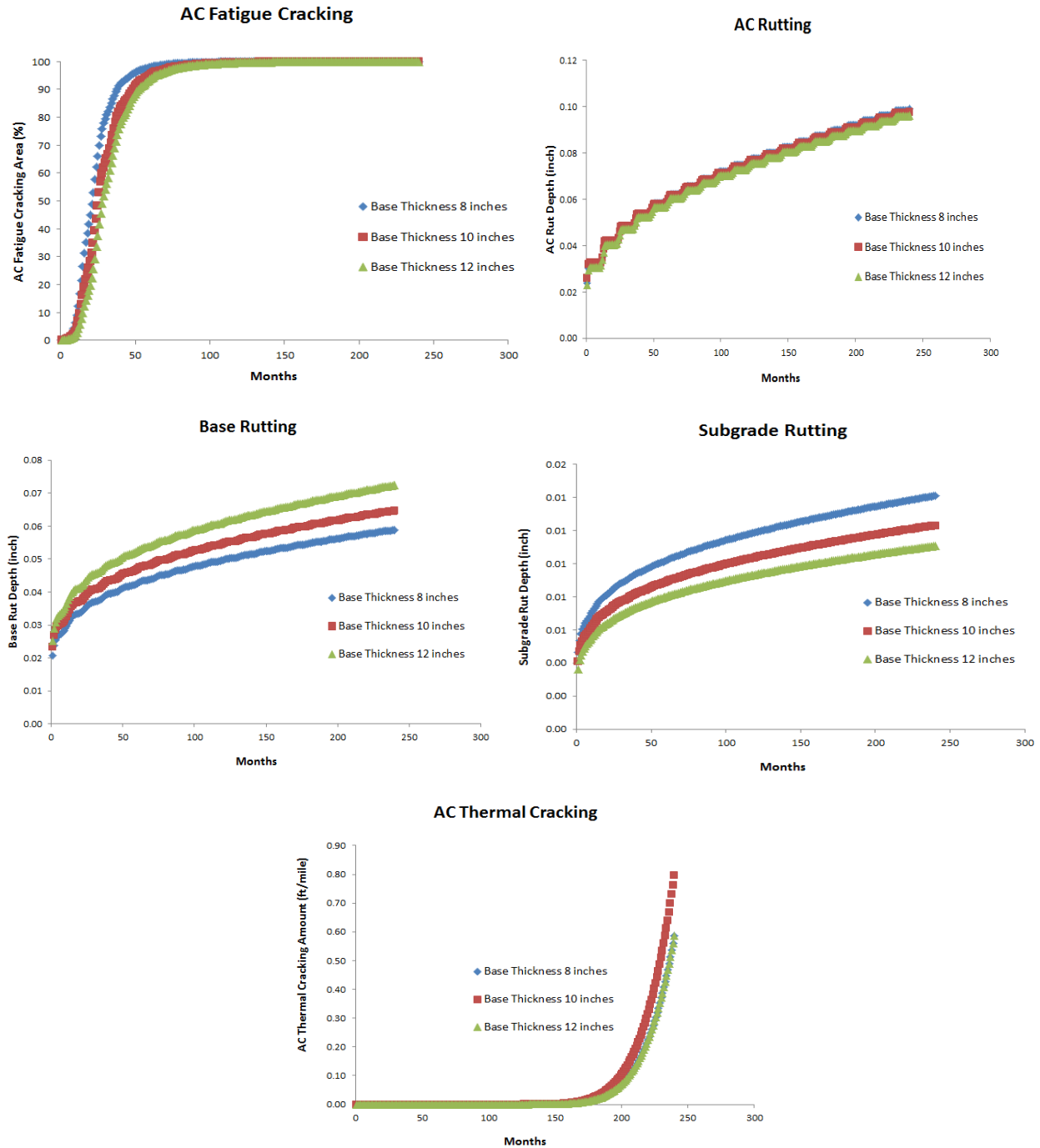
Figure 6-9. Influence of Base Thickness.

Influence of Subgrade Modulus

Figure 6-10 shows the influence of subgrade modulus. The subgrade modulus has significant influence on subgrade rutting but minor influences on other layer performance.
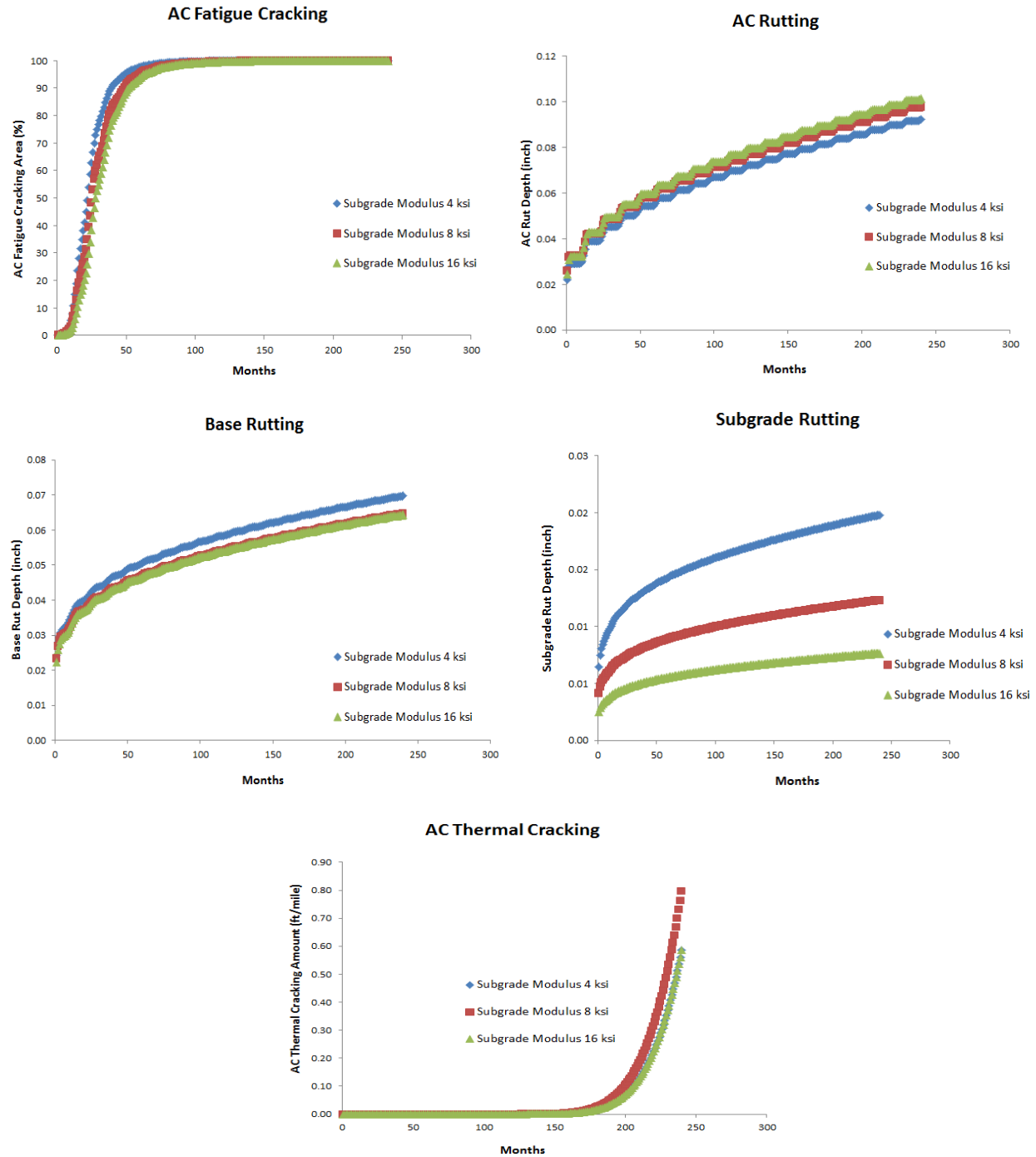
Figure 6-10. Influence of Subgrade Modulus.

Influence of Optimum Moisture Content

The previous sensitivity analysis is based on unbound base or subgrade materials. There is another option to determine the base modulus: users input the modulus at optimum moisture content (M_{opt}) and related base material properties; the TxME program automatically determines

the monthly base/subgrade modulus based on the estimated monthly pavement layer moisture content (obtained from EICM result). The user input interface is presented in Figure 6-11. Obviously, the specific gravity Gs, Maximum dry density γ_{dmax}, and optimum gravimetric moisture content W_{opt} all have influence on the determined base/subgrade modulus.

Figure 6-11. TxME Moisture Consideration in Base/Subgrade Modulus Determination.

As an example, Figure 6-12 shows the influence of W_{opt} of the base layer. It impacts the base modulus and, in turn, has significant influence on all pavement performance predictions, except the AC thermal cracking.
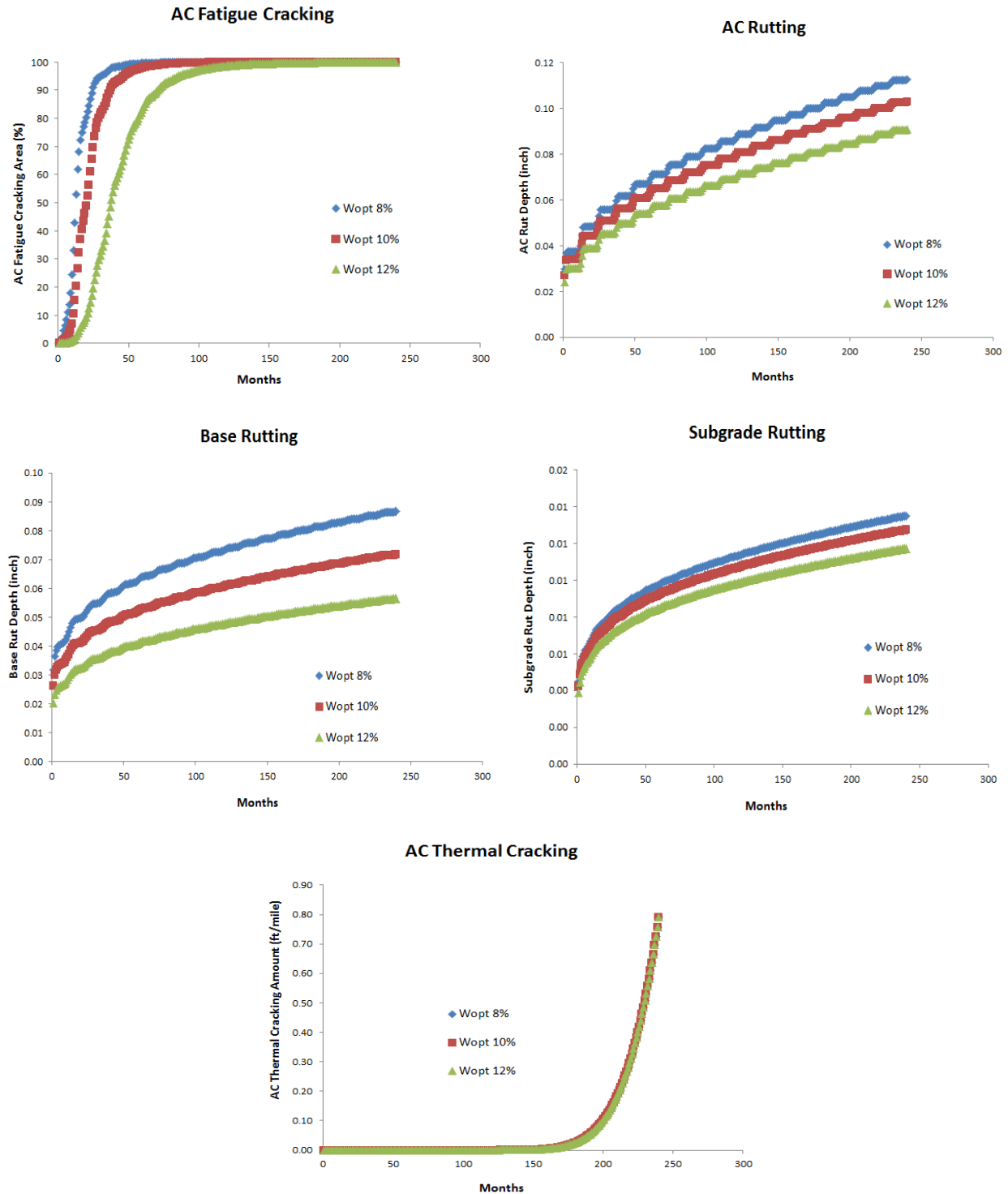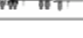
Figure 6-12. Influence of Optimum Moisture Content.

6.2 COMPARISONS OF LOAD SPECTRUM CASES
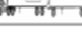
The following makes pilot comparisons among different load spectrum cases. The pavement structure and weather station used to demonstrate these comparisons are the same as Figure 6-1.

6.2.1 Comparisons of Different Vehicle Class Distributions
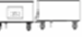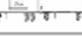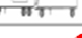
Three types of vehicle class distribution are selected: 1) only class 9, mainly tandem-axle; 2) only class 7, mainly tridem-axle; and 3) all vehicle classes, mixed axles. Figure 6-13 shows their TxME input interfaces, respectively.

Figure 6-13. Selected Vehicle Class Distributions for Comparison.

For each type of vehicle class distribution, the ESALs were determined according to the AASHTO 1993 Guide (AASHTO 1993) recommended equivalent axle load factors. For example, the load factor is 1.38 for a 36 kip tandem axle and 1.66 for a 54 kip tridem axle. So the AADTT inputs were adjusted to make sure that all these three types of vehicle distribution have the same ESALs (10 million during 20 years).

Figure 6-14 shows the comparison results among these different vehicle class distribution cases. The results of traffic input level two (ESALs) are presented in the figure as well. Generally the results are comparable to each other since all these cases have the same ESALs; however, differences among them do exist, which implies the necessity of load spectrum analysis.

99
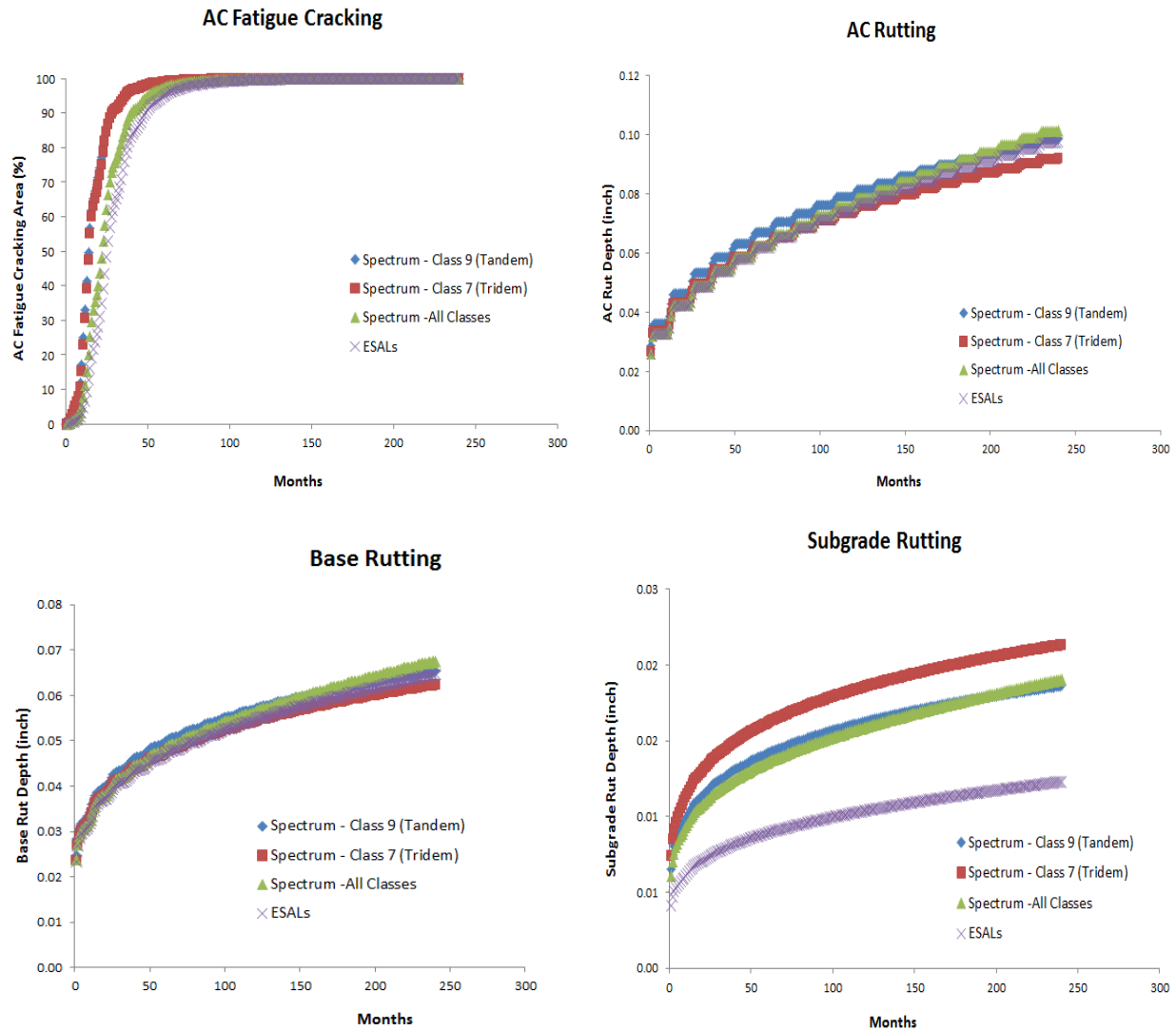
Figure 6-14. Comparison Results of Different Vehicle Class Distributions.

6.2.2 Comparisons of Different Axle Types

Four axle types are selected for comparison: 1) 18 kip single axle (dual tire), 2) 36 kip tandem-axle, 3) 54 kip tridem-axle, and 4) 72 kip quad-axle. Figure 6-15 shows the related "Axles per Truck" input information. The AADTT for all axle load scenarios are the same, which assures that the applied axle repetitions are the same.

Vehicle Class	Steering Axle	Other Single Axle	Tandem Axles	Tridem Axles	Quad Axles
Class 4	0	1	0	0	0
Class 5	0	1	0	0	0
Class 6	0	1	0	0	0
Class 7	0	1	0	0	0
Class 8	0	1	0	0	0
Class 9	0	1	0	0	0
Class 10	0	1	0	0	0
Class 11	0	1	0	0	0
Class 12	0	1	0	0	0
Class 13	0	1	0	0	0

18Kips Single Axle

Vehicle Class	Steering Axle	Other Single Axle	Tandem Axles	Tridem Axles	Quad Axles
Class 4	0	0	1	0	0
Class 5	0	0	1	0	0
Class 6	0	0	1	0	0
Class 7	0	0	1	0	0
Class 8	0	0	1	0	0
Class 9	0	0	1	0	0
Class 10	0	0	1	0	0
Class 11	0	0	1	0	0
Class 12	0	0	1	0	0
Class 13	0	0	1	0	0

36 Kips Tandem-axle

Vehicle Class	Steering Axle	Other Single Axle	Tandem Axles	Tridem Axles	Quad Axles
Class 4	0	0	0	1	0
Class 5	0	0	0	1	0
Class 6	0	0	0	1	0
Class 7	0	0	0	1	0
Class 8	0	0	0	1	0
Class 9	0	0	0	1	0
Class 10	0	0	0	1	0
Class 11	0	0	0	1	0
Class 12	0	0	0	1	0
Class 13	0	0	0	1	0

54 Kips Tridem-axle

Vehicle Class	Steering Axle	Other Single Axle	Tandem Axles	Tridem Axles	Quad Axles
Class 4	0	0	0	0	1
Class 5	0	0	0	0	1
Class 6	0	0	0	0	1
Class 7	0	0	0	0	1
Class 8	0	0	0	0	1
Class 9	0	0	0	0	1
Class 10	0	0	0	0	1
Class 11	0	0	0	0	1
Class 12	0	0	0	0	1
Class 13	0	0	0	0	1

72 Kips Quad-axle

Figure 6-15. Axles per Truck Input Information for Different Axle Types.

Figure 6-16 shows the comparison results of the different axle types. It can be observed that multiple axles cause more damage than single axle; the damage differences among them depend on the distress type and pavement structure.
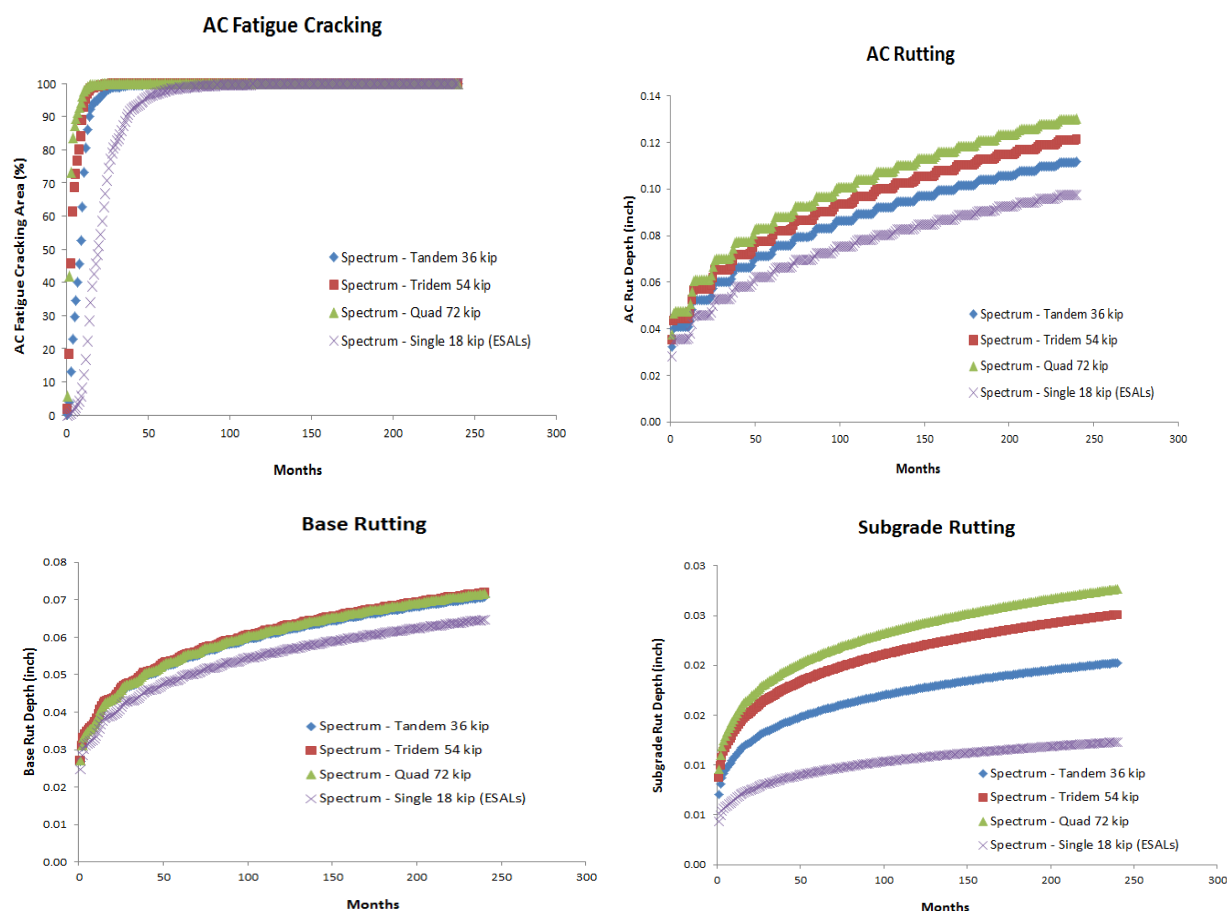
Figure 6-16. Comparison Results of Different Axle Type Scenarios.

101

6.2.3 Comparisons of Different Vehicle Loading Scenarios

Figure 6-17 shows three vehicle loading scenarios of an 18-wheeler (vehicle class 9) for comparison: 1) normal 80 kips, 2) 25 percent overloaded (100 kips), and 3) about 50 percent overloaded (125 kips). The assumed number of passes per day for each scenario is 100, 80, and 64, respectively. Thus the total weight per day for each scenario is the same.

	Tandem Axle Weight (Kips)		Tandem Axle Weight (kips)	Single Axle Weight (kips)	Vehicle Weight (kips)	No. of Passes Per Day	Total Weight Per Day (Kips)
Scenario 1	34		34	12	80	100	8,000
Scenario 2	42		42	16	100	80	8,000
Scenario 3	54		54	17	125	64	8,000

Figure 6-17. Three Vehicle Loading Scenarios.

Figure 6-18 shows the comparison results of the three different scenarios. It can be observed that although the total weight per day for each scenario is the same, the predicted distresses are completely different. The scenarios with overloaded trucks cause much more damage than that with the normally (legally) loaded trucks.
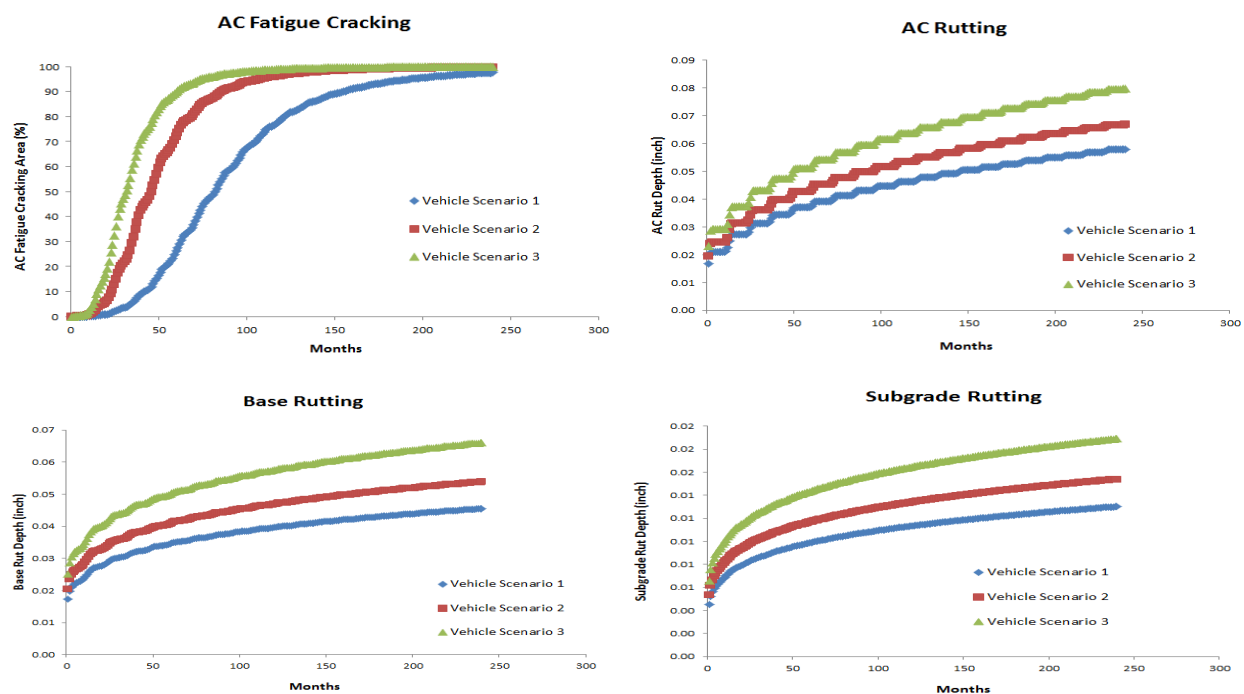
Figure 6-18. Comparison Results of Three Loading Scenarios.

6.3 COMPARISONS ON PERPETUAL PAVEMENT STRAIN DISTRIBUTIONS

For perpetual pavement analysis, TxME has implemented two types of endurance limit analysis:

- When traffic input is in ESALs, the maximum AC bottom tensile strain under the standard 18 kip axle load is determined and compared to a single endurance limit value (the default value is 70 με and can be a users' input).
- When traffic input is a load spectrum, the corresponding AC bottom strain distribution curve under the load spectrum is evaluated and compared to a strain distribution limit curve.

The following demonstrates the different strain distribution curves under different load spectrum cases.

The perpetual pavement structure used for this demonstration is shown in Figure 6-19. Note that the subgrade is assumed to be infinite thickness.
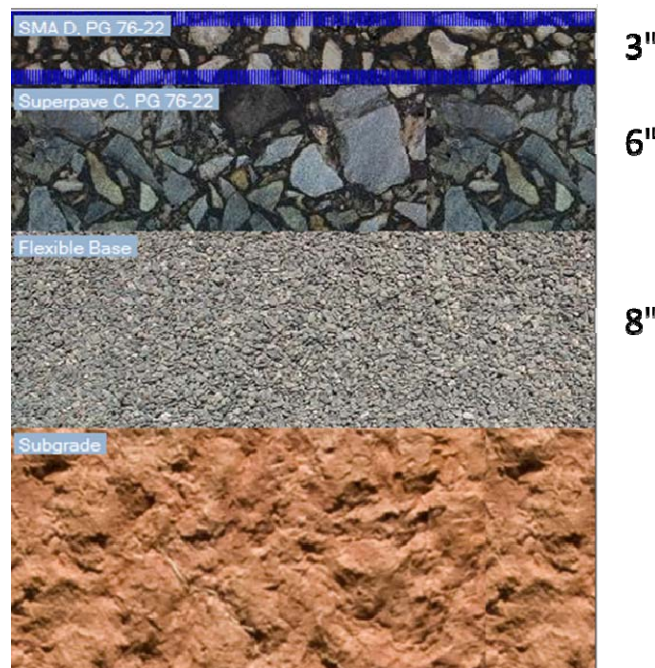
Figure 6-19. Perpetual Pavement Structure.

The load spectrum cases used for demonstration are:

- The vehicle class distribution factor is 10 percent for each vehicle class (class 4 to class 13).
- The vehicle class distribution factor is 100 percent for class 4 and 0 percent for all the others.
- The vehicle class distribution factor is 100 percent for class 13 and 0 percent for all the others.

103

The resulting AC bottom strain distribution curves for each load spectrum case are presented in Figure 6-20. The differences in the strain distribution curves can be observed in this figure.
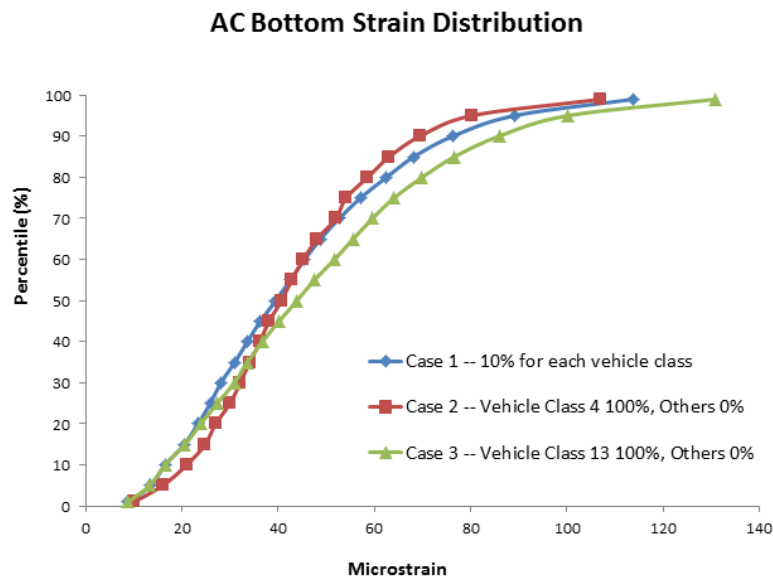
Figure 6-20. AC Bottom Strain Distribution Curves.

6.4 COMPARISONS ON STABILIZED BASE FATIGUE CRACKING

A surface treated pavement with cement stabilized base is used for these comparisons, as shown in Figure 6-21. Note that the surface treated layer thickness is often less than 1 inch and the subgrade is assumed to be infinite thickness.
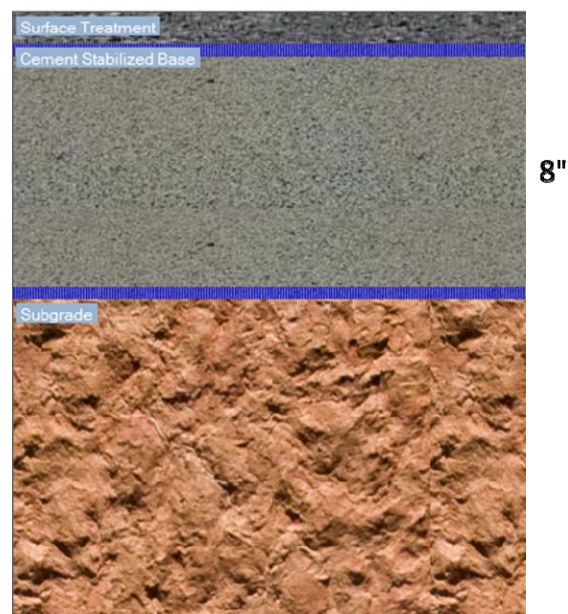
Figure 6-21. Surface Treated Pavement with Cement Stabilized Base.

Several tentative analysis input parameters are listed below. The traffic loading level was assumed to be 10 million ESALs (20 YR), and the climate data from the Austin weather station was used.

- Stabilized Base Modulus: 100ksi, **200ksi**, 300ksi.
- Stabilized Base Modulus of Rupture: 100 psi, **150 psi**, 200psi.
- Stabilized Base Thickness: 6 inches, **8 inches**, 10 inches.
- Subgrade Modulus: 4 ksi, **8 ksi**, 16 ksi.

Note that the "median" value for each parameter above is marked in bold font. TxME will run analyses based on these median values–each time only the value of the investigated parameter varies. The influence of the base modulus, base modulus of rupture, base thickness, and subgrade modulus are presented in the Figures 6-22 to 6-25, respectively. Note that in these cases, stabilized base fatigue cracking is very sensitive to these factors, which sounds reasonable since stabilized base is prone to either crack very soon or not crack at all. However this still needs further validation from field observations.
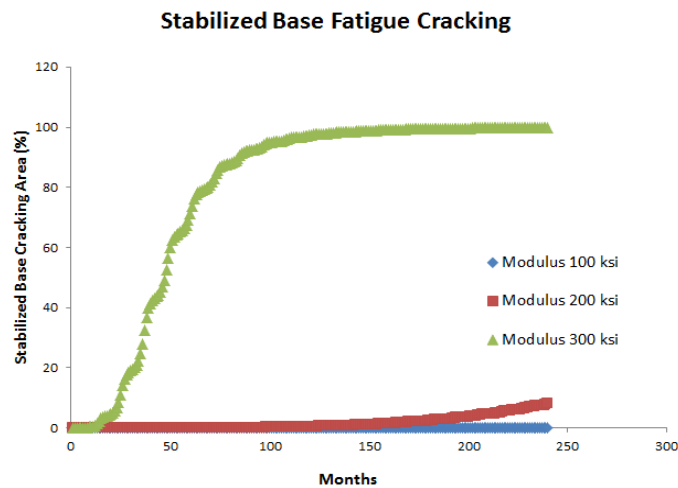
Figure 6-22. Influence of Base Modulus on Stabilized Base Fatigue Cracking.
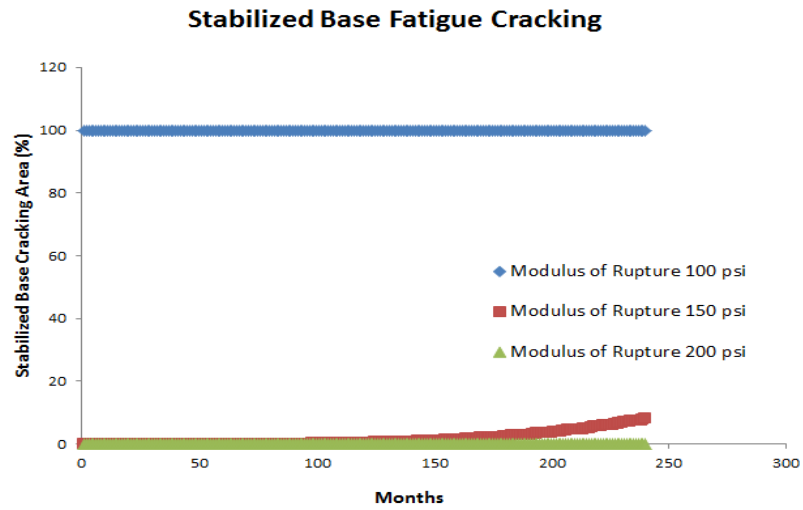
Figure 6-23. Influence of Base Modulus of Rupture on Stabilized Base Fatigue Cracking.
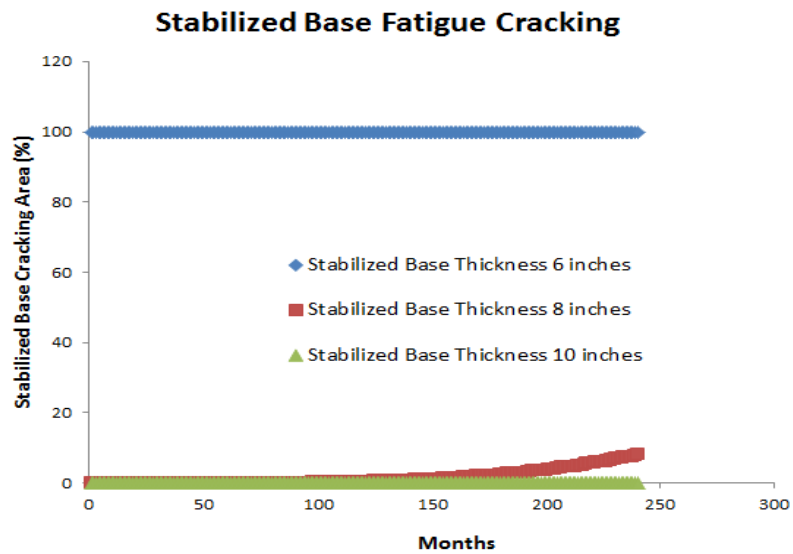
Figure 6-24. Influence of Base Thickness on Stabilized Base Fatigue Cracking.

Stabilized Base Fatigue Cracking
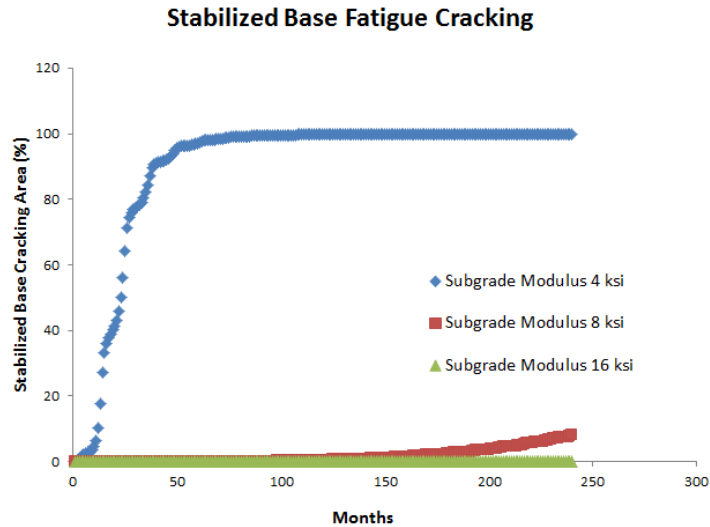
Figure 6-25. Influence of Subgrade Modulus on Stabilized Base Fatigue Cracking.

6.5 SENSITIVITY ON RELIABILITY ANALYSIS

As described in Chapter 5, the reliability level and CV of input parameters have direct impact on the reliability analysis results. The values listed below are used to demonstrate the influence of the reliability level and CV of input parameters.

- Reliability Level: 50 percent, 75 percent, **95 percent**, 99 percent.
- CV of Input Parameters: 5 percent, **15 percent**, 25 percent, 35 percent.

The numbers marked as bold font are the "median" values and the analyses are based on these median values–each time, only the value of the investigated parameter varies.

6.5.1 Comparisons of Different Reliability Levels

The pavement structure shown in Figure 6-1 is selected to perform the comparison among different reliability levels. The investigated variables include ESALs, AC thickness, AC modulus, base thickness, base modulus, subgrade modulus, etc. The mean values of these variables are the same as in Figure 6-1, and the CVs of these variables are all 15 percent. The corresponding comparison results are presented below.

Traffic Input (ESALs) CV 15 Percent

Figure 6-26 shows the reliability analysis results when traffic (ESALs) has a 15 percent CV. It is reasonable that the higher reliability level, the higher predicted distress value. It implies that to design a pavement with higher reliability level, thicker layers (or better materials) have to be considered to lower the predicted distress values.

107

Note that the AC thermal cracking curves at different reliability levels all coincide with each other, since AC thermal cracking has nothing to do with traffic.
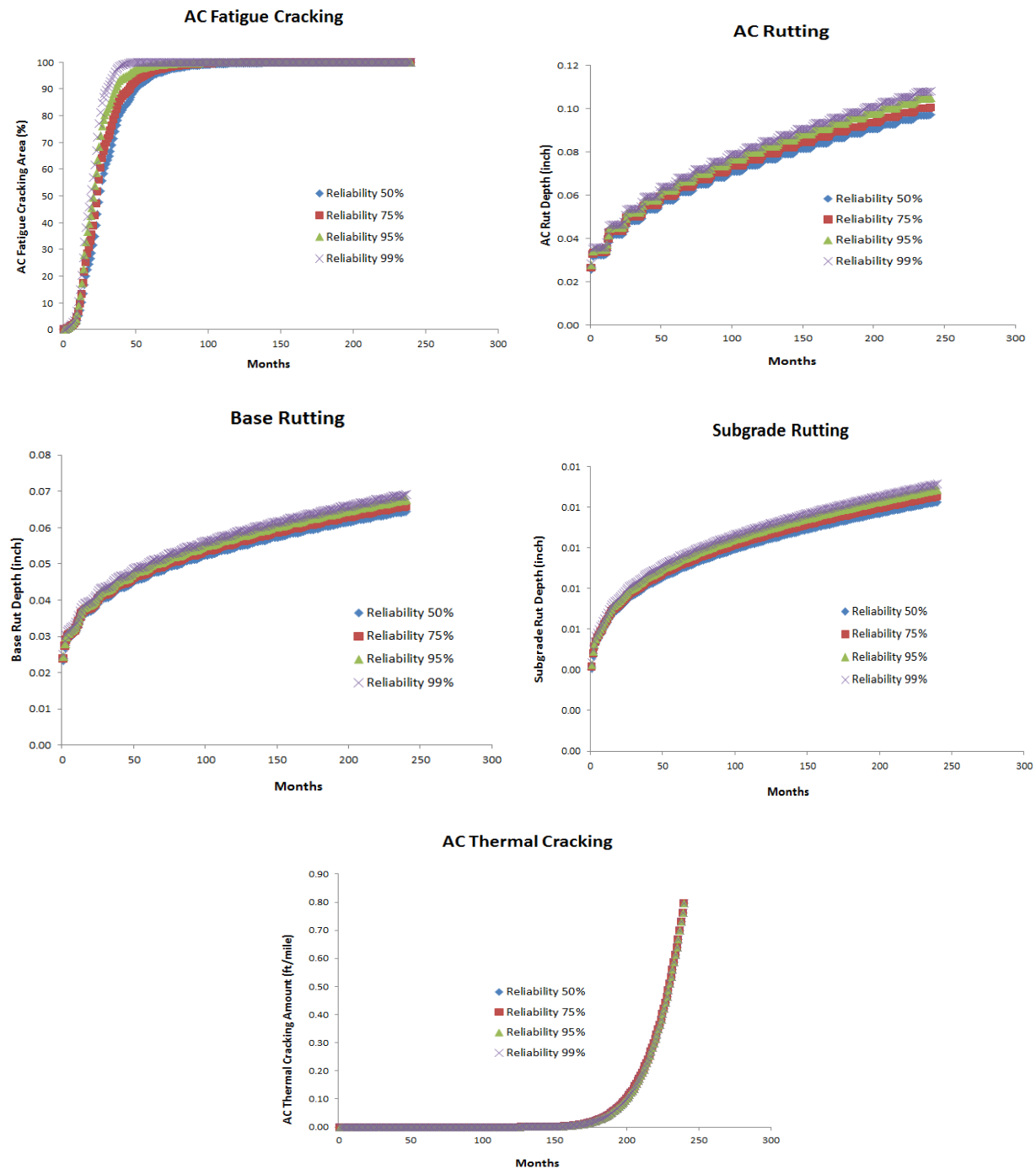
Figure 6-26. Reliability Analysis Results Due to Variability of Traffic (ESALs).

AC Thickness CV 15 Percent

Figure 6-27 shows the reliability analysis results when AC thickness has a 15 percent CV. Again, the higher the reliability level, the higher the predicted distress value.
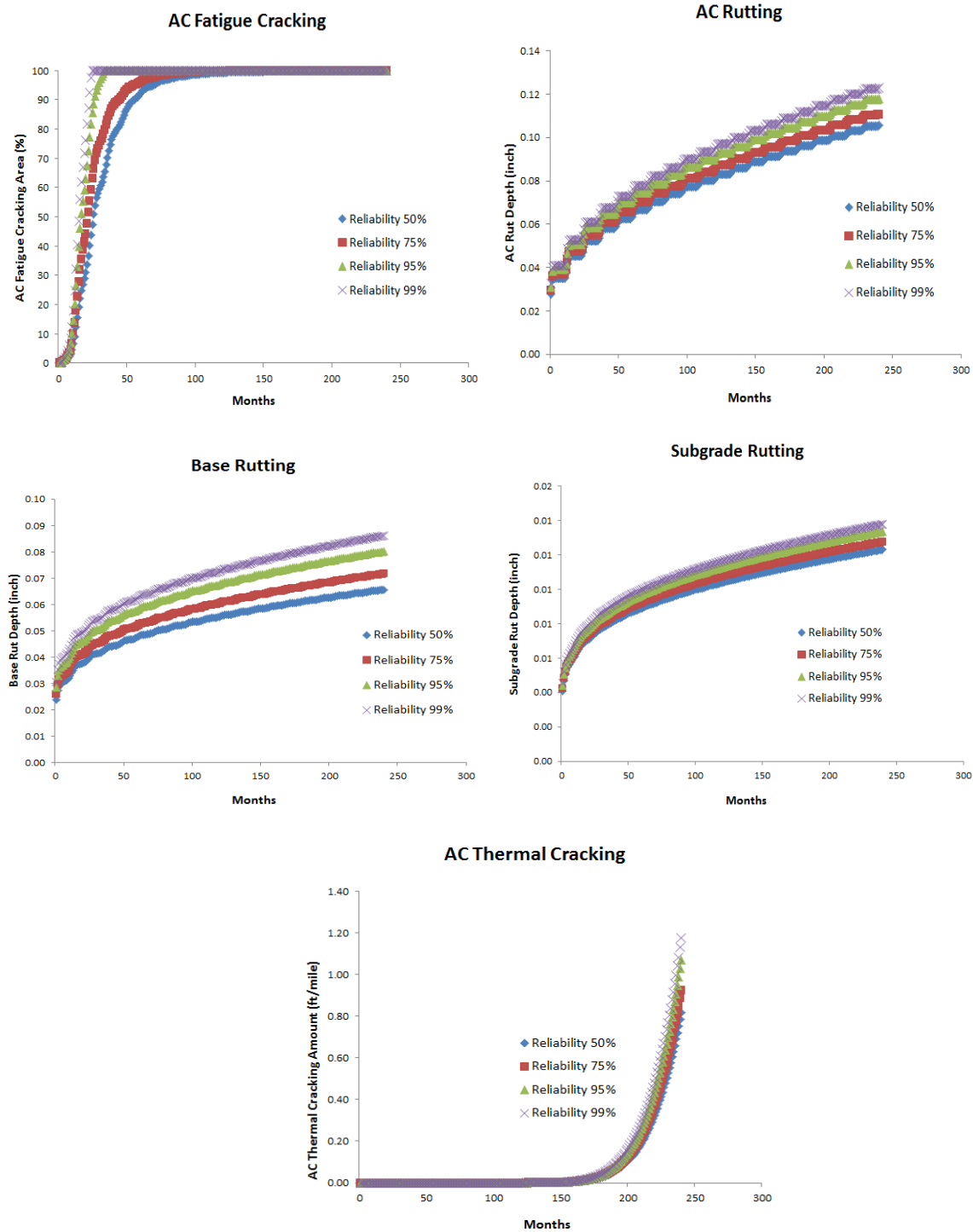
Figure 6-27. Reliability Analysis Results Due to Variability of AC Thickness.

Similar trends have been found when analyzing the other variables such as AC modulus, base thickness, base modulus, subgrade modulus, etc. For reasons of brevity, the corresponding figures are not presented in this report.

To check the TxME capability and processing speed, the researchers also performed the reliability analysis, assuming that all the variables have variability (CV=15 percent) at the same time. The TxME run time was about 4 minutes to complete the analysis and the results are shown in Figure 6-28.
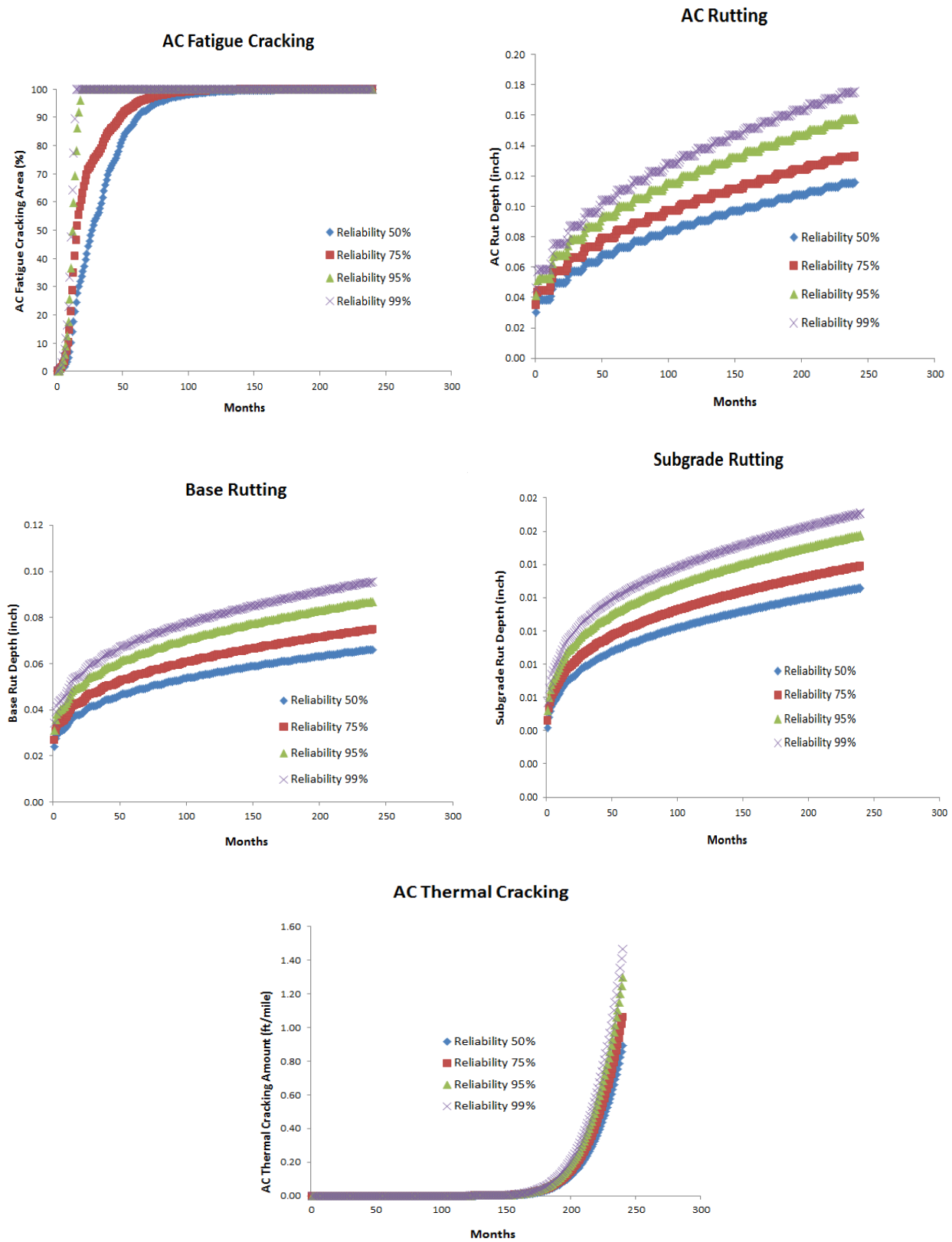
Figure 6-28. Reliability Analysis Results When All Variables Have Variability.

6.5.2 Comparisons of Different CVs

To investigate the impact of CV of each variable, the same pavement structure and the same variables as above are selected. The reliability analyses were performed at the reliability level of 95 percent. As examples, the impact of CV on Traffic Loading and AC Thickness are shown in Figure 6-29 and Figure 6-30, respectively.

The figures show that the higher the variability (CV value), the higher the predicted distress value. It is reasonable since high variability should lead to worse performance for a given climate condition.
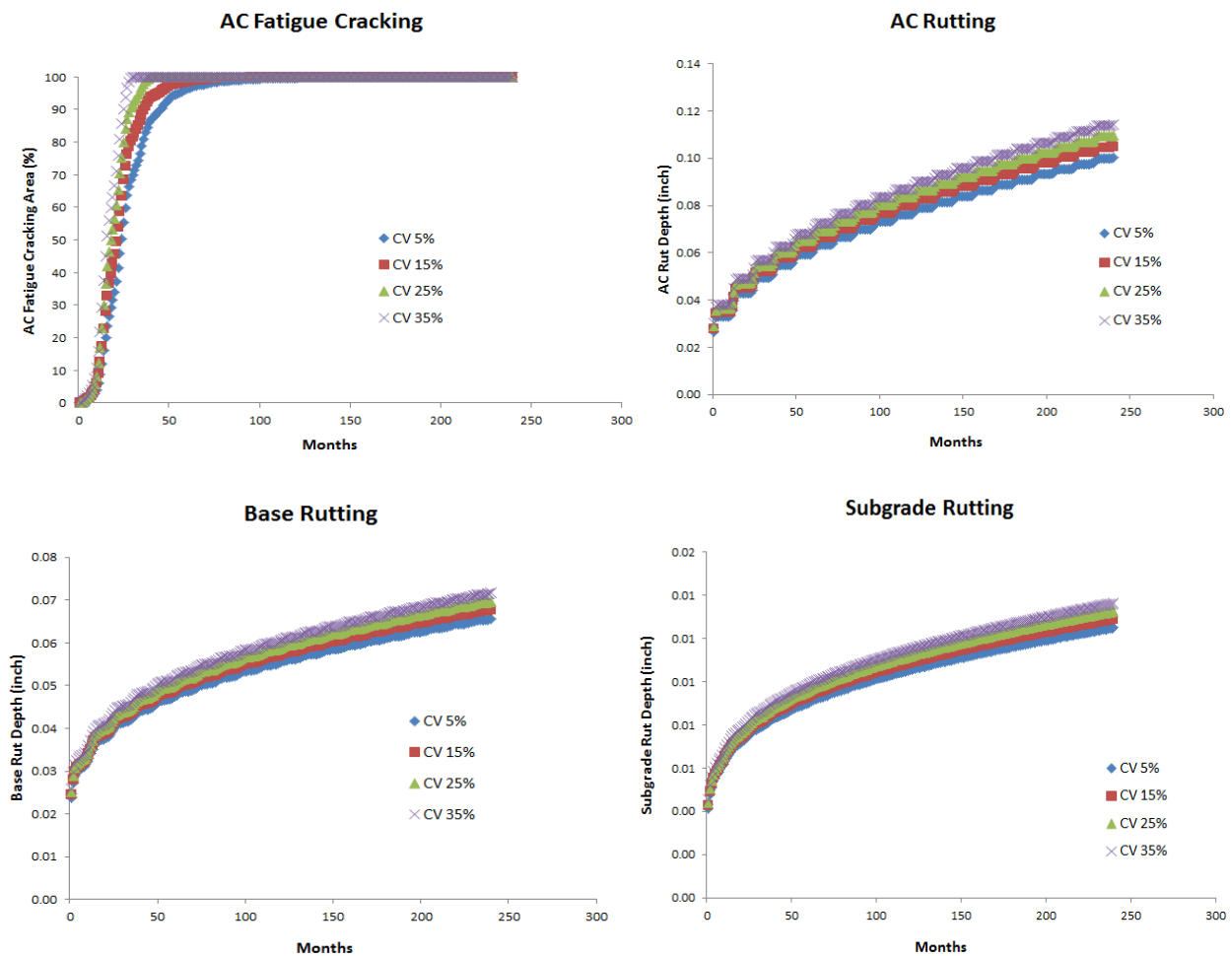
Figure 6-29. Reliability Analysis Results at Different CV of Traffic Loading (ESALs).
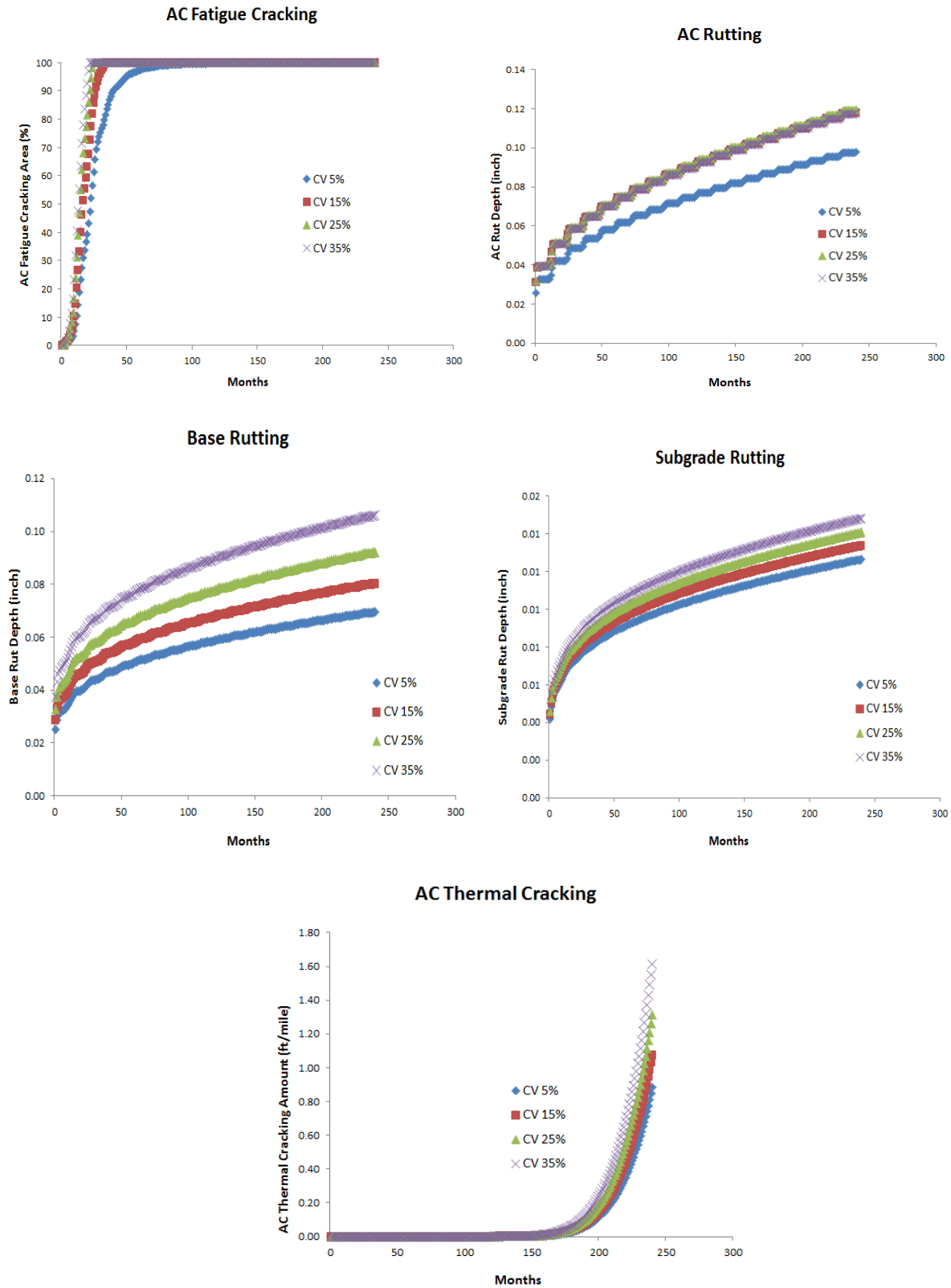
Figure 6-30. Reliability Analysis Results at Different CV of AC Thickness.

6.5.3 Comparisons of Perpetual Pavement Strain Distribution Reliability Analysis Results

The perpetual pavement structure shown in Figure 6-19 is employed to perform the strain distribution reliability analysis. As an example, the second AC layer (Superpave C) thickness is chosen as the parameter with variability. The traffic input is the load spectrum with the default values in the TxME. The corresponding strain distribution reliability analysis results are presented in Figures 6-31 and 6-32.

Note that the figures show that, at a given percentile, the predicted microstrain is higher when the reliability level or the CV value is higher, which is consistent with the previous conclusions.
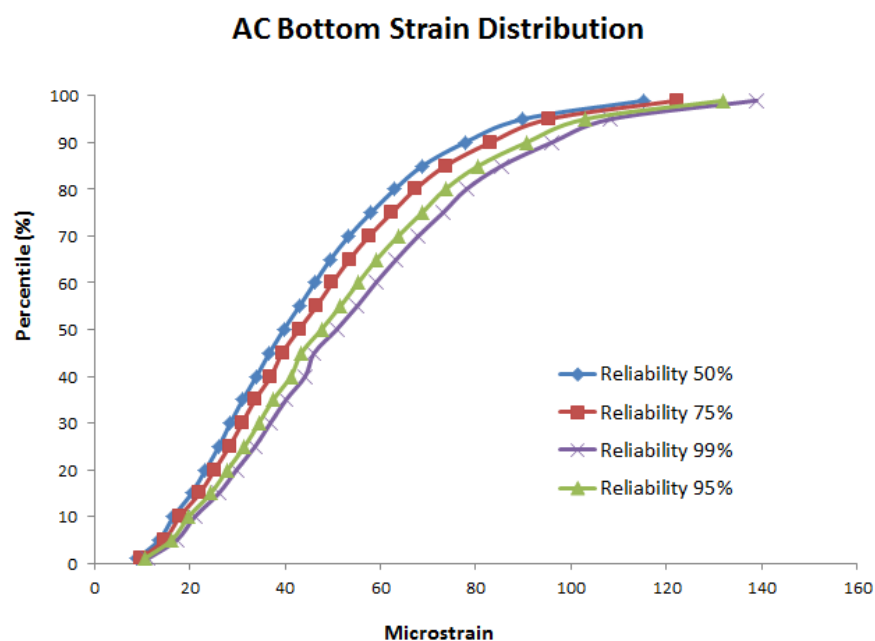
Figure 6-31. Strain Distribution Reliability Analysis Results at Different Reliability Levels.

AC Bottom Strain Distribution
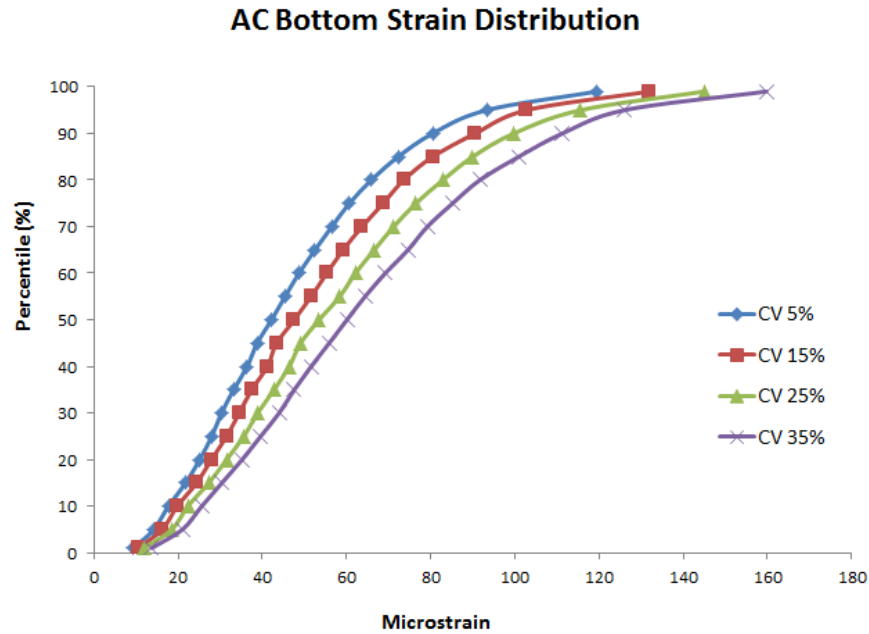
Figure 6-32. Strain Distribution Reliability Analysis Results at Different CV.

6.5.4 Comparisons of Stabilized Base Fatigue Cracking Reliability Analysis Results

To perform the stabilized base fatigue cracking reliability analysis, the surface treated pavement structure shown in Figure 6-21 is employed. As an example, the stabilized base layer thickness is chosen as the parameter with variability. The corresponding stabilized base fatigue cracking reliability analysis results are presented in Figures 6-33 and 6-34.

The figures show the higher the reliability level or the higher the CV value, the higher the predicted stabilized base fatigue cracking area value at the same given time (months).
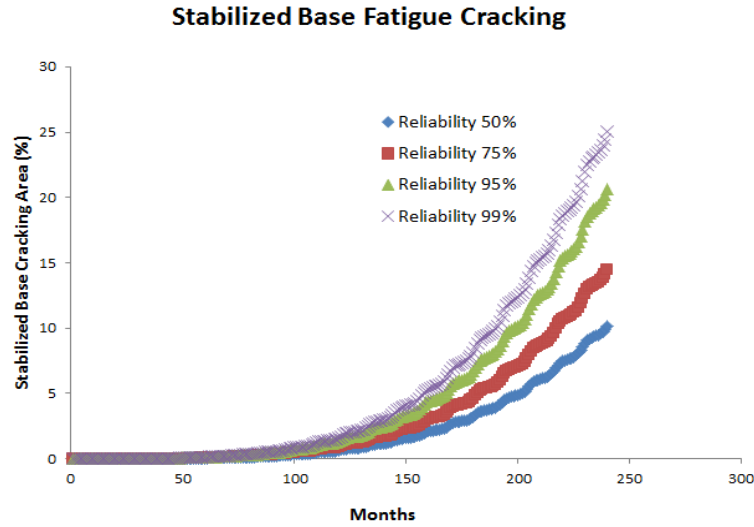
Figure 6-33. Stabilized Base Fatigue Cracking Reliability Analysis Results at Different Reliability Levels.
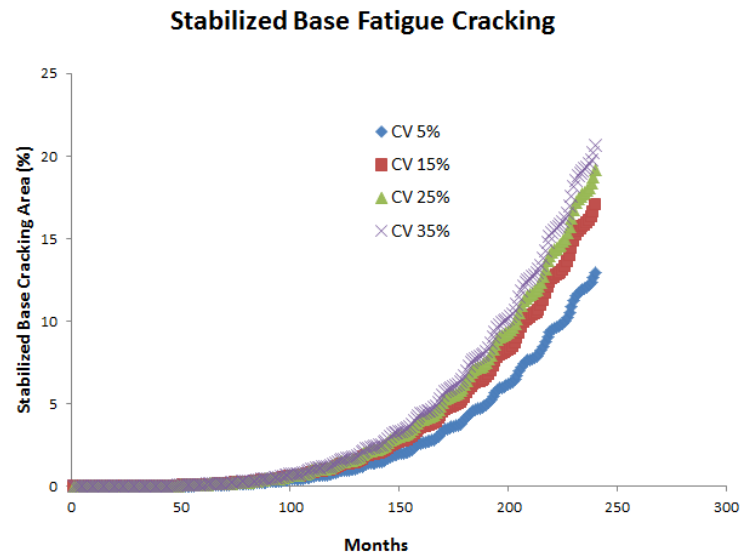
Figure 6-34. Stabilized Base Fatigue Cracking Reliability Analysis Results at Different CV.

6.6 SUMMARY

In accordance with the sensitivity analysis and pilot comparison results, the potential influences of input parameters to the predicted distresses are summarized in Table 6-1. Note that during the sensitivity analysis, the changing of AC mix type and AC binder type corresponds to the changing of AC modulus, AC cracking properties, and AC rutting properties. Also, changing the moisture content of the flexible base corresponds to changing the base modulus.

116

Table 6-1. Potential Influences of Input Parameters to the Predicted Distresses.

	AC Fatigue Cracking	AC Rutting	AC Thermal Cracking	Flexible Base Rutting	Stabilized Base Cracking	Subgrade Rutting	AC Bottom Strain Distribution
Traffic	**	**	/	**	**	**	**
Climate	**	**	**	*	*	*	**
AC Thickness	**	**	**	**	**	**	**
AC Modulus	**	**	**	**	**	**	**
AC Cracking Properties	**	/	**	/	/	/	/
AC Rutting Properties	/	**	/	/	/	/	/
Base Thickness	*	*	*	**	**	*	*
Base Modulus	**	**	*	**	**	**	**
Stabilized Base Modulus of Rupture	/	/	/	/	**	/	/
Subgrade Modulus	*	*	*	*	*	**	*

Note: **–significant influence; *–minor influence; /–no influence.

Other findings and conclusions are listed below.

- For some pavement structures, the predicted AC fatigue cracking in a cold area is less than that in a hot area, which is somewhat counterintuitive. The reason is that the AC fatigue cracking life depends on both the crack initiation life and the crack propagation life. Stiff AC materials (corresponding to the cold area) may have a shorter crack propagation life but a longer crack initiation life than the soft AC materials (corresponding to the hot area), since the AC bottom strain is smaller.
- Pavements with thicker AC layers may have a larger AC rut depth than that of thinner AC layers, but may have a smaller total rut depth since the thicker AC layers lead to smaller rut depth in base and subgrade layers.
- Load spectrum analyses show that multiple axles (i.e., 36 kip tandem axle, 54 kip tridem axle, or 72 kip quad axle) cause more damage than a single axle (i.e., 18 kip single axle). The damage differences among them depend on the distress type and pavement structure.
- The varied vehicle loading scenario comparison results show that although the total weight per day for each scenario is the same, the predicted distresses are completely different. The scenarios with overloaded trucks cause much more damage than that with normally (legally) loaded trucks.

- The stabilized base fatigue cracking prediction results are very sensitive to base modulus, base modulus of rupture, and base thickness, which sounds reasonable since the stabilized base is prone to either crack very soon or not crack at all. However, this still needs further validation from field observations.
- The reliability analysis results show that the higher the reliability level, the higher the predicted distress value. It implies that to design a pavement with higher reliability level, thicker layers (or better materials) have to be considered to lower the predicted distress values.
- The reliability analysis results also show that the higher the variability (CV value), the higher the predicted distress value. This is reasonable since high variability should lead to worse performance when all other conditions are equal.

CHAPTER 7.
CONCLUSIONS AND RECOMMENDATIONS

TxME is developed to enable Texas pavement designers to take full advantage of new or premium materials, with a full consideration of the influential factors including pavement structure, traffic volume, and environmental condition. The main features of TxME include:

- Mechanistic-Empirical modeling.
- Performance-based material characterization.
- Traffic load spectrum incorporation.
- Design input variability- based reliability methodology.
- Incremental distress prediction.
- Fast running speed.
- Friendly user interface.
- Convenient connection with relevant FPS inputs and thickness outputs.

This report mainly focuses on how the M-E models, load spectrum methodologies, and reliability approaches are implemented into the TxME program. Sensitivity analyses are also performed to analyze the impact of design input levels and demonstrate the advantages of the TxME.

Based on the work presented in the previous chapters, the conclusions and recommendations are provided below.

7.1 SUMMARIES AND CONCLUSIONS

The summaries and conclusion are listed in the following:

- Three types of flexible pavement structures and corresponding performance predictions can be handled in the TxME, which include:
  - Surface treated pavement, with predictions of:
    - Granular base rutting (for pavements with granular base).
    - Stabilized base fatigue cracking (for pavements with stabilized base).
    - Subgrade rutting.
  - Conventional or thin HMA, with predictions of:
    - AC rutting.
    - AC fatigue cracking.
    - AC thermal cracking.
    - Granular base rutting (for pavements with granular base).
    - Stabilized base fatigue cracking (for pavements with stabilized base).
    - Subgrade rutting.
  - Perpetual pavement, with predictions of:
    - AC rutting.

- AC thermal cracking.
- Granular base rutting (for pavements with granular base).
- Subgrade rutting.
- Endurance limit.

- TxME provides a seamless tie with FPS 21 to conduct the performance check for each FPS 21 recommended design option. The information of each design option is automatically imported from FPS 21 into TxME and the benefits of improved base materials or superior asphalt mixes can then be determined by TxME. In addition, TxME will predict the impact of climate and axle load spectrum on the performance of the structure.

- The report describes the implementation methods, models, and preliminary calibrations, which are listed below. No doubt all these calibrations need to be further validated and refined based on Texas field data.
  - Asphalt layer rutting model, calibrated by NCAT test track data.
  - Asphalt layer fatigue cracking model, calibrated by NCAT test track data.
  - Granular base and subgrade rutting model, calibrated by several APT test results and trench studies.
  - Asphalt layer thermal cracking model, preliminarily calibrated by Lamount test road data.
  - Stabilized base fatigue cracking model, temporarily adopting MEPDG calibration factors.
  - Perpetual pavement endurance limit model, not calibrated.

- The report describes the methodologies of incorporating axle load spectrum into the TxME, which includes how to determine the monthly axle applications and how to apply these axle applications in performance predictions. The equations and algorithms are provided for each specific performance prediction such as AC fatigue cracking, rutting (AC rutting, granular base/subgrade rutting), and stabilized base fatigue cracking.

- TxME incorporates the reliability concept to address uncertainties and variation issues in pavement design. This report describes the implementation approach of Rosenblueth's $2n+1$ (n is number of variables with uncertainty) method, which has high practical benefit for reliability analysis of flexible pavement designs.

- This report conducts sensitivity analysis by running several factorial combinations of the input parameters and some pilot comparisons through TxME. This information will help to identify the input parameters that appear to substantially influence predicted performances. The sensitivity analyses conducted include:
  - Factorial combinations of AC/Granular base/Subgrade Rutting and AC Fatigue/Thermal Cracking, based on a conventional pavement with a flexible base.
  - Pilot comparisons on the impact of performance predictions using alternate axle load spectrum, for the same conventional pavement structure.

- o Pilot comparisons on endurance limit trends by varying the axle load spectra and resulting strain distributions for a perpetual pavement.
- o Pilot comparisons on stabilized base fatigue cracking, based on a surface treated pavement with a stabilized base.
- o Factorial combinations on reliability based analyzing, varying reliability inputs, using pavement structures previously described.
- According to the sensitivity analyses and pilot comparison results, the following findings and conclusions are made:
  - o Traffic loading (ESALs or load spectrum) has significant influence on all the predicted distresses except the AC thermal cracking, since thermal cracking model has nothing to do with traffic.
  - o Climate has significant influence on AC layer performance, while it has minor influence on base rutting and subgrade rutting. This is reasonable since climate mainly impacts AC layer modulus and cracking/rutting properties, which have a direct influence on AC layer performance but has an indirect influence on the other layers' performance.
  - o For some pavement structures the predicted AC fatigue cracking in a cold climate is less than that in a hot climate, which is somewhat couterintuitive. The reason is that the AC fatigue cracking life depends on both the crack initiation life and the crack propagation life; stiff AC materials (corresponding to a cold climate) may have shorter crack propagation life but longer crack initiation life than that of soft AC materials (corresponding to a hot climate), since the AC bottom strain is smaller.
  - o AC thickness has significant influence on all pavement performance predictions. It is also found that pavements with thicker AC layers may have larger AC rut depth than that of thinner AC layers, but may have smaller total rut depth since the thicker AC layers lead to smaller rut depth in the base and subgrade layers.
  - o Both AC mix type and asphalt binder type have significant influence on AC thermal cracking and AC rutting, but has only a minor influence on base rutting and subgrade rutting. This is reasonable since the AC mix type/binder type mainly impacts AC layer modulus, AC cracking properties, and AC rutting properties, which have a direct influence on the AC layer's performance but have indirect influence on the other layer's performance.
  - o Base modulus has significant influence on all pavement performance predictions, except the AC thermal cracking; while base thickness mainly impacts base and subgrade rutting and has minor influence on AC layer performance.
  - o The subgrade modulus has significant influence on subgrade rutting but minor influences on other layers' performance.
  - o Load spectrum analyses show that multiple axles (i.e., 36 kip tandem axle, 54 kip tridem axle, or 72 kip quad axle) cause more damage than single axle (i.e., 18 kips

121

single axle); the damage differences among them depend on the distress type and pavement structure.

o The vehicle load spectrum distribution scenario comparison results show that although the total weight per day for each scenario is the same, the predicted distresses are completely different. The scenarios with overloaded trucks cause much more damage than that with normally (legally) loaded trucks.

o The stabilized base fatigue cracking prediction results are very sensitive to base modulus, base modulus of rupture, and base thickness, which sounds reasonable since the stabilized base is prone to either cracking very soon or not cracking at all. However this still needs further validation from field observations.

o The reliability analysis results show that the higher the reliability level, the higher the predicted distress value. It implies that to design a pavement with a higher reliability level, thicker layers (or better materials) have to be considered to lower the predicted distress values.

o The reliability analysis results also show that the higher the variability (CV value), the higher the predicted distress value. It is reasonable since high variability should lead to worse performance, given that all other conditions remain the same.

7.2 RECOMMENDATIONS

Overall, the TxME developed in this study offers great promise for accurately predicting distresses for flexible pavements. The software is user-friendly and available to TxDOT pavement engineers; its prediction is rational and reasonable. Therefore, it is strongly recommended to:

▪ Use TxME to evaluate pavement rehabilitation designs for oil and gas development locations, since considering the influence of overloaded truck is very important to the success of these pavement designs.

▪ Use TxME for implementation in select candidate districts, and to develop additional typical default values for asphalt mixes, granular bases, stabilized bases, and subgrade soils within those districts.

▪ Use TxME to perform design checks for FPS 21 solutions for state-wide implementation, and to conduct further performance calibrations based on Texas field data.

REFERENCES

AASHTO Guide for Design of Pavement Structures, American Association of State Highway and Transportation Officials, 1993.

AASHTO TP62-03, *Standard Method of Test for Determining Dynamic Modulus of Hot-Mix Asphalt Concrete Mixtures*, 2003.

AASHTO T180, *Standard Method of Test for Moisture-Density Relations of Soils Using a 4.54-kg (10-lb) Rammer and a 457-mm (18-in.) Drop*, 2004.

AASHTO T100, *Standard Method of Test for Specific Gravity of Soils*, 2010a.

AASHTO T99, *Standard Method of Test Moisture-Density Relations of Soils Using a 2.5-kg (5.5-lb) Rammer and a 305-mm (12-in.) Drop*, 2010b.

Bagowsky, I. *Reliability Theory and Practice*, Prentice Hall, Englewood Cliffs, New Jersey, 1961.

Bonaquist, R., and D. W. Christensen, Practical Procedure for Developing Dynamic Modulus Master Curves for Pavement Structural Design. In *Transportation Research Record: Journal of the Transportation Research Board*, No. 1929, Transportation Research Board of the National Academies, Washington, D.C., 2005, pp. 208–217.

Brademeyer, B. D. *Flexible Pavement Systems: An Analysis of the Structural Subsystem's Deterioration,* Master of Science Thesis, Massachusetts Institute of Technology, February 1975.

Darter, M., L. Khazanovich, T. Yu, and J. Mallela. Reliability Analysis of Cracking and Faulting Prediction in the New Mechanistic-Empirical Pavement Design Procedure, In *Transportation Research Record: Journal of the Transportation Research Board*, No. 1936, pp. 150–160, 2005.

Dunn, L. and J. Gavin. *The C-Sharp Lamont Test Road Five Years of Performance Monitoring*, Proceedings of the 8th International Conference on Asphalt Pavements, Seattle, Washington, pp.487–506, 1997.

El-Basyouny, M. and M. W. Witczak. Verification of the Calibrated Fatigue Models for the 2002 Design Guide, *Proceedings of the Association of Asphalt Paving Technologists*, Vol. 74; 2005.

Hu, S., F. Zhou, and T. Scullion. *Thermal Reflective Crack Propagation,* International Conference on Advanced Characterization of Pavement and Soil Engineering Materials, Athens, Greece, Vol. 2, pp. 1173–1182, 2007.

Hu, S., X. Hu, F. Zhou., and L. Walubita. SA-CrackPro: A New Finite Element Analysis Tool for Pavement Crack Propagation, In *Transportation Research Record: Journal of the Transportation Research Board*, No.2068, pp. 10–19, 2008.

Hu, S., F. Zhou, and L. F. Walubita. Development of a viscoelastic finite element tool (*VE2D*) tailored for asphalt pavement low temperature cracking analysis, the *International Journal on Road Materials and Pavement Design (IJRMPD)*, Vol. 10, pp. 833–858, 2009.

Hu, S. and F. Zhou. New Interconversion Tool for HMA Linear Viscoelastic Functions, *Canadian Journal of Civil Engineering*, Vol. 37, pp. 1071–1081, 2010a.

Hu, S., F. Zhou, and T. Scullion. Reflection Cracking-Based Asphalt Overlay Thickness Design and Analysis Tool, In *Transportation Research Record: Journal of the Transportation Research Board*, No. 2155, pp. 12–23, 2010b.

Hu, S., X. Hu, F. Zhou, and L. Walubita. Development, Calibration, and Validation of a New M-E Rutting Model for HMA Overlay Design and Analysis, *Journal of Materials in Civil Engineering*, Vol. 23, pp. 89–99, 2011.

Hu, S., F. Zhou, and T. Scullion. *Texas M-E Flexible Pavement Design System: Literature Review and Proposed Framework*, 0-6622-1, Texas Transportation Institute, College Station, TX, USA, http://tti.tamu.edu/documents/0-6622-1.pdf, 2012a.

Hu, S., F. Zhou, T. Scullion, and J. Leidy. Calibrating and Validating Overlay Tester-Based Fatigue Cracking Model with Data from National Center for Asphalt Technology, In *Transportation Research Record: Journal of the Transportation Research Board*, No. 2296, pp. 57–68, 2012b.

Hu, S., F. Zhou, and T. Scullion. *Implementation of Texas Asphalt Concrete Overlay Design System*, FHWA/TX-12/5-5123-03-1, Texas Transportation Institute, College Station, Texas, USA, http://tti.tamu.edu/documents/5-5123-03-1.pdf, 2013.

Huang, Y. H. *Pavement Analysis and Design, Second Edition*, Pearson Education, Inc., Upper Saddle River, New Jersey, 2004.

Kenis, W. J. *An Interim Design Method for Flexible Pavements Using the VESYS Structural Subsystem*, FHWA Report, RD-77-154, 1978.

Levenberg, K. A method for the solution of certain problems in least squares, *Quarterly Applied Mathematics*, 2: pp. 164–168, 1944.

Li, X., and R. C. Williams. A Practical Dynamic Modulus Testing Protocol, *Journal of Testing and Evaluation*, Vol. 40, No. 1, 2011.

Liu, W. and T. Scullion. *MODULUS 6.0 for Windows: User's Manual*, Report No. FHWA/TX-05/0-1869-2, Texas Transportation Institute, Texas A&M University, College Station, Texas, 2001.

Liu, W. and T. Scullion. *Flexible Pavement Design System FPS 19W: User's Manual (Reprint)*, TxDOT Research Report 0-1869-1, Texas Transportation Institute, Texas A&M University System, 2006.

Lytton, R. L., F. Tsai, S. Lee, R. Luo, S. Hu, and F. Zhou. *Models for Predicting Reflection Cracking of Hot-Mix Asphalt Overlays*, TRB's National Cooperative Highway Research Program (NCHRP) Report 669, 2010.

Marquardt, D. An algorithm for least-squares estimation of nonlinear parameters, *SIAM Journal on Applied Mathematics*, 11: pp. 431–441, 1963.

Maupin, G. W. and J. R. Freeman. *Simple Procedure for Fatigue Characterization of Bituminous Concrete*, Final Report No. FHWA-RD-76-102, Federal Highway Administration, Washington, D.C., 1976.

Moavenzadeh, F. and J. F. Elliott. *Moving Load on Viscoelastic Layered Systems*, Civil Engineering Department, MIT, Cambridge, Massachusetts, 1968.

Monismith, C. L. and D. B. McLean. Structural Design Considerations, *Proceedings of the Association of Asphalt Paving Technologists*, Vol. 41, 1972.

Navarro, E., J. Garibay, I. Abdallah, and S. Nazarian. *Development of Models to Estimate Modulus and Permanent Deformation of Texas Bases*, Technical Memorandum 0-6622-4a, Center for Transportation Infrastructure Systems, the University of Texas at El Paso, Texas, 2012.

NCHRP, *Guide for Mechanistic-Empirical Design of Pavement Structures*, NCHRP Project 1-37A, National Cooperative Highway Research Program, Washington, D.C., 2004.

Nishizawa, T., S. Shimeno, and M. Sekiguchi. Fatigue Analysis of Asphalt Pavements with Thick Asphalt Mixture Layer, *Proceedings of the 8th International Conference on Asphalt Pavements*, Vol. 2, University of Washington, Seattle, Washington, pp. 969–976, August 1997.

Nunn, M. Long-Life Flexible Pavement, *Proceedings of the 8th International Conference on Asphalt Pavements*, Seattle, Washington, 1997.

Park, S.W. and R. A. Schapery. Methods of interconversion between linear viscoelastic material functions, Part I: A numerical method based on Prony series. *International Journal of Solids and Structures*, 36: pp. 1653–1675, 1999.

Priest, A. L. *Calibration of Fatigue Transfer Functions for Mechanistic-Empirical Pavement Design,* Master's Thesis, Auburn University, Auburn, Alabama, 2005.

Prowell, B. D., E. R. Brown, R. M. Anderson, J. S. Daniel, H. Von Quintus, S. Shen, S. H. Carpenter, S. Bhattacharjee, and S. Maghsoodloo. *Endurance Limit of Hot Mix Asphalt Mixtures*

to Prevent Fatigue Cracking in Flexible Pavements, NCHRP Report 646, Transportation Research Board, National Academy of Science, Washington, D.C., July 2010.

Romanoschi, S. A., A. J. Gisi, M. Portillo, and C. Dumitru. The First Findings from the Kansas Perpetual Pavements Experiment, *Transportation Research Board 2008 Annual Meeting*, CD-ROM, 2008.

Rosenblueth, E. Point Estimates for Probability Moments, In *Proceedings of National Academic of Science*, USA, 72(10): pp. 3812–3814, 1975.

Scullion, T., J. Uzan, S. Hilbrich, and P. Chen. *Thickness Design System for Pavements Containing Soil Cement Bases*, Research Report 400381-1, Texas Transportation Institute, Texas A&M University, College Station, Texas, July 2006.

Ullidtz, P., J. T. Harvey, I. Basheer, D. Jones, R. Wu, J. Lea, and Q. Lu. CalME, a Mechanistic–Empirical Program to Analyze and Design Flexible Pavement Rehabilitation. In *Transportation Research Record: Journal of the Transportation Research Board*, No. 2087, Transportation Research Board of the National Academies, Washington, D.C., pp. 143–152, 2010.

White, H. *Artificial Neural Networks: Approximation and Learning Theory*, Blackwell Publishers, Cambridge, Massachusetts, 1992.

Willis, J. R. *Field-Based Strain Thresholds for Flexible Perpetual Pavement Design,* Doctoral Dissertation, Auburn University, Auburn, Alabama, 2008.

Witczak, M. W., R. Roque, D. R. Hiltunen, and W. G. Buttlar. *Project Report NCHRP Project 9-19: Modification and Re-Calibration of Superave Thermal Cracking Model*, Arizona State University, Tempe, Arizona, 2000.

Wu, Z., S. Hu, and F. Zhou. Prediction of Stress Intensity Factors in Pavement Cracking with Neural Networks Based on Semi-analytical FEA, *Expert System with Applications*, 2013.

Yang, Y., X. Gao, W. Lin, D. H. Timm, A. L. Priest, G. A. Huber, and D. A. Andrewski. *Perpetual Pavement Design in China,* International Conference on Perpetual Pavement, Ohio Research Institute for Transportation and the Environment, 2005.

Zhao, Y., W. Liu, and Y. Tan. Analysis of Critical Structure Responses for Flexible Pavements in NCHRP 1-37A Mechanistic-Empirical Pavement Design Guide, *J. Transp. Eng.*, 138(8), pp. 983–990, 2012.

Zhou, F. and T. Scullion. *VESYS5 Rutting Model Calibrations with Local Accelerated Pavement Test Data and Associated Implementation,* FHWA/TX-03/9-1502-01-2, Texas Transportation Institute, College Station, Texas, 2002.

Zhou, F., S. Hu, T. Scullion, D. Chen, X. Qi, and G. Claros. Development and Verification of the Overlay Tester Based Fatigue Cracking Prediction Approach, *Journal of Association of Asphalt Paving Technologists*, Vol. 76, pp. 627–662, 2007.

Zhou, F., S. Hu, X. Hu, and T. Scullion. *Mechanistic-Empirical Asphalt Overlay Thickness Design and Analysis System,* FHWA/TX-09/0-5123-3, Texas Transportation Institute, College Station, Texas, 2009.

Zhou, F., E. Fernando, and T. Scullion. *Development, Calibration, and Validation of Performance Prediction Models for the Texas M-E Flexible Pavement Design System*, FHWA/TX-08/0-5798-2, Texas Transportation Institute, College Station, Texas, 2010.

APPENDIX A. DEFAULT MATERIAL PROPERTIES OF MOST COMMON PAVEMENT MATERIALS FROM TEXAS DISTRICTS

This Appendix documents the default material properties for common pavement materials that are included in the TxME program. Note that the default values were selected based on historical data collected under Project 0-6622 and previous projects.

Table A-1 lists the default values for asphalt mix properties. The dynamic modulus and associated shift factor equations used in the TxME program are listed below:

$$logE = \delta + \frac{\alpha}{1+e^{\beta+\gamma log(t_{ref})}} \tag{A-1}$$

$$loga_T = aT^2 + bT + c \tag{A-2}$$

where
E	=	dynamic modulus.
$t_{ref.}$	=	loading time at reference $T_{ref.}$
T	=	temperature.
a_T	=	shift factor.
δ, α, β, γ, a, b, c	=	regression factors.

Very limited test results are available for dense-graded Type A and B and Superpave A and B mixes. More effort is needed in this area.

Table A-2 lists the default values of granular base and subgrade soil properties.

Table A-3 lists the stabilized base material properties. The fatigue cracking model for stabilized base material is given below. It is clear that significant additional testing of these materials is necessary.

$$logN_f = B1 - B2\left(\frac{\sigma_t}{MR}\right) \tag{A-3}$$

where
N_f	=	the number of repetitions to fatigue cracking of the stabilized layer.
σt	=	the applied maximum tensile stress.
MR	=	the 28-day modulus of rupture (flexural strength).
B1 and B2	=	material related fatigue parameters.

Certainly, these default values should be updated and more default values for other types of material should be added, when more laboratory test results are available from Project 0-6658 and other research projects. Once a more robust inventory of material properties is acquired, the performance model needs to be calibrated.

Table A-1. Default Values of Asphalt Mixes.

Mix Type	Binder Type	Fracture Properties		Rutting Properties		Dynamic Modulus Properties						
		A	n	Alpha (α)	Mu (μ)	δ	α	β	γ	Shifting Factor *a*	Shifting Factor *b*	Shifting Factor *c*
Type C	PG64-22	5.2041E-06	3.8948	0.7315	0.7234	1.5104	2.9419	−0.8168	0.4525	3.5000E-04	−0.1252	7.0499
Type C	PG70-22	5.5095E-06	3.8792	0.7423	0.7014	1.7302	2.7407	−0.7939	0.4579	2.4132E-04	−0.1063	6.2592
Type C	PG76-22	5.8430E-06	3.8630	0.7485	0.6756	1.8265	2.6491	−0.8322	0.4592	2.1911E-04	−0.1002	5.9375
Type C	PG64-28	2.8039E-06	4.0645	0.7315	0.7306	1.4011	3.0881	−0.7014	0.4329	3.2300E-04	−0.1157	6.5114
Type C	PG70-28	3.3231E-06	4.0179	0.7423	0.6986	1.6035	2.9095	−0.6749	0.4335	2.2940E-04	−0.1000	5.8744
Type D	PG64-22	4.2081E-06	3.9531	0.7465	0.8102	1.5214	2.9058	−0.8074	0.4544	3.5300E-04	−0.1257	7.0658
Type D	PG70-22	4.4280E-06	3.9391	0.7521	0.7792	1.7410	2.7054	−0.7817	0.4595	2.4212E-04	−0.1064	6.2637
Type D	PG76-22	4.6659E-06	3.9248	0.7609	0.7265	1.8349	2.6163	−0.8192	0.4602	2.2032E-04	−0.1004	5.9467
Type D	PG64-28	2.4914E-06	4.0969	0.7465	0.8202	1.4212	3.0408	−0.6915	0.4365	3.2800E-04	−0.1163	6.5353
Type D	PG70-28	2.9215E-06	4.0532	0.7521	0.7892	1.6235	2.8628	−0.6622	0.4369	2.3101E-04	−0.1003	5.8872
Superpave C	PG64-22	4.9238E-06	3.9100	0.7315	0.7234	1.6273	2.7724	−0.7467	0.4782	3.9400E-04	−0.1312	7.2518
Superpave C	PG70-22	5.2041E-06	3.8948	0.7423	0.7014	1.7189	2.7170	−0.7780	0.4608	2.4265E-04	−0.1065	6.2678
Superpave C	PG76-22	5.5095E-06	3.8792	0.7485	0.6756	1.8129	2.6280	−0.8153	0.4613	2.2101E-04	−0.1005	5.9524
Superpave C	PG64-28	2.6934E-06	4.0755	0.7315	0.7306	1.3977	3.0520	−0.6902	0.4387	3.3200E-04	−0.1169	6.5588
Superpave C	PG70-28	3.1804E-06	4.0299	0.7423	0.6986	1.6044	2.8706	−0.6585	0.4390	2.3188E-04	−0.1004	5.8948
Superpave D	PG64-22	4.0044E-06	3.9667	0.7465	0.8102	1.5262	2.9080	−0.8093	0.4537	3.5200E-04	−0.1255	7.0580
Superpave D	PG70-22	4.2081E-06	3.9531	0.7521	0.7792	1.7447	2.7083	−0.7846	0.4589	2.4185E-04	−0.1064	6.2620
Superpave D	PG76-22	4.4280E-06	3.9391	0.7609	0.7265	1.8390	2.6189	−0.8224	0.4598	2.1995E-04	−0.1003	5.9437
Superpave D	PG64-28	2.3989E-06	4.1073	0.7465	0.8202	1.4237	3.0459	−0.6935	0.4353	3.2600E-04	−0.1160	6.5256
Superpave D	PG70-28	2.8039E-06	4.0645	0.7521	0.7892	1.6249	2.8686	−0.6653	0.4357	2.3053E-04	−0.1002	5.8832
SMA-C	PG76-22	9.2769E-08	4.9996	0.7106	0.7761	1.6567	2.8590	0.2599	0.5613	3.3400E-04	−0.0974	5.6739
SMA-D	PG76-22	8.1315E-08	5.0358	0.7106	0.7856	1.5967	2.8590	0.2599	0.5613	3.3400E-04	−0.0974	5.6739
SMA-F	PG76-22	6.0576E-08	5.1166	0.7106	0.8004	1.7460	2.5868	−0.7823	0.4823	2.8489E-04	−0.1092	6.2484
CAM	PG76-22	1.4129E-08	5.5159	0.7670	1.3540	1.7766	2.5105	−0.5469	0.5238	−7.8220E-05	−0.0364	2.9305

Table A-2. Default Values of Granular Base and Subgrade Soils.

Material Type	Elastic Property		Rutting Properties**	
	Resilient Modulus	Poisson's Ratio	Alpha (α)	Mu (μ)
Granular Base	50 ksi	0.35	0.87	0.06
Subgrade Soil	Depending on county*	0.40	0.80	0.10

Note: *–subgrade soil modulus used in TxME is exactly the same values as those in FPS21.

**–Alpha and Mu values were recommended based on the laboratory test results from the University of Texas at El Paso.

Table A-3. Default Values for Stabilized Base Materials.

Stabilized Base Types	Elastic Property		Fatigue Cracking Properties*		
	Modulus	Poisson's Ratio	Modulus of Rupture	Parameter B1	Parameter B2
Cement Stabilized Base	200 ksi	0.2	125 psi	0.972	0.0825
FA or LFA Stabilized Base	100 ksi	0.2	125 psi	0.972	0.0825
Lime Stabilized Base	65 ksi	0.2	125 psi	0.972	0.0825

Note: *–Very little information is available for fatigue cracking properties of stabilized base materials.

APPENDIX B. PROGRAM SPECIFICATIONS FOR TxME

1. INTRODUCTION

1.1 Purpose

The purpose of this specification is to present a clear description of the functionality of the flexible pavement design and analysis system, called TxME, and to eliminate ambiguities and misunderstandings that may exist. For the user, this document explains the functions that the software should perform. For the developer, it is a reference point for use during software design, implementation, and maintenance.

1.2 Overview

This document is divided into four main sections: 1) Introduction, 2) General Description, 3) Specific Requirements, and 4) Flowcharts. Section 1 describes the purpose of the document and the scope of product. Section 2 gives a general description of the product, including its main features. The third section provides the specific requirements for the system, including software and hardware requirements, and the user interface requirements. The last section presents the flowcharts for corresponding models.

2. GENERAL DESCRIPTION

2.1 Product Perspective

Developments over the last several decades have offered an opportunity for more rational and rigorous pavement design procedures. Substantial work has already been completed in Texas, nationally, and internationally, in all aspects of modeling, materials characterization, and structural design. These and other assets provided the technical infrastructure that made it possible to develop the Texas Mechanistic-Empirical (TxME) flexible pavement design system. The development of this new system will enable Texas pavement designers to take full advantage of new and premium materials, with a full consideration of the influential factors including pavement structure, traffic loading characteristics, and environmental conditions.

2.2 Product Features

The TxME design system aims to enable TxDOT designers to take full advantage of new and premium materials and to make more economical and reliable designs. It shall be used for:

- Asphalt Concrete (AC) mixture design selection.

- Thickness design, for surface treatment, conventional or thin Hot-Mix Asphalt (HMA), or perpetual pavement structure.

- Performance predictions of:

- o AC thermal cracking.
- o AC fatigue cracking.
- o Rutting prediction, including AC rutting, flexible base/subgrade rutting.
- o Stabilized base fatigue cracking analysis for surface treatment or thin HMA pavement with stabilized base layer.

- Endurance limit analysis for perpetual pavement.

- Load spectrum and reliability analyses.

- Performance check for design options recommended by current TxDOT Flexible Pavement Design system (FPS).

Three types of flexible pavement structure shall be handled in the TxME, which include

- Surface treated.

- Conventional or thin HMA surfaces.

- Perpetual pavement.

For any type of pavement design and analysis, there shall be four categories of input:

- Pavement structure and associated material properties.

- Traffic Characteristics.

- Climate.

- Reliability related input, including performance criteria and variability, etc.

2.3 User Characteristics

The TxME is designed to be run as a standalone program, where the user interacts with the system directly, to create and run a project file. No multiple users or remote access are supported in this system. Users are expected to have experience in pavement design and be familiar with pavement and material-related terminologies. Users are also expected to have experience using a computer, in particular computers with a Microsoft® Windows and Microsoft Office environment.

3. SPECIFIC REQUIREMENTS

3.1 Software and Hardware Requirements

The system will run on a Microsoft Windows computer, such as Windows XP and Windows 7. For Windows XP, Net Framework 4.0 is required.

The system will use a Microsoft Excel spreadsheet (version 2003 and later) to generate result output.

The system will embed the database of default values; no outside database needs to be accessed.

The computer that will run the system should have a minimum of a 1GHz processor and at least 1GB RAM.

3.2 General Interface Requirements

The interface is described in terms of a main screen, input screens, and results screen.

All windows shall display a title with the names of the system: TxME.

All windows shall include at least a close button.

3.3 Main Screen

The main screen of the system shall provide options of 1) creating a new project, 2) opening an existing project, 3) saving a project, 4) saving a project by another name, 5) running a project, and 6) exiting program.

The user shall be able to select an input screen to enter or select data for a pavement structure.

The user shall be able to select an input screen to enter or select data for climate parameters.

The user shall be able to select an input screen to enter or select data for traffic parameters.

The user shall be able to select an input screen to enter or select data for reliability parameters.

The user shall be able to select an input screen to enter or select calibration factors.

3.4 Pavement Structure Input Screen

The input screen shall allow the user to choose which type of pavement: 1) surface treated, 2) conventional or thin HMA surfaces, or 3) perpetual pavement.

The input screen shall provide a visualized way for the user to select materials and create the pavement structure.

The user shall be able to input design/analysis life, project location, and other optional information.

For each pavement layer, the user shall be able to edit the layer properties conveniently.

Default values or initial values shall be provided according to the layer type.

3.5 Material Properties Input Screens

For AC layer property inputs, the user shall be able to input layer thickness, binder type, gradation, dynamic modulus, fracture properties, rutting properties, Poisson's Ratio, and thermal coefficient of expansion, etc.

For the dynamic modulus input screen, two levels of inputs shall be provided: 1) input test data and 2) default values.

For Stabilized base layer material inputs, the user shall be able to input modulus, modulus of rupture, fatigue cracking properties, and Poisson's Ratio, etc.

For Flexible base layers and subgrade material inputs, the user shall be able to input modulus, rutting properties, and Poisson's Ratio, etc. Two levels of modulus should be provided: 1) typical value and 2) monthly values. The modulus input also needs to provide user with the option of inputting optimum moisture content information with the capability to integrate climatic data to evaluate the effects of moisture variation.

3.6 Traffic Loading Input Screens

Two levels of traffic loading inputs shall be provided: 1) Equivalent Single Standard Axle Load (ESAL) input and 2) load spectrum.

ESALs input should be consistent with current FPS traffic input, which includes 18 kip ESALs (20 years), the beginning average daily traffic number, the ending average daily traffic number, and vehicle operational speed information.

Load spectrum input should include 1) the basic traffic volume information, 2) traffic volume adjusting factors, and 3) axle load information, all in a format compatible with MEPDG traffic characterization inputs.

The basic traffic information should include the average annual daily truck traffic (AADTT) number, operation speed, tire pressure, axle spacing, etc.

The traffic volume adjustment factors should include vehicle class distribution factors, traffic growth factors, and monthly adjustment factors.

The axle load information should include axle configurations, number of axles per truck, and axle load distribution factors.

3.7 Climate Input Screens

Users shall be able to select a weather station, and the system shall provide both the hourly data and the summary of the weather data, such as average temperature or precipitation.

For a project location without a dedicated weather station, the system shall be able to provide the user several adjacent weather stations and "interpolate" climatic data.

3.8 Reliability Input Screens

Two input categories shall be displayed in this screen: performance criteria inputs and variability inputs.

The performance criteria inputs should include the analysis threshold criteria (performance limit) and reliability level in terms of percentage.

The variability inputs should include the potential variables and the coefficient of variation value.

The system shall be able to allow the user to select the variables to be considered by checking the applicable checkboxes.

3.9 Output Screens

The system shall provide a screen indicating the progress of analyzing (progress bar).

The output of TxME shall be organized into an Excel file format.

The output Excel file shall mainly be composed of three parts: the summary of user's inputs, the analysis results table, and the distress plots.

The user shall be able to view the output by selecting corresponding tree nodes in the main screen.

3.10 Error and Warning Messages

The system shall display error message prompts if any invalid input or data is considered as erroneous and/or incomplete.

4. FLOWCHARTS

The algorithms for implementing each distress model are shown in the flowcharts below.

- AC fatigue cracking: Figures B-1 and B-2.

- AC/base/subgrade rutting: Figure B-3.

- Low-temperature cracking: Figure B-4.

- Stabilized base fatigue cracking: Figure B-5.

- Endurance limit: Figure B-6.
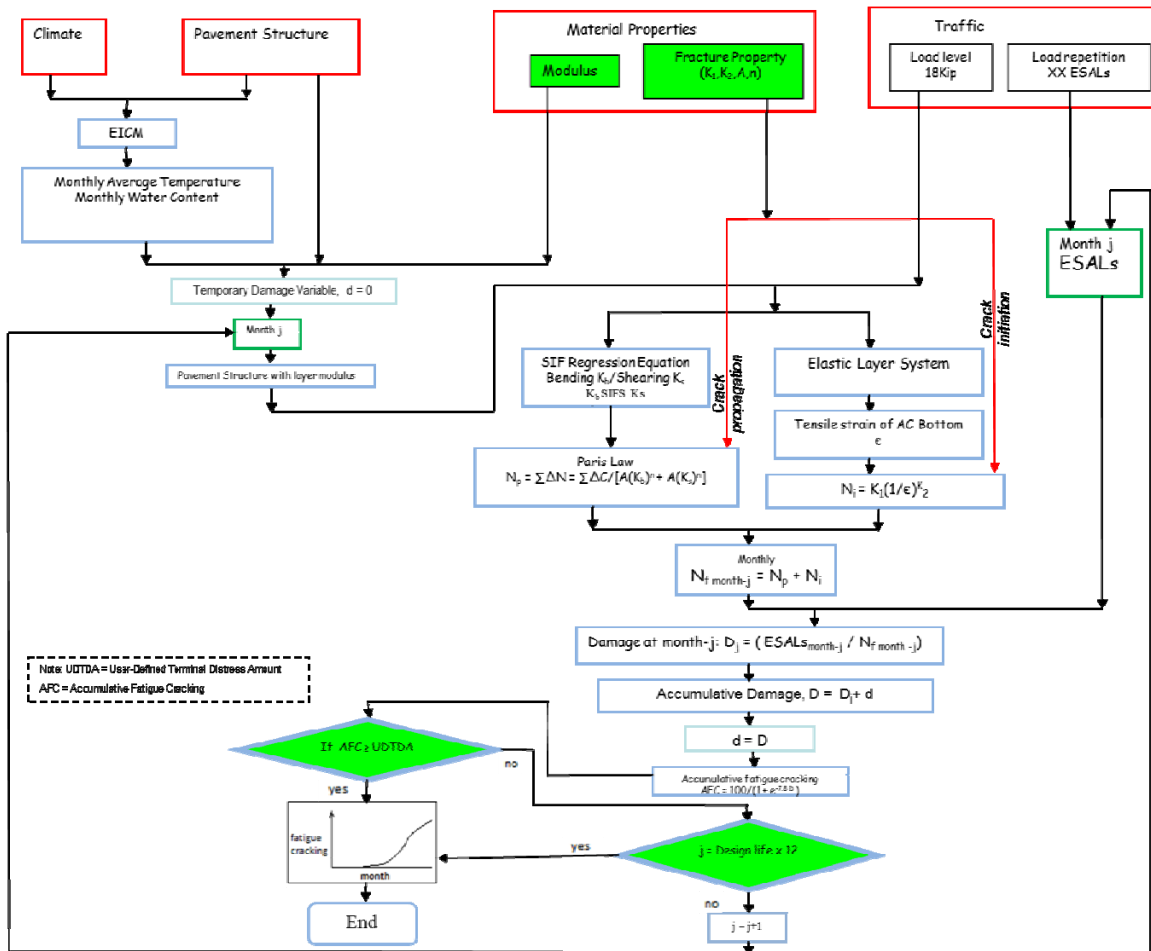
Figure B-1. AC Fatigue Cracking Flowchart for Deterministic Approach without Considering Input Variability.
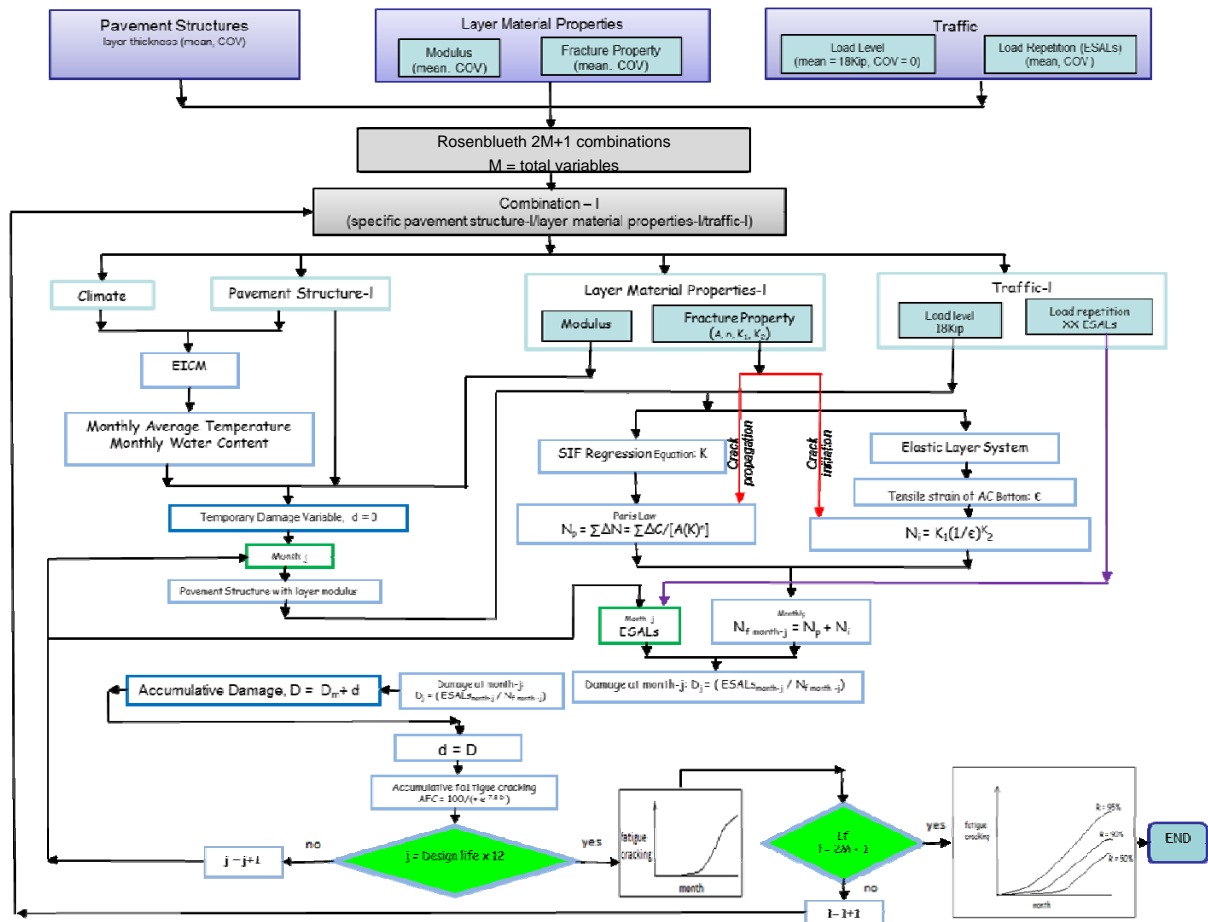
Figure B-2. AC Fatigue Cracking Flowchart for Reliability Approach Considering Input Uncertainty.
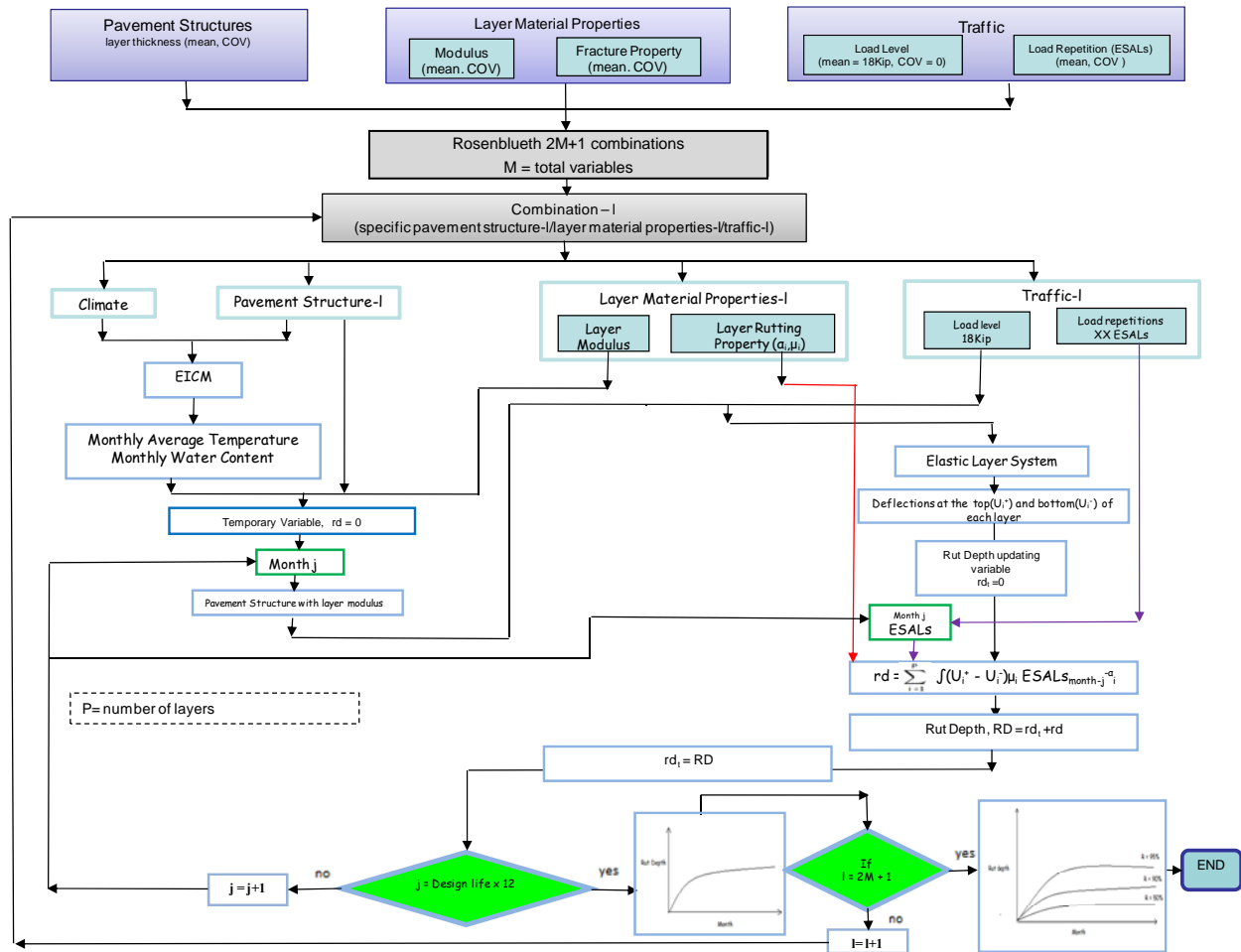
Figure B-3. AC/Base/Subgrade Rutting Flowchart for Reliability Approach Considering Input Uncertainty.

Low Temperature Cracking Flow Chart
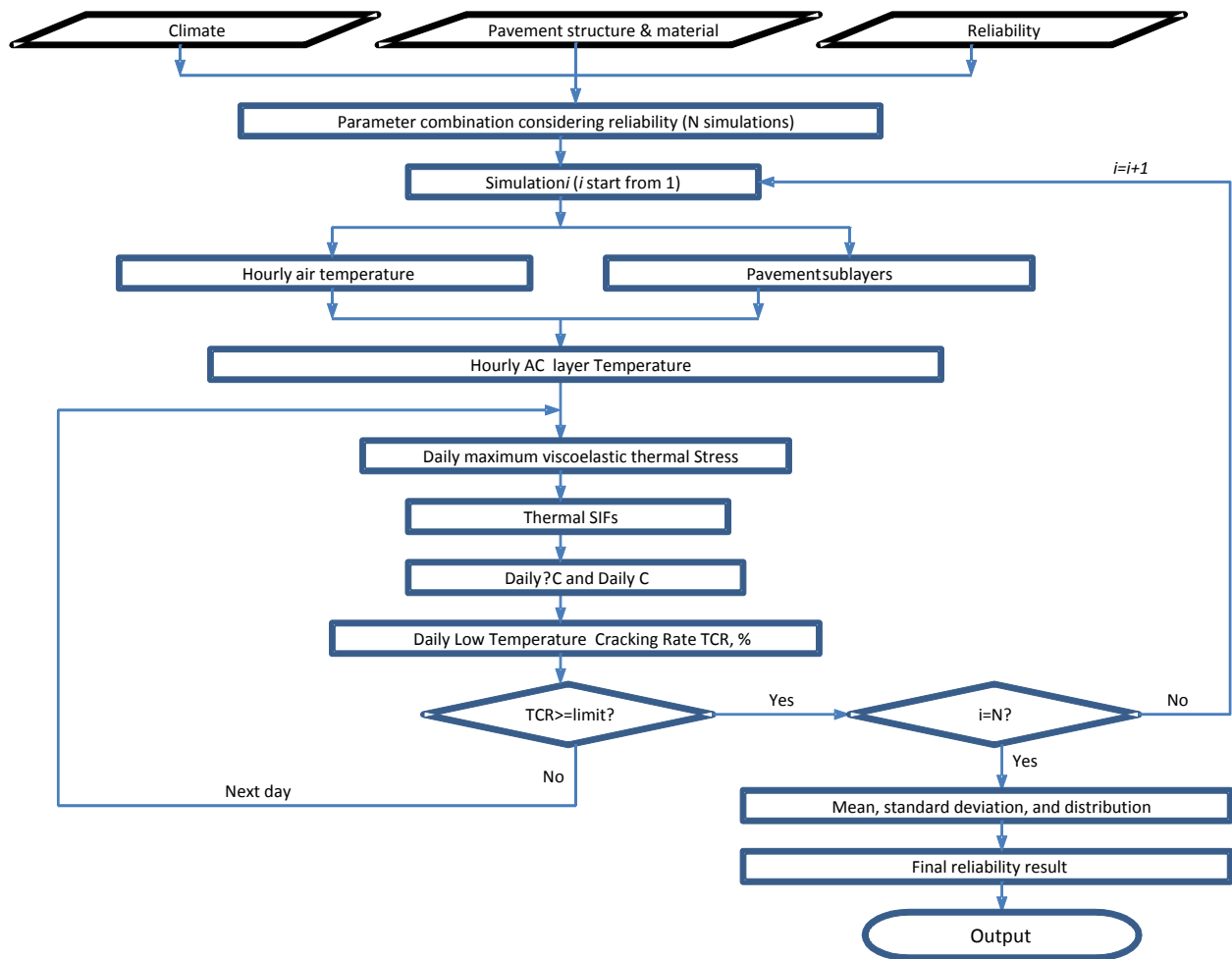
Figure B-4. Low Temperature Cracking Flowchart for Reliability Approach Considering Input Uncertainty.

Pavement Structures
layer thickness (mean, COV)

Layer Material Properties
Modulus (mean. COV)
CTB Modulus of Rupture (M$_r$) (mean, COV)

Traffic
Load Level (mean = 18Kip, COV = 0)
Load Repetition (ESALs) (mean, COV)

Rosenbluth 2M+1 combinations
(M = total variables)

Combination−I
(specific pavement structure/layer material properties/traffic)

Climate

Pavement Structure

Layer Material Properties I
Layer Modulus
CTB Modulus of Rupture (M$_r$)

Traffic I
Load level 18Kip
Load repetitions XX ESALs

EICM

Monthly Average Temperature
Monthly Water Content

Elastic Layer System

Tensile Stress (σ_t) of CTB bottom

Temporary Damage Variable, D$_x$ = 0

Month j

Pavement structure with layer modulus

Month j
ESALs

$N_{f-monthj} = 10^{[A+(\sigma_t/M_r)]/B}$

$d_j = (ESALs_{month-j} / N_{f\,month-j})$

Accumulative fatigue cracking
AFC = 100/(+ e$^{-7.8\,D}$)

D$_x$ = D

Accumulative Damage, D = d + D$_x$

j = j+1

no

j = Design life x 12

yes

fatigue cracking
month

If I = 2M + 1

yes

no

I= I+1

fatigue cracking
R = 95%
R = 90%
R = 50%
month

END

Figure B-5. Stabilized Base Fatigue Cracking Flowchart of Reliability Approach Considering Input Uncertainty.

142
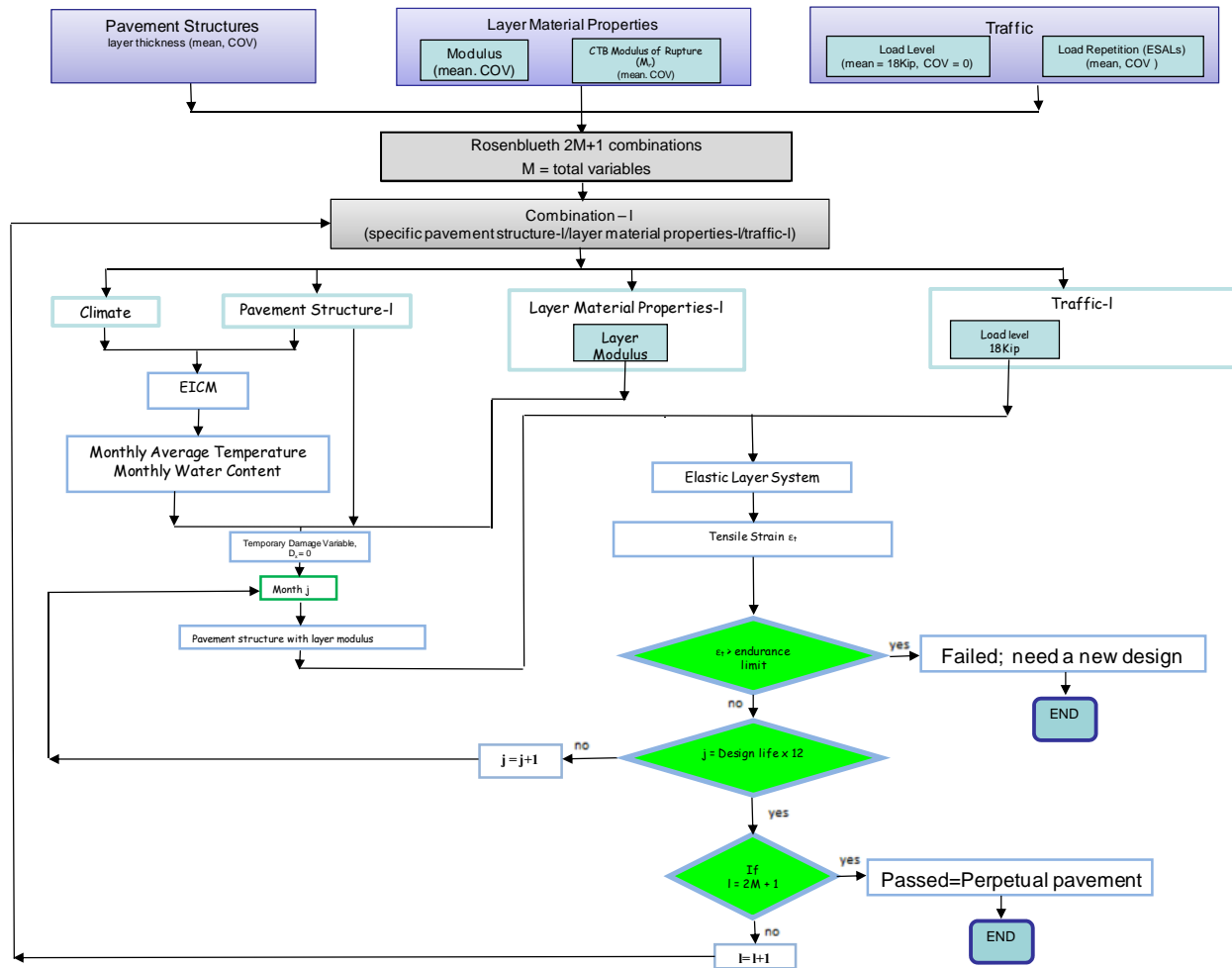
Figure B-6. Endurance Limit Flowchart for Reliability Approach Considering Input Uncertainty.

APPENDIX C. RUTTING DISTRIBUTION IN INDIVIDUAL LAYERS

1. BACKGROUND

The Texas Department of Transportation (TxDOT) is sponsoring two research projects with the objective of establishing a Texas Mechanistic-Empirical pavement design system (TxME).

- Project 0-6622: Texas Mechanistic-Empirical Pavement Design System.

- Project 0-6658: Texas Flexible Pavement Database.

Project 0-6658 will collect field performance data of around 100 field test sections and necessary lab data to characterize materials in the structure. These data will be used as part of the effort to calibrate the TxME system being developed under Project 0-6622. One of the distresses being considered in TxME is pavement rutting. Rutting development is often a gradual process under an increasing number of load applications. Rutting occurs in flexible pavements because of the accumulation of small permanent deformations in any of the pavement layers or the subgrade. It is criti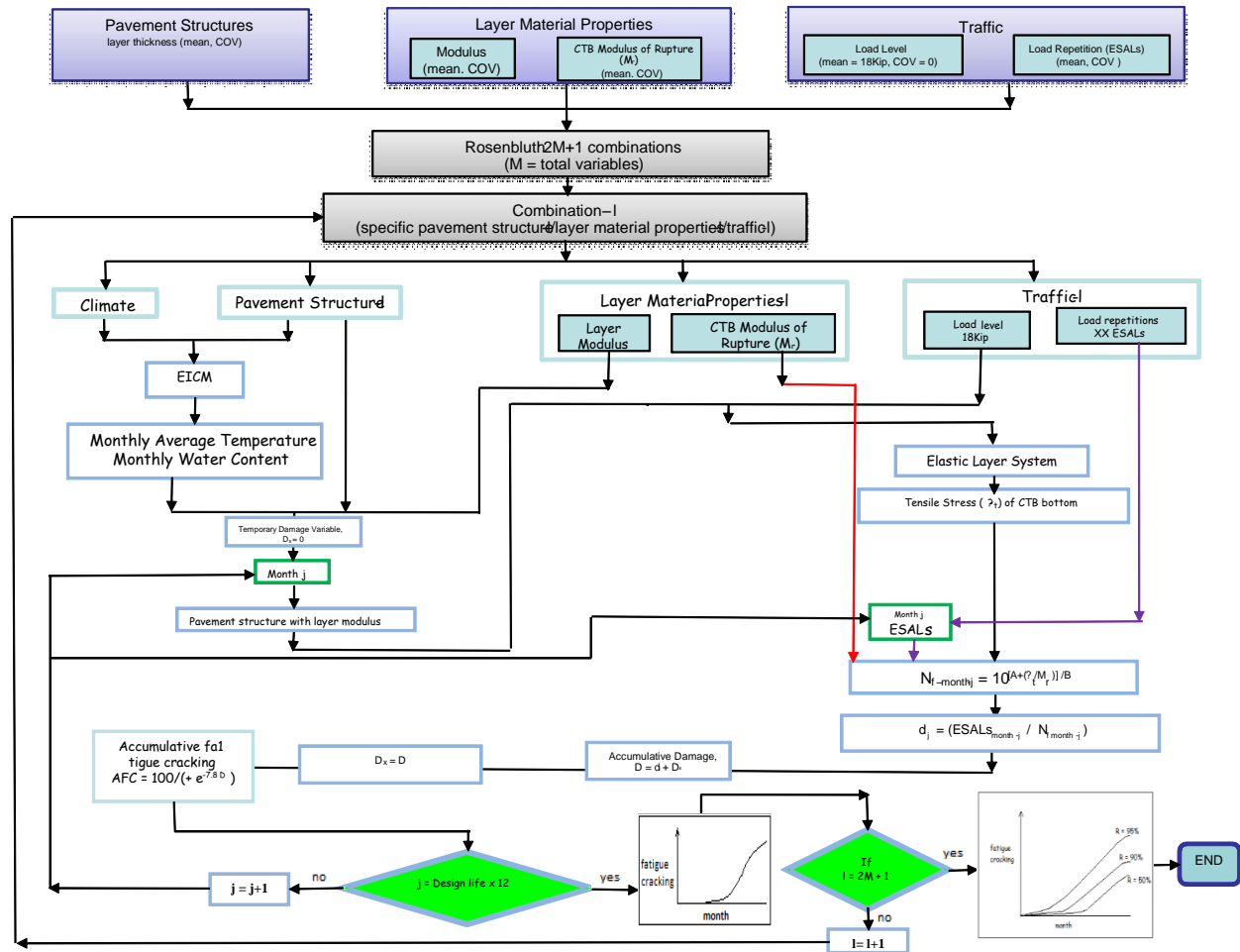cal to know both total rutting and rutting distribution in each individual layer when calibrating rutting models being integrated into TxME. However, rutting distribution information is not currently available from Project 0-6658 due to limited resources. Therefore, researchers under Project 0-6622 compromised by identifying the rutting distribution information through literature review. This technical memorandum summarizes the rutting distribution information found in the literature.

First of all, this document distinguishes the rutting development process. Then field trench studies and APT testing on a variety of asphalt pavements are presented. Finally, a summary is presented at the end.

2. PAVEMENT RUTTING DEVELOPMENT

It is well known that normal rutting development is a gradual process, and follows the power law model (RD=aN^b, N-load repetitions, a and b constants) (Zhou and Scullion 2002). However, this is the case only if there is no fatigue cracking. Field observations clearly indicate that the rutting development will not follow the power law model once fatigue cracking occurs. A few examples are presented below.

2.1 FHWA-ALF Phase III Research Program

From 1993 through 2001, FHWA conducted a series of accelerated pavement tests to validate Superpave asphalt binder and mixture tests and associated criteria for rutting and fatigue cracking. Twelve pavements were constructed in 1993 at the Turner-Fairbank Highway Research Center in McLean, VA (Stuart et al. 2002). Each pavement had a length of 144 ft, a width of 13ft, and was divided into four test sites. The FHWA ALF was used to load these pavements. The pavements were constructed and evaluated under conditions that promoted

either rutting or the formation of fatigue cracks. Figure C-1 shows a layout of the pavements, designated as lanes 1 through 12. For fatigue cracking tests, all pavements were tested at the temperature of 82°, 66°, or 50 °F, and loaded using super-single load of 12000 lb. with a tire pressure of 100 psi. For rutting validation tests, the pavement temperature ranged from 115° to 169 °F and was controlled during trafficking using infrared lamps; the 10000 lb. ALF load was applied using a super-single tire with a tire pressure of 100 psi.

Rut depth in the asphalt layers, without consideration of any upward heaving outside the wheel path, was measured during each distress survey using a survey rod and level. For tested sites at both intermediate and high temperatures, the relationships between the measured rutting depths in asphalt layers and the number of ALF repetitions are shown in Figures C-2 to C-8. In addition, the corresponding fatigue cracking data at intermediate temperature also are depicted in Figures C-2 to C-6.

FHWA-ALF Results at Intermediate Temperatures

For all of the curves in Figures C-2 to C-6, the rate of rutting accumulation does not follow the power law. The most interesting phenomenon is that upon the occurrence of the rapid rutting development, for all test lanes, there was a concurrent initiation and propagation of fatigue cracking. Apparently, the initiation and propagation of cracking accelerates the development of rutting.

FHWA-ALF Results at High Temperatures

For all 17 sites tested at different temperatures, the relationships between the measured rutting depths in the asphalt layer and the number of load repetitions are shown in Figures C-7 to C-8. No fatigue cracking was reported in test sections and no rapid rutting development was observed. All sites followed the power law development. This implies that the development of rutting itself, when not combined with fatigue cracking, generally follows the rule of the power law.
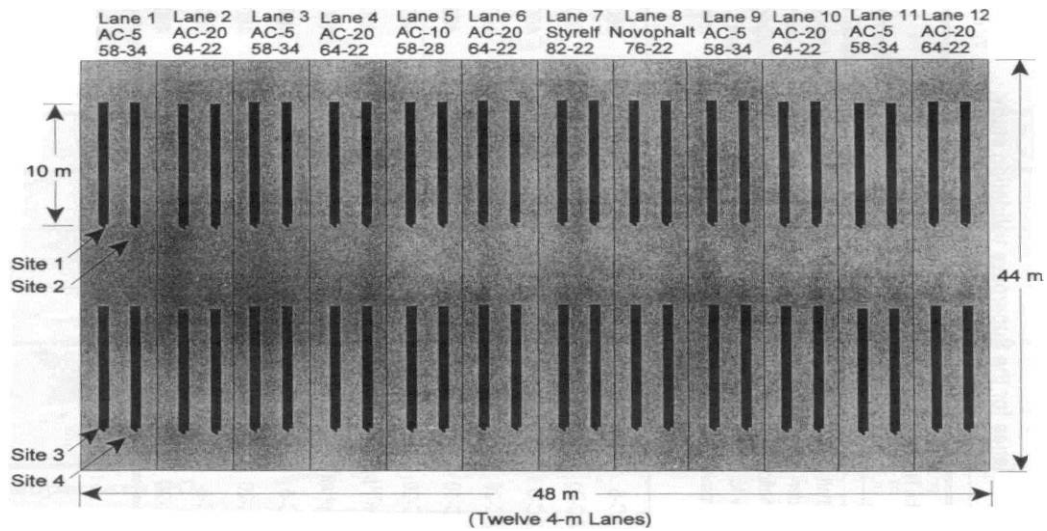
Figure C-1. Layout of the Test Lanes at the FHWA Pavement Test Facility (Stuart et al. 2002).
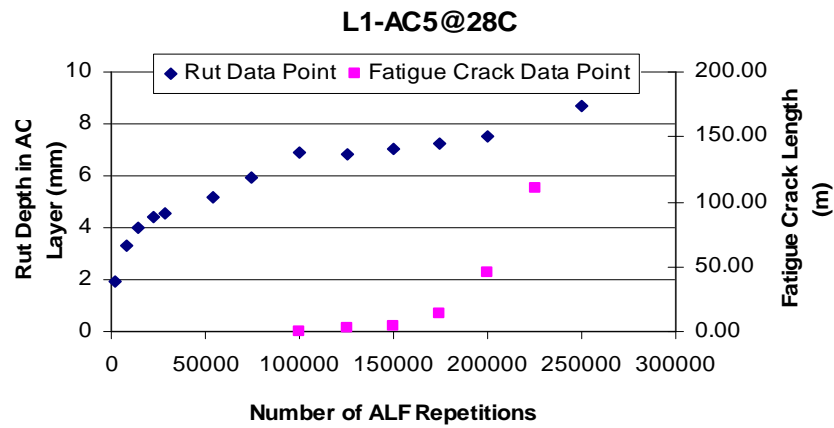
Figure C-2. FHWA ALF Phase III Test Results at Intermediate Temperature: L1-AC5@28°C.
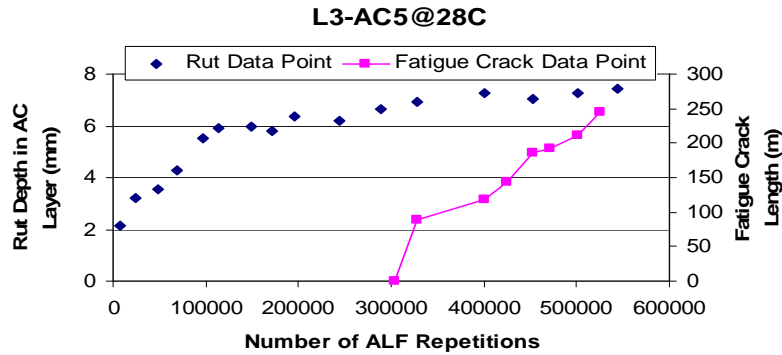
Figure C-3. FHWA ALF Phase III Test Results at Intermediate Temperature: L3-AC5@28°C.

Figure C-4. FHWA ALF Phase III Test Results at Intermediate Temperature: L3-AC5@19°C.

Figure C-5. FHWA ALF Phase III Test Results at Intermediate Temperature: L3-AC5@28°C.

148

L4-AC20@19C
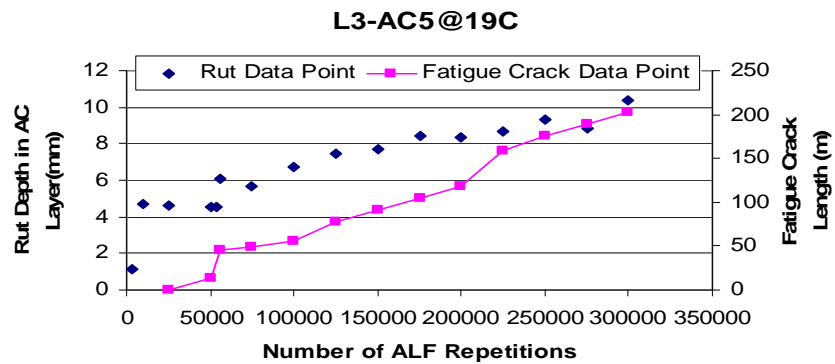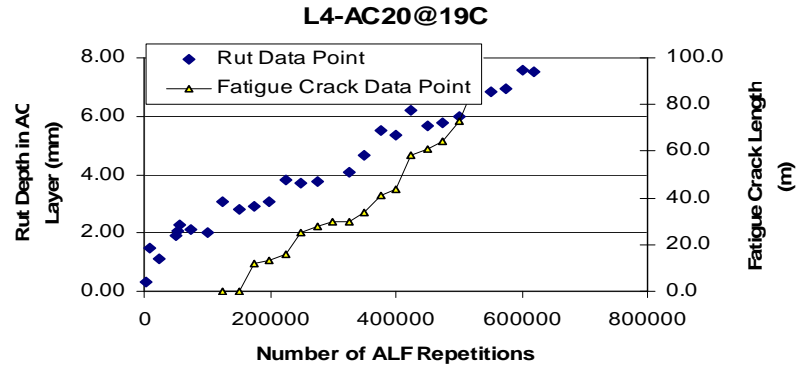
**Figure C-6. FHWA ALF Phase III Test Results at Intermediate Temperature:
L4-C20@19°C.**
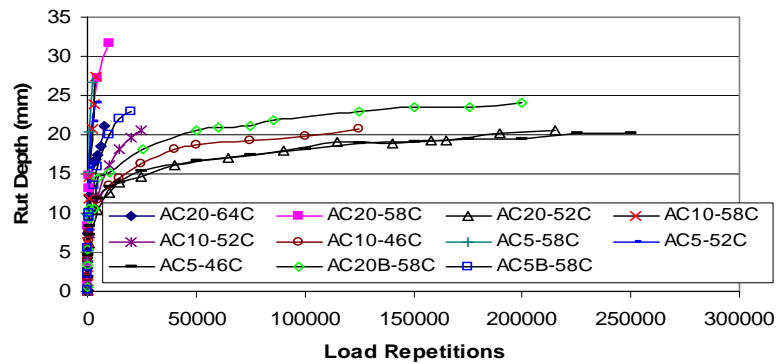
Figure C-7. FHWA ALF Phase III Test Results at High Temperatures: Unmodified Binder
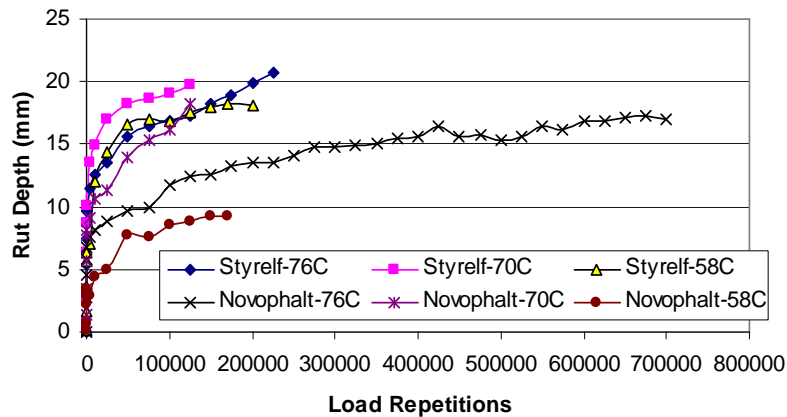
Figure C-8. FHWA ALF Phase III Test Results at High Temperatures: Modified Binder.

149

All asphalt pavements discussed previously are APT sections, which behave somewhat differently from field highway conditions. Therefore, it is necessary to look at the performance of in-service highway sections. This is discussed as follows.

2.2 Lake Wales Test Road

The construction of the Lake Wales test road with a four-lane facility (Tseng 1988) was completed in January 1971. Traffic in terms of annual daily traffic was approximately 725 vehicles in 1971 and had a 5.5 percent growth rate in the following years. Various base and surface thickness combinations were included in the test sections. The performance data including the cracking and rutting was continuously collected for 15 years. These data are shown in Figures C-9 and C-10 for two pavement sections, No. 1A and 4B, respectively. The detailed combinations of pavement structure layers are also presented in the Figures. In addition, the predicted rutting curve from the three-parameter model (Tseng 1988) is also presented in the figures. For pavement section No. 1A shown in Figure C-9, there was no cracking during the 15 years of service. Moreover, after initial rapid accumulation, rut depth stopped increasing, which may partially result from the aging of asphalt binder. As shown in Figure C-10, however, Section No. 4B indicates a rapid development of the cracked area with increased rutting in later years. As discussed in the author's paper (Zhou et al., 2002), the three-parameter model is similar to the power law model. Thus, the performance of these sections clearly indicates that the occurrence of fatigue cracking results in an increased rate of rutting appearing in later periods of service.
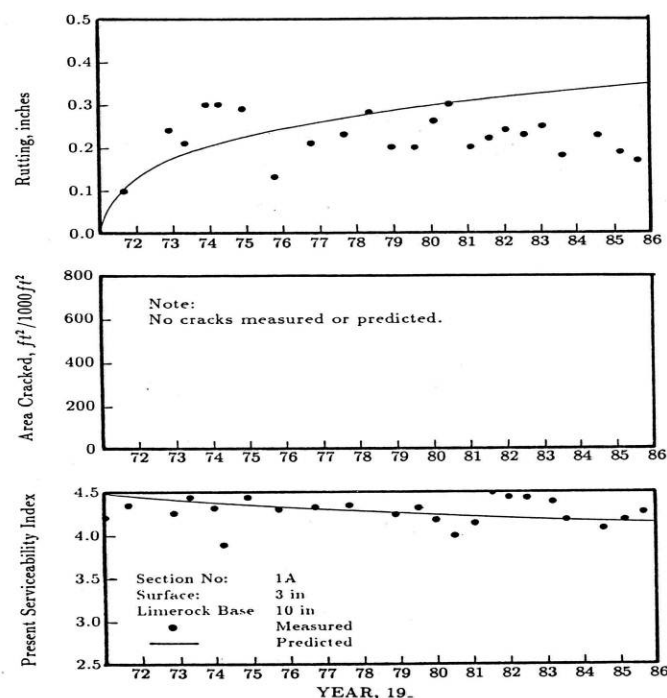
Figure C-9. Performance Data of Section No. 1A on Lake Wales Test Road (Tseng, 1988).

150
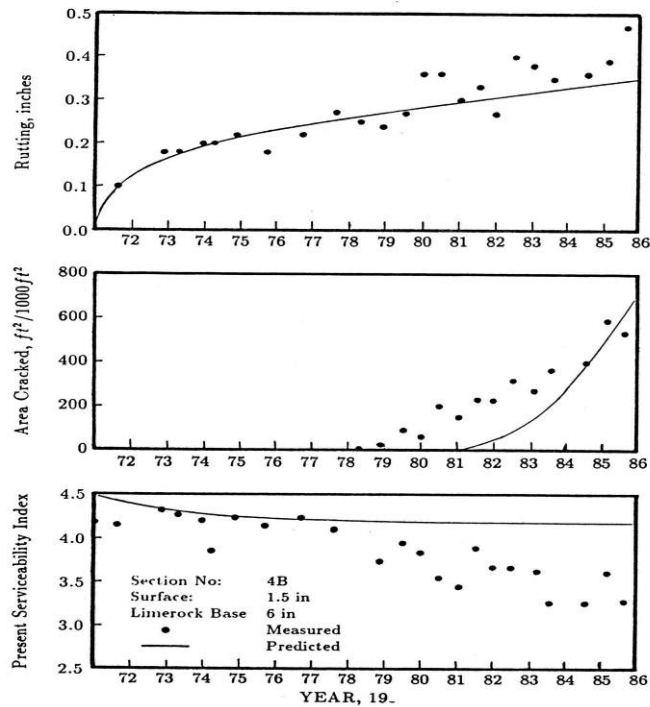
Figure C-10. Performance Data of Section No. 4B on Lake Wales Test Road (Tseng 1988).

2.3 NCAT Test Track

Eight structural test sections with three different asphalt layer thicknesses (5, 7, and 9 inches) and two different binder types (PG 67-22 and an SBS modified PG 76-22) were constructed at the NCAT test track in 2003. All eight sections had an underlying 6-inch crushed granite granular base over fill material, which was constructed over the existing embankment. Figure C-11 shows the cross sections of the structural study sections, N1-N8. Notice that the sections were a full factorial experiment with N7 serving as a duplicate to N6, both with an SMA surface, and N8 is a duplicate of N7, both with an asphalt-rich bottom layer. Field performance of these eight test sections, in terms of rutting and fatigue cracking, is shown in Figure C-12. Note that Section N8 should be excluded from consideration here, because a portion of Section N8 was milled and inlaid with new mix due to extensive fatigue cracking in spring 2005.

While reviewing the performance data of Sections N1-N7 in Figure 13, researchers noted that fatigue cracking in Sections N1 and N2 induced their rapid rutting development in the later stage. Without fatigue cracking, rapid rutting development in later stages is not observed.

151
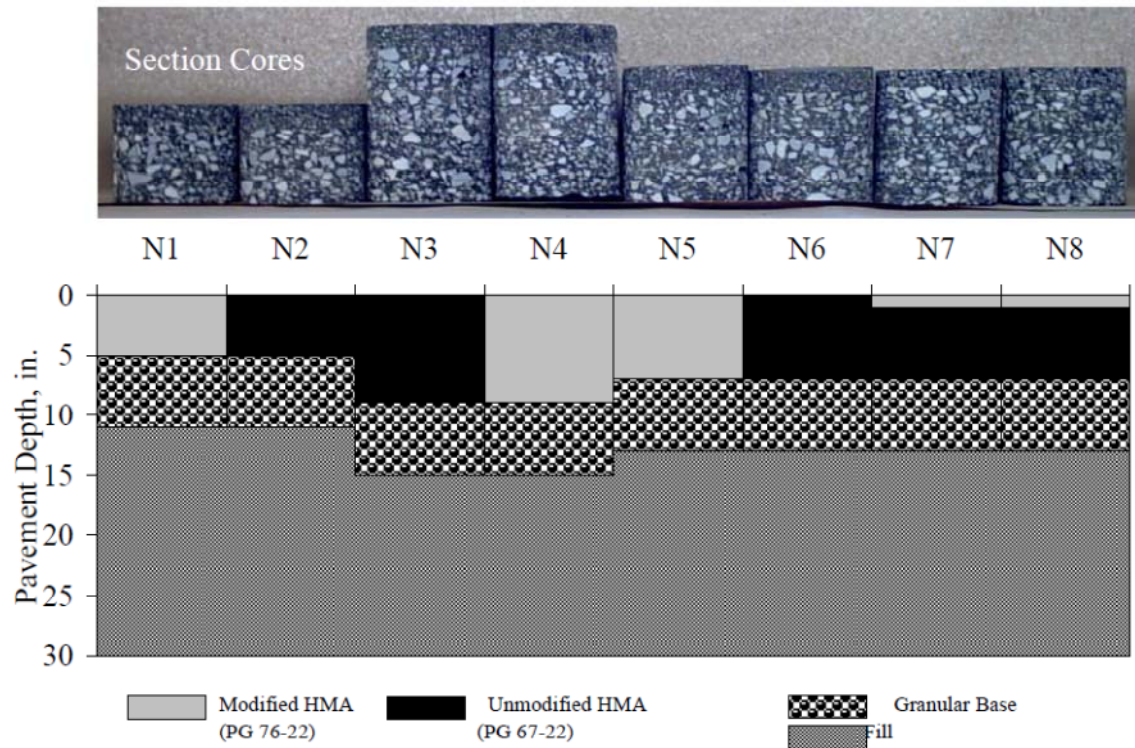
Figure C-11. Structural Experimental Section Layout (Priest and Timm 2006).
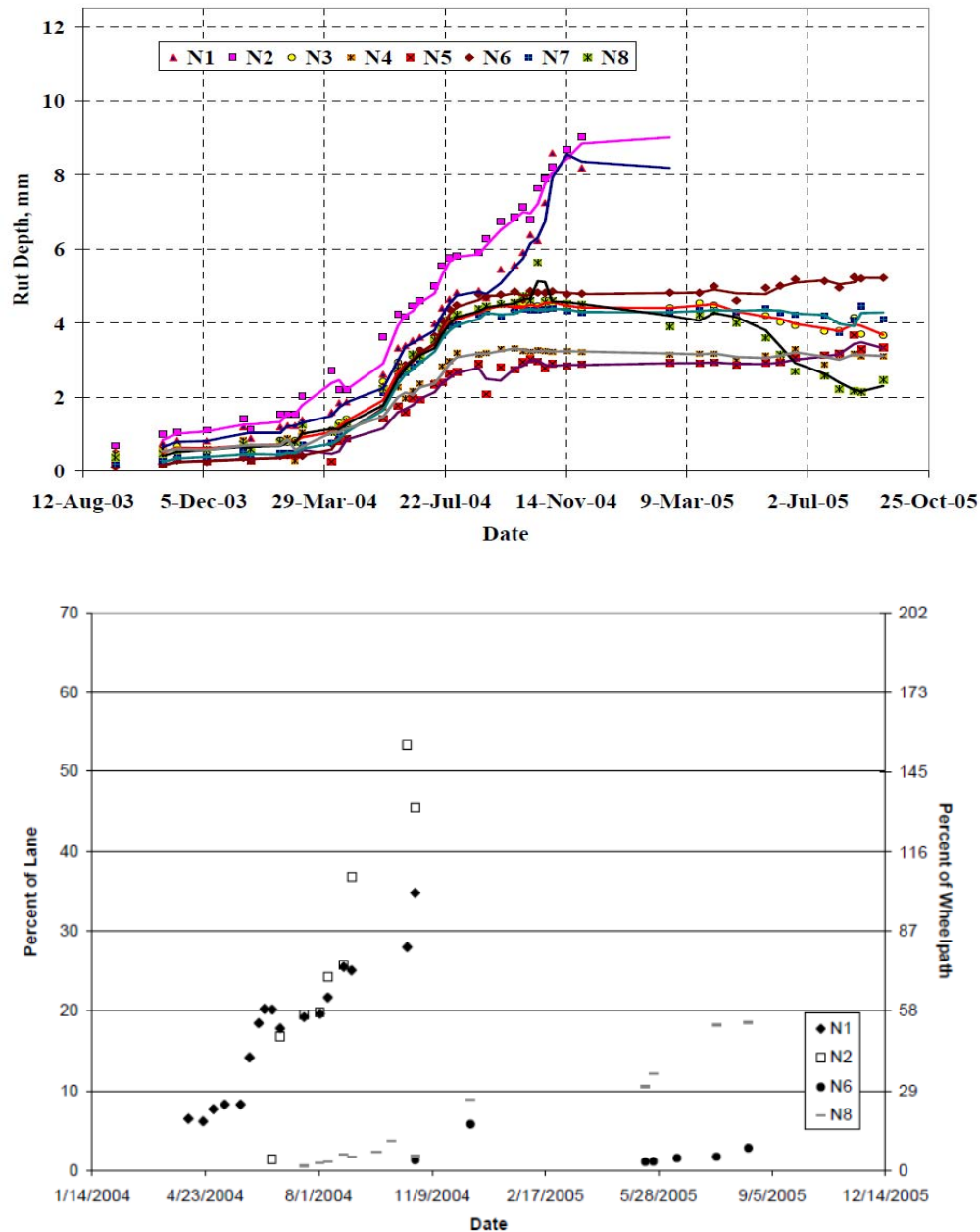
Figure C-12. Observed Field Performance of NCAT Test Sections (Priest and Timm 2006).

In summary, for itself, the development of pure rutting follows the well-known power law. Meanwhile, the occurrence of fatigue cracking will accelerate rutting development in later stages of pavement service. This observation also implies that one should be very careful when determining rutting distribution in individual layers based on trenching information. If the trenched section is already fatigued, the associated rutting distribution may not represent the true distribution before fatigue occurrence.

3. RUTTING DISTRIBUTION IN INDIVIDUAL LAYERS

In general, for thicker asphalt pavements, asphalt layers are the main contributor to the total rutting measured at the surface as noted in the MEPDG report (Table C-1). The main concern with identifying layer contribution to total rutting is with thinner pavements. However, there is not much trenching information available about rutting distribution in the thinner pavements in the literature. The researchers of Project 0-6622 turned to the NCHRP 4-30A study and a recent APT study conducted at the Cold Regions Research & Engineering Laboratory (CRREL). More detailed information is discussed below.

Table C-1. Average Percentage of Surface Rutting for Different Pavement Layers and Subgrade.

Layer	Asphalt Layer Thickness		
	Less than 4 inches	4–8 inches	>8 inches
Asphalt concrete	70	80	100
Granular base	15	10	0
Granular subbase	10	5	0
Subgrade	5	5	0

3.1 Thicker Asphalt Pavements

NCAT Study

Brown and Cross (1989) surveyed a variety of pavements in the late 1990s. Their trench results showed that permanent deformation is limited to the upper 100 mm (4 inches) of the mix. It also indicated that, at least for reasonably stiff supporting materials, most pavement rutting is confined to the asphalt pavement layer.

Rutting Study in Alabama

Parker and Brown (1991) investigated rutting problems in Alabama in late 1980s. Thirteen sections with a minimum of 4 inches asphalt layer(s) were trenched; five of them were considered to have good rutting performance and the other eight sections, considered poor. After reviewing the trenching results, Parker and Brown concluded that the rutting was generally confined to the top 3–4 inches of asphalt layer(s) (surface and binder courses).

TxDOT's Trench on SPS1-US281 Sections

The two trench profiles (Chen et al. 2001) indicated that the rutting was coming primarily from the top 50 mm (2 inches) of the HMA layer. As shown in Figure C-13, the rutting was accompanied by the considerable lateral shear flow.

Figure C-13. Trench Profiles for 161 (Top) and 162 (Bottom).

3.2 MnRoad Mainline Trench Study

Mulvaney and Worel (2002) documented the forensic rutting investigation of the MnRoad mainline Test Road. The main purpose was to identify the rutting distribution in individual layers. Figure C-14 presents the mainline layout and pavement structure of each cell. The minimum asphalt layer is around 6 inches thick. The trench results indicated that all the rutting was from asphalt layer(s). Table C-2 details the rutting distribution in asphalt layers. Therefore, basically the surface rutting comes mainly from asphalt layers when the total asphalt layers are close to or thicker than 6 inches.
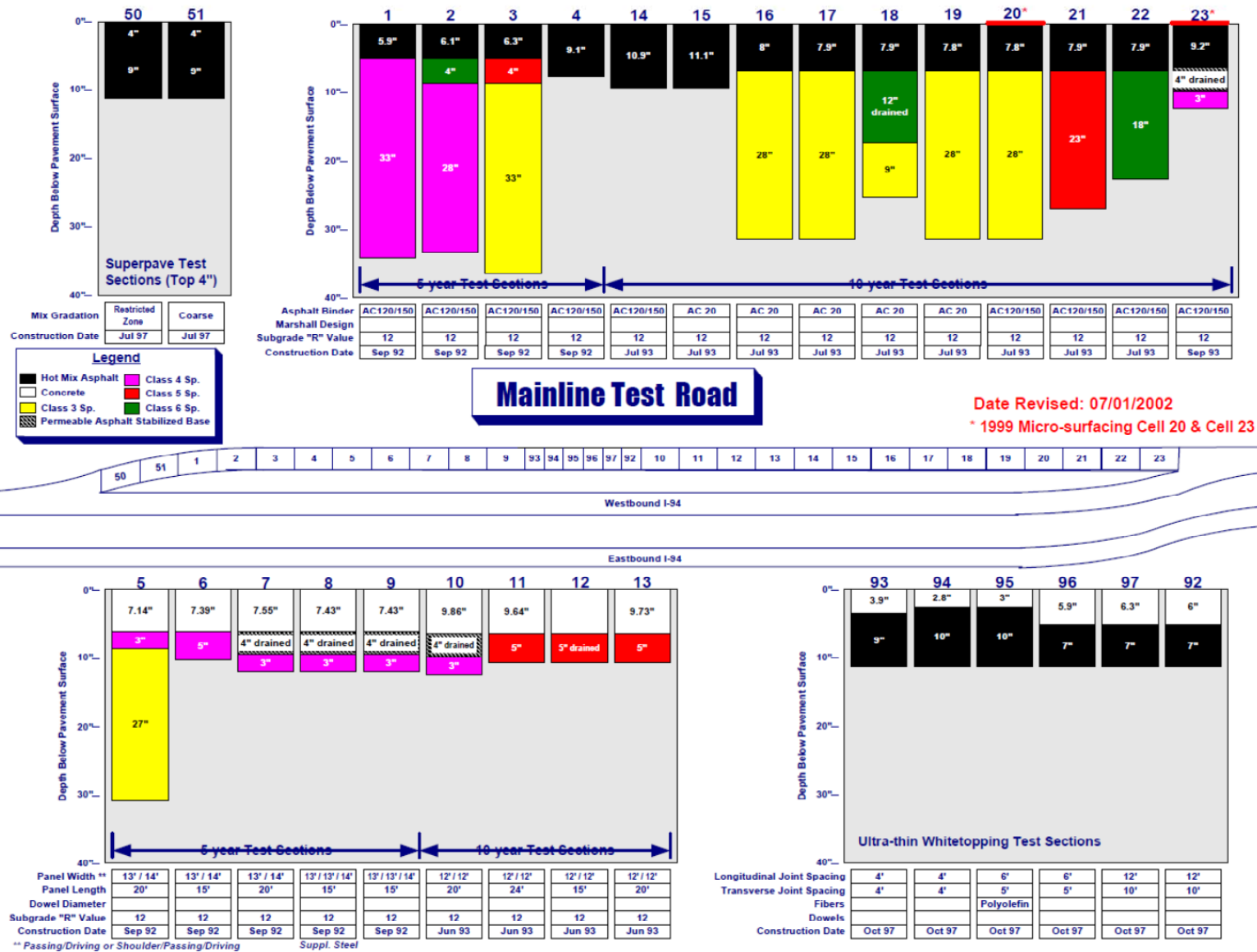
Figure C-14. MnRoad Test Road (Mulvaney and Worel 2002).

156

Table C-2. Rutting Distribution in Asphalt Layers.

Left Wheel Path Rutting (inches)								Right Wheel Path Rutting (inches)							
Calculated Rutting Contribution per Lift										Calculated Rutting Contribution per Lift					
Bottom		Surface			Forensic Trench	Cell AVG	Cell	Cell AVG	Forensic Trench	Surface			Bottom		
5	4	3	2	1						1	2	3	4	5	
		NR	0.167	0.289	0.229	0.232	1	0.210	0.250	0.202	0.128	0.018			
		0.080	0.190	0.363	0.531	0.321	2	0.273	0.385	0.447	0.239	0.124			
		0.075	0.082	0.329	0.302	0.248	3	0.166	0.302	0.330	0.099	0.088			
	NR	NR	0.015	0.123	NMT	0.228	4	0.397	NMT	0.384	0.260	NR	NR		
NR	0.106	0.208	0.287	0.360	0.328	0.266	14	0.260	0.391	0.421	0.372	0.305	0.108	0.169	
NR	0.219	0.120	0.066	0.244	0.250	0.247	15	0.219	0.266	0.251	0.303	0.087	0.069	NR	
	NR	NR	0.104	0.160	NMT	0.153	16	0.116	NMT	0.162	0.008	NR	NR		
	NR	NR	0.124	0.219	NMT	0.197	17	0.122	NMT	0.132	0.108	0.104	NR		
	NR	NR	0.015	0.084	NMT	0.207	18	0.197	NMT	0.220	0.102	0.083	NR		
	NR	0.092	0.259	0.257	NMT	0.235	19	0.185	NMT	0.197	0.119	0.083	NR		
	NR	0.111	0.229	0.426	NMT	0.531	20	0.394	NMT	0.305	0.171	0.132	0.061		
	0.026	0.211	0.389	0.785	0.719	0.467	21	0.270	0.391	0.352	0.114	0.022	0.156		
	NR	NR	0.142	0.247	NMT	0.263	22	0.238	NMT	0.103	0.048	NR	NR		
NMT	NMT	NMT	NMT	NMT	NMT	0.563	23	0.588	NMT	0.395	0.244	0.163	0.147	0.026	

3.3 Thinner Asphalt Pavements

Mississippi Trenching Study

White et al. (2002) trenched two highways in Mississippi under NCHRP 4-30A, one being on SH302 and the other on SH28. Detailed trenching information is described below.

SH302 E, Mississippi

The pavement structure on SH302 consists of 80 mm (3.2 inches) of HMA, 230 mm (9 inches) of asphalt-treated base, 330 mm (13 inches) of subbase, on natural subgrade. Figure C-15 shows the trenching results. Close examination of the enlarged trench profile showed that rutting occurred predominantly in the HMA layer, with a minor contribution from the base layer.

On-site visual inspection using a string line indicated that no pavement failure was present below the base layer.
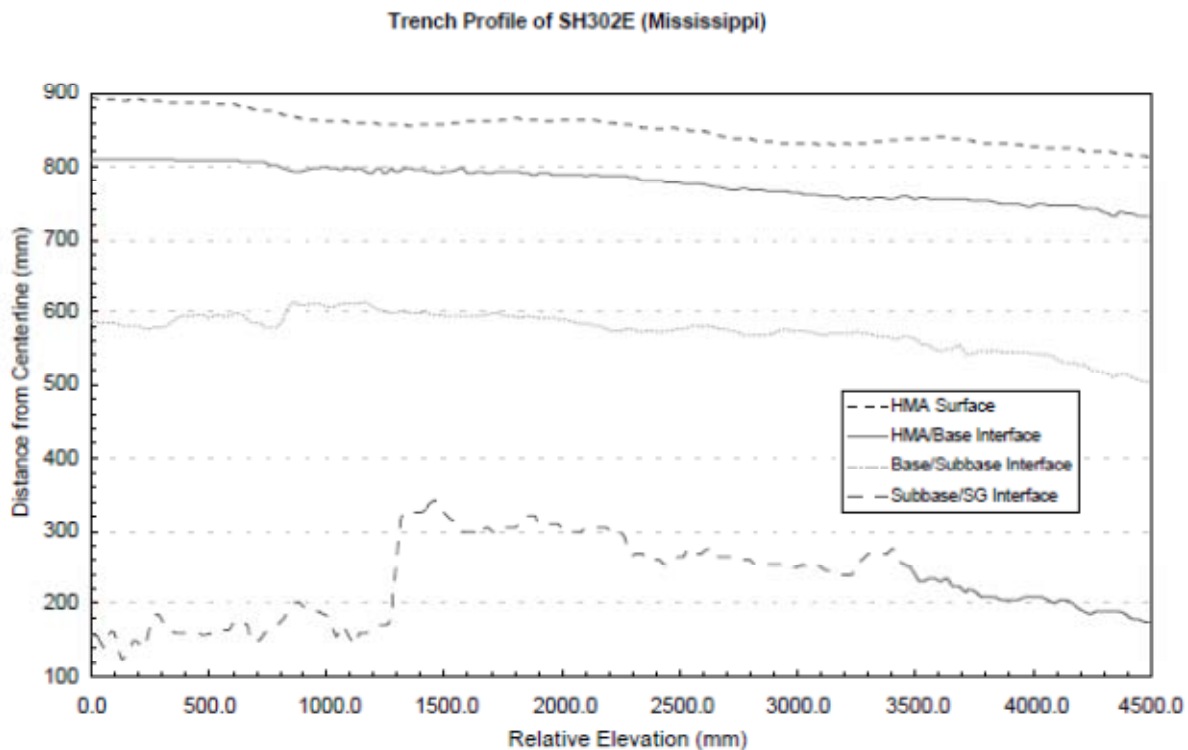

Figure C-15. Trench Information on SH302E, Mississippi (White et al. 2002).

SH28E, Mississippi

The pavement structure on SH28 includes 1.2 inches (30 mm) of HMA, 7 inches (180 mm) of asphalt treated base layer, 7 inches (180 mm) of subbase layer, and a subgrade layer. The trenching results are shown in Figure C-16. Close examination of the enlarged trench profile

showed that rutting occurred primarily in the base layer. This occurrence was verified by an on-site visual inspection using a string line; no rutting was found below the base layer.

Trench Profile of SH28E (Mississippi)
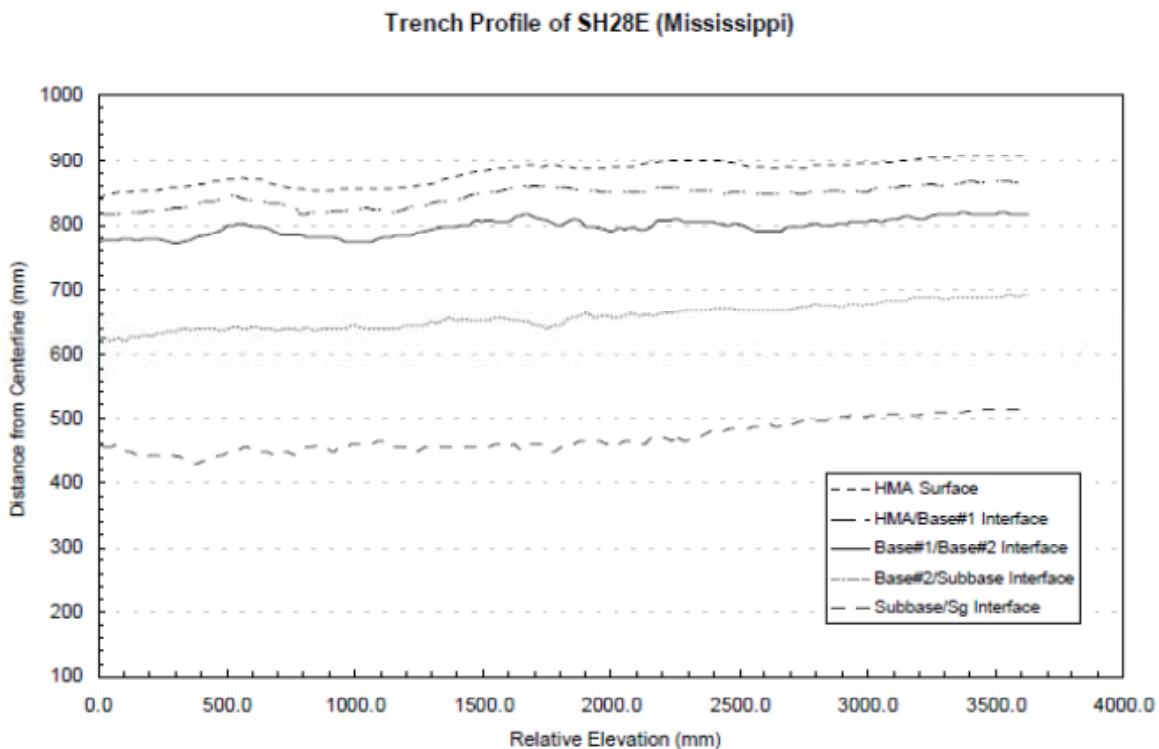
Figure C-16. Trench Information on SH28E, Mississippi (White et al. 2002).

CRREL Subgrade Test Sections

A national pooled fund was recently completed in CRREL, focusing on pavement subgrade performance. Table 3 shows the test matrix. A total of 12 test sections were instrumented and tested under HVS loading. All these 12 sections have the same (or similar) pavement structure: 3 inches asphalt layer, 9 inches granular base, and 60 inches subgrade soil and concrete bottom.

The same asphalt mix and base material were used for all test sections. The only difference among these test sections is subgrade soil type (see Table C-3).

Table C-3. CRREL HVS Test Matrix.

Subgrade Moisture Content	AASHTO Soil Type			
	A-2-4	A-4	A-6	A-7-5
Moisture 1	Optimum–10% TS701	Optimum–17% TS702	Optimum–16% TS709	Optimum–20.4% TS712
Moisture 2	12% TS707	19% TS704	19% TS708	21% (soil borderline to A-6) TS710
Moisture 3	15% TS703	23% TS705	22% TS706	25% TS711

After reviewing the reports produced, it was found that only four of 12 sections had full permanent deformation data in different depth of pavement: TS703, TS704, TS709, and TS712. As an example, Table C-4 shows the rutting distribution in individual layers of TS703. Table C-5 summarizes the averaged rutting distribution in individual layers of these four test sections. Note that all HVS testing was conducted at around 68°F so that little rutting was from the asphalt layer. It is believed that the rutting distribution shown in Table C-5 is applicable to thin pavements with a 1- to 2-inch asphalt layer.

Table C-4. Rutting Distribution in Individual Layer of TS703.

HVS Applications	Asphalt Layer	Granular Base Layer	Subgrade
500	14	29	57
1000	14	39	47
2500	15	41	44
5000	16	43	41
10000	17	44	38
25000	18	45	37
50000	19	43	37
Average	16	41	43

Table C-5. Rutting Distribution in Individual Layers of TS703, TS704, TS709, and TS712.

Test section	Soil Type	Asphalt Layer	Granular Base Layer	Subgrade
TS703	A-2-4	16	41	43
TS704	A-4	11	49	40
TS709	A-6	13	55	32
TS712	A-7-5	15	60	25
Average		14	51	35

4. RUTTING DISTRIBUTION RECOMMENDATION

Based on the information presented above, the author makes the following recommendation on rutting distribution in individual pavement layers, as indicated in Table C-6. Please note that this recommendation is not applicable to rutting development after fatigue cracking in the later stages of pavement life.

Table C-6. Average Rutting Distribution in Individual Layer.

Layer	Surface treated	Asphalt Layer Thickness			
		1–2 inches	2–4 inches	4–6 inches	>6 inches
Asphalt concrete	0	10	60	80	100
Granular base	70	55	25	15	0
Subgrade	30	35	15	5	0

5. REFERENCES

Brown, E. R. and S. Cross. A Study of In-Place Rutting of Asphalt Pavements, *Proceedings, Association of Asphalt Paving Technologists*, Volume 58, 1989.

Chen, D., J. Bilyeu, T. Scullion, D. Lin, and F. Zhou. Forensic Evaluation of Premature Failures of Texas Specific Pavement Study-1 Sections, *Journal of Performance and Construction Facility*, Vol. 17, pp. 67–74, Nov. 2, 2003.

Cortez, E. *Pavement Subgrade Performance Study, Test Section 712: Subgrade AASHTO Soil Type A-7-5 at 20 Percent Gravimetric Moisture Content,* U.S. Army Cold Regions Research and Engineering Laboratory, Handover, New Hampshire.

Janoo, V., E. Cortez, R. Eaton, and M. Ferrick. *Pavement Subgrade Performance Study, Volume 2-Results from Accelerated Pavement Testing of an A-2-4 Subgrade Soil at Higher Than Optimum Moisture Content*, U.S. Army Cold Regions Research and Engineering Laboratory, Handover, New Hampshire.

Janoo, V. and E. Cortez. *Pavement Subgrade Performance Study, Volume 4-Results from Accelerated Pavement Testing of an A-4 Subgrade Soil,* U.S. Army Cold Regions Research and Engineering Laboratory, Handover, New Hampshire.

Janoo, V. and E. Cortez. *Pavement Subgrade Performance Study, Test Section 708: Subgrade AASHTO Soil Type A-6 at Wet of Optimum (19%),* U.S. Army Cold Regions Research and Engineering Laboratory, Handover, New Hampshire.

Mulvaney, R. and B. Worel. *MnRoad Mainline Rutting Forensic Investigation*, Minnesota Department of Transportation, St. Paul, Minnesota, 2002.

Parker, F. and E. R. Brown. A Study of Rutting of Alabama Asphalt Pavements, Final Report Project Number ST 2019-9, Auburn University Highway Research Center, Auburn University, Alabama, 1990.

Priest, A. and T. David. Methodology and Calibration of Fatigue Transfer Function for Mechanistic-Empirical Flexible Pavement Design, NCAT Report 06-03, National Center for Asphalt Technology, December 2006.

Stuart, K. D., W. S. Mogawer, and P. Romero. *Validation of the Superpave Asphalt Binder and Mixture Tests that Measure Rutting Susceptibility Using an Accelerated Loading Facility*, FHWA-RD-99-204, the Federal Highway Administration, McLean, Virginia, 1999.

Tseng, K. A Finite Element Method for the Performance Analysis of Flexible Pavements, Dissertation of the Texas A&M University, College Station, Texas, 1988.

White, T. D., J. E. Haddock, A. J. Hand, and H. Fang. *Contributions of Pavement Structural Layers to Rutting of Hot Mix Asphalt Pavements*, NCHRP 468, 2002.

Zhou, F. and T. Scullion. Discussion: Three Stages of Permanent Deformation Curve and Rutting Model. *International Journal of Pavement Engineering*, Volume 3, Number 4, pp. 251–260, 2002.